12-1-2016

Radiation Therapy and Dosing Material Transport Methodology

Robert O'brien
University of Nevada, Las Vegas, obrienrjo@gmail.com

Repository Citation

O'brien, Robert, "Radiation Therapy and Dosing Material Transport Methodology" (2016). *UNLV Theses, Dissertations, Professional Papers, and Capstones*. 2891.
https://digitalscholarship.unlv.edu/thesesdissertations/2891

RADIATION THERAPY AND DOSING MATERIAL TRANSPORT METHODOLOGY

By

Robert James O'Brien

Master of Science, Materials and Nuclear Engineering
University of Nevada, Las Vegas
2006

Bachelor of Science, Mechanical Engineering
University of Nevada, Las Vegas
2005

Bachelor of Science, Applied Physics
University of Nevada, Las Vegas
2005

A dissertation submitted in partial fulfillment
of the requirements for the

Doctor of Philosophy in Engineering – Mechanical Engineering

Department of Mechanical Engineering
Howard R. Hughes College of Engineering
The Graduate College

University of Nevada, Las Vegas
December 2016

UNLV | GRADUATE COLLEGE

Dissertation Approval

The Graduate College
The University of Nevada, Las Vegas

November 16, 2016

This dissertation prepared by

Robert James O’Brien

entitled

Radiation Therapy and Dosing Material Transport Methodology

is approved in partial fulfillment of the requirements for the degree of

Doctor of Philosophy in Engineering – Mechanical Engineering
Department of Mechanical Engineering

William Culbreth, Ph.D.
Examination Committee Chair

Yitung Chen, Ph.D.
Examination Committee Member

Woosoon Yim, Ph.D.
Examination Committee Member

Brendan O’Toole, Ph.D.
Examination Committee Member

Steen Madsen, Ph.D.
Graduate College Faculty Representative

Kathryn Hausbeck Korgan, Ph.D.
Graduate College Interim Dean

ABSTRACT

A technique is examined here that utilizes high energy beta decays from a short lived radioisotope to treat medical conditions such as shallow cancerous lesions. A major benefit of beta particle interaction in tissue is a fixed penetration depth for the charged particle, with dose limited to the ultimate range of the beta particle. This method improves on some current techniques of radioactive brachytherapy, where "seeds" are placed inside patients through temporary or permanent implantation in order to kill cancerous cells or inhibit growth of tissue. The use of low energy gamma-rays is the most common method of treatment currently for brachytherapy, with Ir-192 used in most high dose rate procedures. The 73.8 day half-life of Ir-192 means frequent replacement and the requirement to deal with the logistics of constantly decaying, fixed radioactive sources.

This method instead utilizes the short 14.1 second half-life of indium-116 to quickly deliver dose to a treatment area while decaying to a stable ground state. Since the isotope is very short lived, pumping is used to transport the isotope in a room temperature liquid eutectic between the “activation site” where the In-116 is created, and the “application site” where it is allowed to decay over a target area. In-116 is produced at the activation site through neutron capture on the stable isotope In-115. This radioactive In-116 is then pumped through a sealed, closed loop system using a peristaltic to an application site where it is allowed to decay for one minute, enough time to pass through over four 14.1 second half-lives and reach a stable ground state. This applicator is a sealed spreader surface with a thin barrier to allow passage of the decay betas. The loop is then repeated with the In-115 activated again and pumped.

This work examined the feasibility of this method with three types of neutron sources including a fixed Pu-Be source, a Dense Plasma Focus pulsed fusion neutron source and an X-Ray producing accelerator using photoneutrons from a beryllium target. Radiation transport modeling was used to determine the efficacy of this technique on two higher output neutron sources, including the use of a standard clinical accelerator used for external beam therapy, the Varian Clinac 2200C. Neutron output from the Clinac was modeled based on photonuclear production in the accelerator components when operated at 20MeV. Dose outputs were found to be viable for clinical use when the system is used on a Clinac due to the substantial photoneutron output.

In addition to therapy, this work demonstrated the ability to measure neutron fluence at a remote location by measuring decaying In-116 from the eutectic after irradiation. In particular, this was demonstrated with the pulsed DPF source and compared with existing yield measurement techniques. The yield of neutrons from pulsed sources can be difficult to measure due to the intense and brief burst, preventing the use of normal radiation detectors that measure radiation over time. Pulsed sources instead require activation of materials to create a signature of the yield magnitude which is then counted after the pulse. This method showed excellent agreement with an existing method of beryllium activation detection.

ACKNOWLEDGMENTS

This work would not have been possible without the support and encouragement of both my advisor and committee members during the course of my entire education and my coworkers over the past decade. I’d like to thank my advisor Dr. William Culbreth for his constant support and insights during both my doctoral and master’s thesis work. He constantly encouraged me to continue and finish with this research despite my constant distractions at work. Next I must thank Dr. Daniel Lowe, both a coworker and friend since undergraduate days, for his help in data acquisition for this project. Critical data for this work would not have been possible without his assistance. I’d also like to thank Dr. Chris Hagen and the entire dense plasma focus crew including Steve Molnar, Larry Robbins, Dennis Dalley, Al Mitlyng and Tim Meehan. I could not have asked for a better crew to work with at the DPF for the past decade. Thanks to Dr. Trevor Wilcox for constant MCNP and parallel processing support over the years. I also must thank my committee members Dr. Brendan O’Toole, Dr. Woosoon Yim, Dr. Yitung Chen, and Dr. Steen Madsen. Not only were they dissertation committee members but I’ve had the pleasure of being a student of theirs from undergraduate to graduate classes. Special thanks to Matthew Hodges for his assistance with the accelerator model. I’d also like to apologize to my poor dog Fi for missing many walks during the final days of finishing this work.

Finally, and most importantly, I’d like to thank my family for their unwavering belief that I would finish this work. Thank you to my parents for their support through my entire education and constant encouragement during dire times when this dissertation seemed in peril of being left unfinished!

TABLE OF CONTENTS

LIST OF TABLES

LIST OF FIGURES

CHAPTER 1

INTRODUCTION

Despite being originally developed as a method of delivering radiation dose in a therapeutic capacity, this work evolved to also target an additional application in the field of radiation detection. While both applications of this method, radiotherapy and detection, utilize a similar system of material activation and transport, their ultimate uses are distinctly different and warranted the inclusion of several sections that are unique to one application or the other. The physical activation, transport and application of the activated isotope along with the theory, modeling and experimental testing are the same for both concepts and so those sections are combined whenever possible. Descriptions of theory and results specific to each possible application are described separately.

1.1 Background - Radiotherapy

Treatment methods for cancer using radiation therapy have been in use since 1896 when X-Rays were first reportedly used to treat cancer [1]. This treatment was just months after Roentgen first discovered how to produce X-Rays in a laboratory setting without the use of radioisotopes. The ability to treat parts of the body inaccessible to traditional surgery has led to the widespread adoption of additional forms of radiation therapy, each method taking advantage of the properties of differing types of radiation. Radiation therapy today utilizes everything from X-Rays, electrons and protons, to the emerging use of neutrons, heavier nuclei such as helium or carbon [2], and exotic particles like muons [3]. Proton therapy for the treatment of prostate cancer, which has only recently become accessible to most patients, was first proposed for use in cancer therapy in 1946 [4]. While the usefulness of radiation in destroying cancer cells has been apparent for quite some time, an increased understanding of radiation effects and rapid technological advancements have led to safer, more targeted and effective use in treatments. Patients now have broad access to radiation therapy as the technology to both produce and deliver the radiation has been making steady advances.

Radiation treatments can be generalized into either external or internal delivery methods, depending on how energy reaches the targeted area. External delivery requires that the radiation be produced outside the body and is the method by which a majority of the previously mentioned radiation types are applied. Most of these sources of radiation are produced through accelerators or high energy gamma ray emitting radioisotopes. Internal delivery of radiation is typically known as brachytherapy, derived from the Greek word “brachys” meaning short in reference to distance. Radiation applied in this manner has a short range in tissue to avoid depositing energy outside the targeted area. Brachytherapy consisting of the insertion of an actual radioisotope into or near a cancer tumor was first proposed in 1901 with the use of Radium isotopes [5]. This method of treatment has advanced in the current day to the use of multiple types of radioactive isotopes to deliver a targeted dose to a tumor when a localized dose is preferable to external radiation therapies. The placement of a radioisotope inside or in close proximity to a tumor often spares surrounding tissue, and a recent 2012 study has shown that external beam X-Ray therapy and brachytherapy have offered similar outcomes for prostate cancer treatment with brachytherapy costing hospitals substantially less than X-Ray therapy [6]

Brachytherapy utilizes isotopes that decay with known emissions of low to medium energy gamma-rays and high energy electrons, and this decay radiation is used to treat tumors rather than using artificially generated X-Rays or electrons from an accelerator as is typical in external beam therapies. X-Rays and gamma-rays, while both referring to high-energy photons, are typically used to describe ionizing photons emitted from the electron shell and photons emitted from the nucleus, respectively. While X-Rays emitted from the electron shell possess lower energies than gamma-rays emitted from the nucleus, artificially created accelerator based X-Rays emitted in the bremsstrahlung process can greatly exceed electron-shell X-Rays. This work will follow this naming convention with gamma-rays referring to nucleus emitted photons and X-Rays referring to both electron shell and accelerator bremsstrahlung produced sources.

Traditional high dose rate (HDR) brachytherapy involving the use of a radioactive source has been an effective but involved process. The HDR brachytherapy procedure uses a physical, constantly decaying radioactive source that is placed directly adjacent to cancerous or other tissues that are targeted for treatment, allowing decay radiation to damage and kill the tissue. HDR therapy is generally defined as a dose rate of at least 12 gray per hour (Gy/hr) with a gray being a unit of radiation dose equal to 1 joule/kilogram of energy deposition. In comparison, a low dose rate (LDR) therapy is 0.5 to 2.0 Gy/hr and is typically used for permanent or semi-permanent implantation of radioactive “seeds” [7]. Both HDR and LDR therapies have enabled hospitals and clinics to provide outpatient treatment for patients since dose can be delivered quickly in as few as four treatments with HDR or a single implantation procedure with LDR, compared to 20 or more clinical visits with external beam X-Ray therapy [6].

An effective HDR brachytherapy treatment must deliver radiation dose quickly since the procedure involves surgical application of catheters to allow a radioactive isotope to be placed in close proximity to the treatment volume. Several catheters are inserted near the treatment site and the radioactive material is inserted using remote handling into each catheter at intervals corresponding to the desired dose. This process of source insertion using a shielded system that is remotely operated is known as remote afterloading, and has been in use since the 1960's. This system does not require a doctor or therapist to handle or manually insert the source and spares support personnel from unwanted dose [7]. HDR afterloading treatment rooms require substantial shielding and safety interlocks, on the order of 18 inches or more of concrete compared to LDR treatment rooms which can often be performed in existing retrofitted X-Ray rooms.

Candidate isotopes for use in both HDR and LDR procedures must possess half-lives of at least several days since they cannot be produced on site and must be shipped to treatment clinics and hospitals after being produced in reactors or accelerators. The shortest half-life used for permanent implants is gold-198 (Au-198) with a half-life of just 2.7 days. These isotopes therefore must be manufactured continually and quickly shipped in order to be utilized in treatments. A traditional isotope used for HDR therapy, iridium-192 (Ir-192) has a half-life of 73.8 days and requires replacement three to four times a year at an annual cost of up to $15,000 as of 1993 [8]. Additional complications arise from the issue of dealing with shipping and receiving of these isotopes which must be shielded during storage in between patient treatments. These very active sources require remote handling procedures at the treatment site to prevent unwanted dose to therapy personnel [9].

Treatment plans for patients must account for the continuously weaker source used in HDR brachytherapy as the isotope decays between treatments. As is the case in treatments using the common isotope Ir-192, with a half-life of about 74 days, the intensity of the source is cut in half every ten weeks and procedure times must therefore increase in duration by an inverse amount in order to deliver an equivalent radiation dose. Because of this continual decay, the Ir-192 seeds used are replaced every three to four months to maintain a high dose rate delivery system [10]. Isotopes with longer half-lives such as ruthenium-106, Ru-106, with a half-life of over 1 year do not require replacement as frequently but still require twice as much treatment time after one half-life has passed. Ru-106 requires replacement if a sufficient dose delivery rate over time can no longer be maintained, especially if a high dose rate is required for cancer cell control or if a short procedure time is required. Replacement costs and complexity can quickly add up as the sources have a fixed limited shelf life, whether or not they are being utilized in treatments.

Because radioisotopes are not typically produced onsite at treatment locations, isotopes with half-lives sufficiently long to survive shipping and transport must be used. In contrast, half-lives must not be exceedingly long since the isotopes must also decay quickly enough to deliver radiation dose in a desired amount of time. Additionally, a longer lived isotope also requires a larger mass of isotope to deliver dose due to a reduced specific activity (activity per unit mass) compared to shorter lived isotopes, placing an upper limit on half-life since large masses become non practical for clinical use. Longer lived isotopes used in brachytherapy include cobalt-60 (Co-60 half-life 5.27 years) and cesium-137 (Cs-137 half-life 30.08 years) with source diameters up to 6-8mm. These sources are used in LDR, MDR (medium dose-rate) or intracavity irradiation where source diameter is not as critical. The shorter lived Ir-192 sources have diameters down to 0.59mm [8], small enough for usage in 20 gauge needles, and can be used for size restricted intraluminal applications, or uses of the source in small openings like vessels and organs. This dual requirement for quick dose delivery and small source size makes very slow decaying isotopes impractical for brachytherapy use. These two conflicting needs for an isotope that can both survive shipment while still providing fast dose delivery places a half-life time window around useful brachytherapy isotopes and greatly limits the potential candidates for therapy. The most common isotopes in use for brachytherapy are typically constrained in half-lives from 2.7 days for Au-198, used in seed implantation, to an upper end of 30 years for Cs-137 used in LDR procedures [7]. This window of useful half-lives is illustrated below in Figure 1.1 with comparative isotopes including potassium-40 (K-40) and carbon-14 (C-14), two isotopes present in organic matter. By contrast, In-116 is an order of magnitude shorter lived than Au-198.

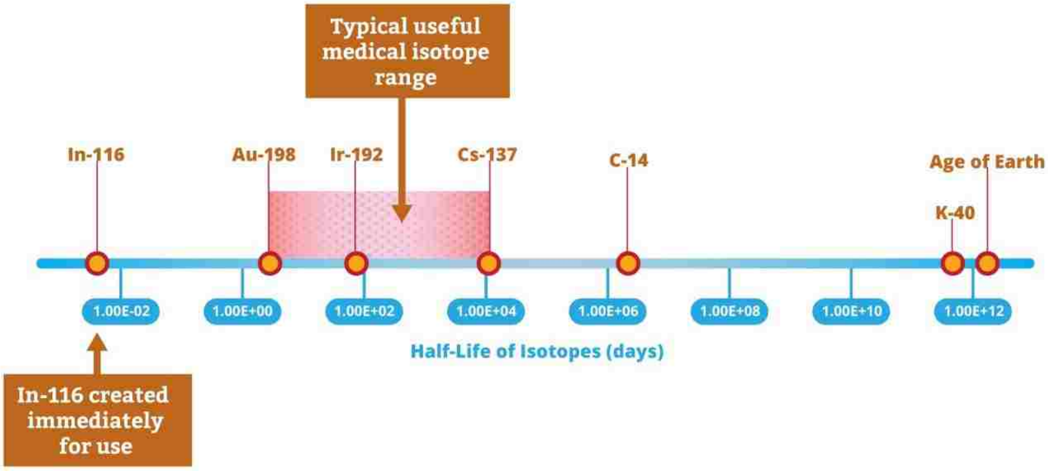

Figure 1.1 Half-life comparison for medically useful brachytherapy isotopes (highlighted region).

This half-life window also limits the type of decay radiation that can be used in treatments to gamma-ray emitters with a few exceptions. While electrons may be superior to x-rays in many applications, isotopes with at least a several day half-life tend to emit lower energy beta decay radiation with energies on the order of or less than 1 MeV . These low energy betas are not useful for treatments due to their limited range in tissue. A rough range estimate for electrons in tissue is energy in MeV divided by 3 or 4 resulting in a depth in centimeters at which percent depth dose is 80 to 90% of maximum dose, respectively [11]. Using this rule of thumb an accelerator produced mono-energetic 6MeV electron beam would deliver a depth dose line of 80% at 2cm, making electrons useful for shallow treatments in patients. With most beta decay isotopes emitting electrons below 1MeV, gamma-ray emitters of several hundred keV are instead used since these allow sufficient tissue penetration in addition to these types of isotopes possessing a sufficiently long half-life to be useful after shipping. For an isotope with pure beta emission to be useful in brachytherapy, high energy decay electrons (greater than 2 to 3 MeV) are required that can penetrate a distance of at least several millimeters in tissue to provide a targeted dose to a shallow depth. Since electrons interact continuously with tissue due to their negative charge, they have a finite range and never deposit dose beyond a cutoff distance that is dependent on their energy. The maximum range for beta decay electrons in any material can be determined by equation 1.1:

$$Range_{max}\left(\frac{cm^2}{g}\right) = \begin{cases} 0.412 * E_\beta^{1.265-0.0954*\ln(E_\beta)} & 0.01 \leq E_\beta \leq 2.5MeV \\ 0.530 * E_\beta - 0.106 & E_\beta \geq 2.5MeV \end{cases} \qquad 1.1$$

with E_β the electron energy in MeV and maximum range in units of cm^2/g, allowing range to be computed for any density of material [12]. A 3MeV end point decay beta in tissue, for example, with density $1.0g/cm^3$ has a maximum range of 1.48 cm or 14.8mm. This results in tissue beyond this depth being spared any radiation dose.

Gamma-rays, on the other hand, interact probabilistically along their path length, sometimes depositing all of their energy in the first interaction, scattering several times and depositing energy in random locations, or occasionally passing straight through tissue with zero interaction. If critical structures are to be spared, the use of electrons ensures that no dose is deposited by the electron beyond a certain depth.

In theory, the ideal therapy isotope would emit high energy electrons that possess enough penetrating potential, on the order of several MeV, to treat tumors and lack gamma-ray emissions that would travel beyond the desired treatment volume. This isotope would also have a high enough specific activity to deliver dose in a reasonable amount of time, but not decay too quickly to be used. One isotope partially satisfying these requirements in current use is Ru-106 (and associated daughter product Rh-106), with a peak beta emission energy of 3.541MeV and a half-life of 372 days. A beta decay spectrum of this energy, averaging 1.5MeV, can deliver effective dose to treat tumors down to more than 4mm in depth, while sparing deeper tissue. This isotope has been in use for quite some time and has seen increasing use for treatments of shallow intraocular tumors [13] of the eye where short range of energy deposition is critical. A long half-life of 372 days means that specific activity is reduced and treatments typically require that the source be temporarily implanted in the eye to deliver dose over several days due to a low dose rate**.** No pure high energy beta emitters with a half-life less than Ru-106 are currently in use for therapy since a majority of energetic pure beta emissions occur with short half-lives on the order of hours or less. While isotopes with a much shorter half-life would allow quicker dose delivery of the beta radiation and a simplified treatment, production and transport to the clinic or hospital for onsite use is not possible since most of the isotope would have decayed during transportation. Even traditional therapy isotopes like Ir-192 and Cs-137 require expensive production infrastructure and are created in large accelerators or nuclear reactors, making on-site production impractical.

An illustration of the challenges in the medical community's dependency on manufacturing and shipping infrastructure for medical isotopes is the recent disruption to supplies of technetium-99m, or Tc-99m. This isotope is critical to the medical diagnostic field for its usage in myocardial stress tests. Tc-99m is a daughter product of molybdenum-99, Mo-99, with half-lives of 6 hours and 66 hours, respectively. Mo-99 is produced in only a few nuclear reactors around the world and then immediately shipped to facilities for use. None of the Mo-99 used in the US is produced in domestic reactors with 100% of the supply coming from outside the country. With a 2.75 day or 66 hour half-life, Mo-99 must be rapidly transported to customers and used before decay eliminates medical effectiveness. Any temporary interruption in the production at the reactors creates an instant supply shortage within days. With around 9 million of these procedures performed every year in the US, a reactor outage for just a few days creates significant issues for the healthcare system [14]. Mo-99 is a unique case in that it is produced through the intentional fission of highly enriched uranium-235 (U-235) foils, a heavily regulated material, and is not produced in any US reactors despite a high volume of use in diagnostic imaging. A main source of Mo-99 from Canada, the NRU reactor at

Chalk River, is scheduled to eventually cease production which is driving demand for alternatives to the current method of U-235 target materials as a source [15]. Many therapy isotopes, including Ir-192 and Au-198, are manufactured using neutron capture on stable metals, making their production subject to less regulation and expense compared to Mo-99. Longer half-lives for therapy isotopes like Ir-192 and Cs-137 also reduce the dependency on a continually renewed supply and can withstand short disruptions in supply. Nevertheless, radiation therapy clinics remain dependent on an external manufacturer for delivery of their isotopes.

Even with a reliable supply of manufactured therapy isotopes, rapid decay of isotopes during transport to the treatment facility still prevents the use of very short half-life isotopes, eliminating the possibility of using potentially superior decay radiation properties. This lag time between production and use means that if short lived isotopes are desired for treatment or diagnostic applications, they must be produced on site or in very close proximity to the application location. Short lived isotopes that can only be produced in a sufficient quantity in nuclear reactors or that require large accelerator infrastructure have severely limited practicality and are not feasible for clinical use. This limits the use of short lived isotopes to those that can be produced on site with a cost effective method such as a small accelerator.

1.2 Summary of the Current Work - Radiotherapy Application

The ability to produce a radioactive isotope on-site at a clinic has been hampered by the traditional requirements of a large accelerator or nuclear reactor to either transmute an isotope or for production through fission products. If instead a radioactive therapy isotope could be produced with a neutron source directly at a clinic or hospital site and immediately used for treatment, the potential number of elements to be used for treatment or imaging procedures increases dramatically. Neutron production technology is advancing rapidly with sources becoming more compact and higher yielding. Additionally, existing accelerators that produce high energy X-Rays for external beam therapy (EBT) are already in use at most radiation therapy clinics. These existing units possess sufficient electron/photon energy to produce neutron fields [16] and can actually be optimized to produce even more significant neutron fields, a normally unwanted byproduct in high energy X-Ray use. These fields can be utilized in the activation and immediate pre-treatment production of medical isotopes. Therefore the potential exists for the production of a medically useful isotope onsite at therapy locations using either new, compact neutron production technology or existing infrastructure.

An ideal candidate for radiation therapy to tissues of shallow depths emits a pure high energy beta spectrum. Therapies that currently use or could benefit from energetic beta radiation treatment include shallow eye lesions [17] and intravascular brachytherapy [18] where radiation dose is restricted to depths of only millimeters. With the brachytherapy placement of sources in multiple locations using small needles in HDR treatments, even larger tumors can be targeted with short range beta particles. A pure beta spectrum removes the unwanted dose delivered by gamma-rays which can travel great distances through a patient. High energy means a minimum of several MeV, providing these betas enough penetration capability to reach tissue depths of several millimeters and making them effective for tumor and lesion treatments. This ideal therapy candidate also should decay rapidly to a ground state, allowing it to quickly deliver dose to the target tissue and then require zero shielding in between patient treatments, unlike traditional therapy isotopes. It should not decay so rapidly, however, that it decays away before moving from onsite production to the patient. Finally, this isotope should reach sufficient radioactive levels when exposed to a neutron source of moderate intensity, such as what might be possible to achieve with a small accelerator in a hospital or clinic setting. When dealing with neutron interactions the cross section, a unit of area, is used to quantify the probability of an interaction taking place. Therefore this candidate isotope must have a high activation cross section, or probability of capturing a neutron, when exposed to a neutron source.

An ideal candidate matching all of these qualifications is an isotope of indium, In-115. This metal exhibits several properties that can be capitalized on for dose delivery in tissue. First, the activated isotope of indium, In-116, is a nearly pure beta emitter, decaying by beta emission in 99.977% of decays. This decay process is almost completely beta emission as only about 2% of these decays result in the emission of an associated gamma-ray. Additionally, the beta decay process emits a single high energy beta in 99% of beta decays with a maximum end point of 3.274 MeV [19] and an average energy of 1.365 MeV , penetrating tissue to a depth of more than 9mm [20]. This single emission of a beta particle makes dose calculations substantially easier and the small fraction of gamma-rays, in only 2% of emissions, greatly reduces dose to surrounding tissues. Additionally, this isotope quickly decays to a stable ground state of tin (Sn-116) with a half-life of only 14.1 seconds. This short half-life means rapid transport from an on-site production location to the patient is possible and quick dose delivery to the patient. Fast decay also eliminates the need to shield the indium both before and in between treatments. Finally, In-115 exhibits an excellent neutron capture cross section, with strong resonance regions in the thermal range where the probability of capture is even higher. In fact, this high probability of neutron capture is often used to quantify neutron fields with indium foil activation being a common method of measuring neutron energies and fluences at reactors, accelerators and medical facilities [38].

The isotope of indium chosen here as a candidate for therapy, In-115, is a 95.71% component in natural indium. The only other stable isotope of indium, In-113, makes up the remainder at 4.29%. This high natural weight percent of In-115 provides a major additional benefit in that indium can be used in a natural form without the need for isotopic separation, a costly procedure used to "purify" elements into their isotopic constituents. Neutron capture on the minor isotopic component, In-113, produces In-114 with a half-life of 71.9 seconds and decays by beta emission with an endpoint energy of 1.99 MeV and average energy of 778 keV. A single rare gamma is associated with this decay in only 0.139% of decays. Neutron capture on In-113 for thermal neutrons are also one order of magnitude lower than that of In-115, making the fraction of activated In-114 less than 0.5% and its contribution to dose negligible.

Indium in a pure form exists as a metallic element with a relatively low melting point of 157 degrees Celsius. In a metallic form, indium is very soft and malleable making it common for use in manufacturing and the low melting point makes it a common addition to solder [39]. Solid indium could be irradiated in a neutron field, producing In-116, and then moved to a treatment site to be used in a similar fashion to traditional brachytherapy sources. However with a half-life of only 14.1 seconds this process would need to happen quickly for the In-116 to remain useful.

This work investigates a novel method of applying the activated indium beta decay to a treatment site by rapid creation, transport and flexibility in application to treatment sites by using a very unique form of indium in a liquid at room temperature eutectic mixture. When mixed with the elements gallium and tin, indium forms a eutectic mixture that does not solidify until -19 degrees Centigrade [40]. This mixture consists of, by weight percent, 68% gallium, 9.5% tin and 22.5% indium [41] with a density of 6.44g/cc and creates great flexibility in how the indium can be irradiated, transported, and applied to the treatment site. This eutectic mixture is often marketed under the commercial registered trademarked name Galinstan® as a portmanteau of the components gallium, indium and stannum (Latin for tin), and is generally considered non-toxic to humans [42] and relatively inexpensive at $2 to $3 a gram in small quantities. Since it is generally considered safe for humans Galinstan® is being used as a mercury replacement, especially in thermometers for the healthcare industry [43]. The mixture will generally be referred to as the eutectic or an abbreviation as GaInSn in the work if not referred to by its trademarked name.

Through the use of a liquid metal transport mechanism, the indium can then be transported from the neutron source to the treatment site by pumping the mixture through non-metallic tubing and connections. This allows the patient to be protected from the neutron source while still allowing quick transportation of the activated indium to the treatment site. Additionally, a liquid carrier for the indium means that custom application shapes can be applied and treatment is no longer limited to a physical seed which is moved into place temporarily and moved incrementally to create a dose distribution. This flexibility to spread out the activated isotope opens the possibility to use the indium in the treatment of larger surface area lesions, like skin cancer, by applying radiation to the lesion using custom shaped applicators that contain the mixture but allow radiation to pass into the target area. The system examined here is a closed loop system, and the indium containing eutectic is re-circulated to be activated again after decay. To allow the decay beta particles to reach the treatment area, a thin window applicator is used to reduce attenuation of the energetic electrons while still containing the indium mixture. A conceptual outline of this process is illustrated in Figure 1.2. Despite the flexibility of using GaInSn, a major challenge that must be dealt with is the corrosiveness of the mixture to metals. Galinstan cannot be stored, transported or placed in contact with metallic elements as the mixture will quickly corrode and dissolve the metal. This presents the unique challenge of using completely non-metallic components for the containment and transport of the mixture, including pumping mechanisms.

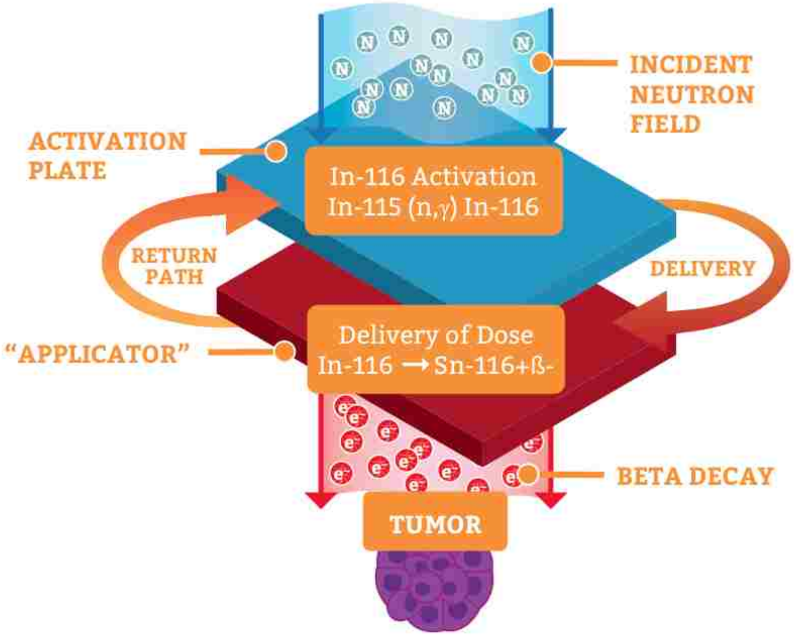

Figure 1.2 Conceptual design of the In-116 activation and dose delivery system.

The work presented here demonstrates the feasibility of such a system and provides models of the effectiveness of this method for the possible treatment of cancerous tissues and lesions. These models consist of both Monte-Carlo radiation transport predictions of activation efficiency and dose delivery using GaInSn activated by three types of neutron sources, and also examines analytically based predictions of the liquid transport system. Physical testing results and dose measurement using actual neutron sources are also presented and analyzed for two of the neutron activation sources. Dose to actual human tissue is predicted based on experimental results with radiation detectors. Finally benefits and challenges of each possible combination of neutron source and activation/delivery mechanism as a clinic treatment method are examined.

1.3 Summary of the Current Work - Radiation Detector

In addition to use in the medical field as a radiation therapy method, a potential use for this technique emerged based on how neutron activation in the material is quantified.   The goal of keeping the activating neutron source and the decay beta source isolated from each other for patient safety translates to this technique also being used to measure the neutron output from a neutron source at a distance. A direct relation between the activating neutron fluence and the resulting beta particle decay emission can be determined with knowledge of the flow properties of the system and the time of irradiation. Using measured irradiation time, flow rate, and beta decay on a detector the original neutron source activity can be determined. This system features a method of placing an activation material, indium in this case, near the neutron source and subsequently transporting the activated material to a detector which can be placed outside of any shielding or obstacles and have no need for electronic components near the neutron source.

The ability to place a radiation detector remotely from the data acquisition or analysis location has several uses in the nuclear power industry including the placement of a probe within a reactor core where space is at a premium and high neutron fluence can quickly damage most traditional detectors. Additionally, a probe such as this can be used in waste mitigation areas like the Hanford superfund site location where cleanup crews need to determine activity and contamination inside pipes and vessels used to house waste. These locations can require that radiation probes travel long distances in confined areas that are difficult to access. In potentially the most beneficial application of the system, a detector making use of a probe with activation material and no electronics near the probe point can be placed near pulsed radiation sources that emit large amount of electromagnetic interference (EMI) in addition to radiation. Application of the system in this type of environment was demonstrated in this testing when used with the Dense Plasma Focus pulsed neutron source.

Current radiation detectors used in harsh, high radiation environments like waste mitigation areas or inside nuclear reactors have typically relied on gas filled detectors due to their ability to utilize gamma-ray discrimination and withstand high fluence rates without damage. These detectors use ionization and collisions with gas molecules by radiation particles, and recombination of the gasses subsequent to detection preserved their ability to detect radiation. Gas filled detectors also offer resistance to transmutation, or the conversion of the atom to a different isotope when impinging radiation changes a proton or neutron in the nucleus. High radiation areas are typically limited to gas detectors due to the effects of radiation on solid detectors. Scintillation detectors, that utilize solid materials which convert radiation to light, are often susceptible to damage from neutron fields and also have trouble distinguishing gammas from neutrons. Neutron activation materials can be used which take advantage of intentional transmutation of the atoms in the material, in contrast to the damaging effects this transmutation causes in most solid detectors. Activation materials must be placed manually and then retrieved and counted on a remote detector every time a measurement is to be made, and continuous measurement is not possible.

The current system solves the issue of placing and retrieving activation materials by containing the activation isotope in the transported liquid medium. With an on demand movement of activation materials, continuous measurements can be made and meet an important need in reactors for tracking radiation fields and neutron fluences over time. In contrast to using the neutron source to induce radioactivity in the GaInSn for production of decay betas for medical use, the decay betas are instead used to infer the amount of neutrons intersecting the material near the neutron source. This can be accomplished by a well characterized system with known flow properties and irradiation times. Of particular interest is the use of this system with a pulsed neutron source like the DPF. The DPF, a high output neutron source, also emits strong pulses of EMI which can damage detector electronics. This pulsed source requires that radiation measurement instrumentation be adequately shielded from EMI or placed at a distance from the source of EMI to reduce damage or interference. Because the system needs to be close to the DPF to pump the GaInSn, the detection electronics used to quantify decay betas were placed in an EMI shielded box with the GaInSn mixture pumped through tubing to the source through a copper pipe extension on the EMI shielded box. This setup served the dual purpose of making decay beta measurements for use in medical application while also demonstrating a detection system capable of measuring neutron radiation from a pulsed source. A direct comparison of measured beta decay radiation amounts to a known, independently measured activating neutron fluence is presented here for several DPF shots to demonstrate the ability of the system to be used as a neutron measurement device.

CHAPTER 2

REVIEW OF RELATED LITERATURE

2.1 Traditional HDR Brachytherapy with Iridium-192

Decay radiation from the most popular HDR brachytherapy source, Ir-192, consists primarily of gamma-rays emitted after beta decay of the parent nucleus. Four primary gammas are emitted during this decay with energies of 316keV, 468keV, 308keV and 295keV respectively in order of intensity. The preceding beta decay emits two betas with relatively low end point energies of 669keV and 533keV, which would exhibit a very short range in tissue but are absorbed in the shell cladding material used to seal the source and therefore do not contribute to tissue dose. The associated gamma-rays are therefore the primary radiation used to treat tissue near the Ir-192 seed. While these gamma-rays deposit most of their energy by Compton scattering within several centimeters, they also can travel much deeper than the tumor volume due to the probabilistic interaction of gamma-rays with matter and deposit dose in unwanted areas of the body. Additionally, these gamma rays are a major hazard when the source is in storage or being transported as they must be adequately shielded. Because of these gamma-rays, the source must be remotely handled and stored and shipped in shielded containers.

Ir-192 is produced by neutron irradiation in nuclear reactors, with the stable Ir-191 being exposed to thermal neutrons and transitioning to Ir-192 through neutron capture. Because Ir-192 can be produced from a stable isotope, there are fewer regulatory and legal issues than the production of Mo-99 and Tc-99 which rely on highly enriched uranium foils. Ir-192 can be produced in most high neutron flux reactors. When used for medical treatments, a source typically is activated to 10Ci or more, while industrial sources for radiography are much hotter at 20 to 150Ci [21]. The most common use for Ir-192 is in non-destructive testing, with decay gammas used for radiography in industrial applications to test for flaws in materials and structures.

While the primary application of Ir-192 seeds is for prostate cancer therapy, this isotope is also used to treat breast cancer and some head and neck tumors. These methods use catheters placed into and around the tumor which then follow with the HDR seed being fed into the catheter attached to a wire. These procedures require careful planning and execution, as a stuck or broken HDR source can cause major complications in such a delicate process. Other uses of brachytherapy include the treatment of lesions using rectal, vaginal, intraluminal, and nasopharyngeal applicators. In contrast to HDR, LDR therapy involves the use of permanent implantation of radioactive seeds into tumor regions that slowly decay and deposit dose until they reach a ground state. This method is not hampered by the need for off-site production of isotopes since the lower activity of LDR seeds makes them suitable for shipping.

2.2 Uses of Beta Decay in Radiotherapy

The use of beta decay in radiotherapy has seen more specialized applications than gamma-ray emitters like Ir-192 due to the short range of the charged beta particles in tissue. However, this short range can be an advantage when treatment of shallow lesions requires that dose be delivered quickly with very little penetration beyond the lesion. An example of this is the use of Rh-106 with a 371 day half-life decaying to Ru-106 with subsequent decay by high energy beta emission (3.54MeV endpoint). Rh-106 has been used in the treatment of ocular lesions, like retinoblastoma, and recently for ocular melanoma [23]. In-116 decays offer a comparable beta decay energy to Rh-106.

Studies have also been examining the use of both beta and gamma emitters for use in intravascular brachytherapy. This process uses radiation dose to inhibit restenosis after angioplasty but requires dose to be delivered within a very narrow depth of millimeters. A study found sufficient depth of penetration can be achieved with electrons above an energy of 1MeV [22]. This application of betas to intravascular brachytherapy requires 10-30 Gy of dose delivery.

2.3 Electronic Brachytherapy

A very new and emerging technology that is competing with some uses of radioactive seed HDR brachytherapy is the utilization of small, low energy X-Ray sources. The novelty of these sources are their miniaturized sizes, on the order of 2 millimeters, allowing them to be used in situations where internal application of radiation is desired. Xoft Inc is one of the leading developers of this technology and uses sources that produce 50 keV X-Rays that can be placed inside catheter tubes [24]. This technology is already FDA approved for the treatment of breast and cervical cancers and is also entering widespread use for skin cancer treatments. The use of 50 keV X-Rays means shallow dose deposition, and delivery of 80% of dose within 2 millimeters. Additionally, the small source mimics the HDR brachytherapy method in that it can be placed directly near cancerous tissue. These sources are often marketed as "electronic brachytherapy" which further exhibits their goal of competing with conventional isotope based therapy. A major benefit of this electronic brachytherapy is the lack of isotopes that need to be stored, replaced, and remotely handled. The miniature X-Ray tube is either "on" or "off", and presents no radiation hazard when powered down. Despite these benefits, however, these sources still utilize X-Rays which travel through and deposit dose in the tissue well beyond the treatment volume.

2.4 Current Uses of GaInSn

The applications for metals like GaInSn have expanded as mercury is removed from the market due to health concerns. Favorable physical properties such as remaining liquid above -20C until a boiling point of 2300C provides for a wide range of applications. GaInSn is generally seen as a safe alternative to mercury for common applications such as thermometers and dental fillings [25][26] and is generally regarded as non-toxic and safe to work with [27]. GaInSn and similar liquid metals are also finding applications in more uncommon areas that utilize the liquid nature of the material such as dynamically tunable antennas [28], varying inductors [29], and even for usage in cooling and heat transfer of electronics [30].

Another intriguing new application of liquid metals with direct application to the usage of a eutectic in radiotherapy is the movement and pumping of the material through the process of Magnetohydrodynamic (MHD) pumping investigated at Purdue University [31]. This method utilizes the Lorentz force generated by passing a current through a material while subject to a magnetic field. Major benefits of this method for a material like eutectics include the ability to pump the fluid with no mechanical parts, eliminating wear or corrosion issues. The researchers at Purdue were able to move liquid GaInSn with a cross sectional area of 4mm x 0.5mm at a rate of 10mm/s using a small MHD micro-pump and gold electrodes. This rate is too slow for the current radiotherapy application being investigated involving a short 14 second half-life. However MHD pumping of GaInSn was shown to be feasible and while this micro-pump was not designed for large volumes, the pump could be scaled up to use higher currents and magnetic fields. Challenges facing this work included dealing with significant surface oxidation of the GaInSn which can make pumping difficult. Correspondence with the authors found that further work was awaiting funding and that providing a thin layer of oxidation to reduce wetting and stalling of the eutectic was being considered [32].

2.5 Neutron Detection Methods

In addition to radiotherapy, this work investigates the feasibility of a pumped eutectic based system as a neutron detection method. Neutron detectors are unique in the world of radiation detection and monitoring due to the uncharged nature of neutrons and their weak interaction with materials. Compared to X-Rays and gamma rays that readily interact with the electron clouds of materials, an uncharged neutron can only interact with the nucleus of a material. The small relative cross section of the nucleus makes neutron interactions less probable than interactions that occur with electron clouds. Additionally, neutrons must be absorbed or scatter off the nucleus and result in either emission of a charged particle through decay or physically impart enough energy to a light nucleus that it recoils as a charged particle, such as scatter from hydrogen.

Neutron detection methods can be generally categorized as scatter reactions that rely on the neutron to impart kinetic energy onto the nucleus causing it to recoil or enter an excited energy state, and capture reactions that rely on physical capture of the neutron in the nucleus with a resulting new isotope that then decays or emits a secondary particle. Which method is utilized depends on the neutron energy of interest and whether energy discrimination is desired. Scatter reactions are generally limited to light isotopes, like hydrogen, where a large portion of the neutron energy can be transferred. These are sometimes called proton recoil detectors, although recent work has been done to utilize heavier elements like helium [34]. Inelastic scattering, with a neutron escaping but leaving a nucleus in an excited state, can be used as a threshold reaction since the neutron must have enough initial energy to excite the nucleus into a quantized state. Inelastic scatter has found recent applications in the measurement of fusion neutrons in new test reactors due to an inherent ability to discriminate high energy from low energy neutrons [35]. Capture reactions, on the other hand, rely on the total absorption of the neutron and result in transmutation of the capturing atom to a different isotope with one additional neutron. Sometimes this new isotope is unstable, or radioactive, and will decay be emission of a particle that can then be detected. Helium-3 (He-3), lithium and boron are the most well known elements used for the capture and detection of thermal neutrons in gas, with lithium and boron also integrated into solid detectors.

Modern needs and drives for neutron detector development tend to be for applications in fusion work, both for energy and stockpile stewardship, and for next generation fission reactors. Indium has become a standard neutron activation material for higher energy fusion neutrons due to an inelastic scattering reaction with a 336 keV threshold, thus eliminating contribution from scattered neutrons. Other novel uses of isotopes are being explored including more exotic metals like the use of praseodymium for the detection of neutrons above 10MeV [36]. Researchers are continually looking at hundreds of isotopes that offer various advantages for the detection of neutrons of varying energies. The ideal isotope for a particular application is chosen based on energy, decay time, decay particles, cost and availability/purity of the activation material.

CHAPTER 3

THEORY

3.1 Neutron and Gamma Material Activation Sources/Accelerators

Transforming a stable element into a radioactive isotope requires altering the proton to neutron ratio in the nucleus in order to push the element towards instability. This is often done through the removal or addition of neutrons, both of which cause the isotope to change in atomic weight and become radioactive if the new isotope is outside the range of stability. Methods for adding and removing neutrons include accelerators and nuclear reactors depending on what reaction is desired.

To remove neutrons, a common technique is the use of an accelerator to bombard the target nuclei with high energy protons, electrons or X-Rays. With proton bombardment a neutron is ejected from the nuclei with replacement by a proton, a process abbreviated as a (p,n) reaction, which increases the proton to neutron ratio of the nucleus. Using electrons or X-Rays, ejection of a neutron occurs by overcoming the binding energy of a neutron in the nucleus, a process that also increases the proton to neutron ratio. The use of X-Rays in this method is referred to as a photonuclear interaction and this process favors higher atomic number nuclei, or high Z material, where the binding energy per nucleon is reduced and strong resonances exist that allow emission of a neutron. Because of this process, high energy X-Ray sources sometimes avoid the use of high Z materials like tungsten for shielding to reduce excessive photoneutron production.

In contrast to removing neutrons from nuclei, increasing the number of neutrons in a nucleus is often accomplished through exposure to a neutron field produced by a reactor. Many commonly used medical isotopes are produced in this fashion. Nuclear reactors typically operate in the thermal range with neutron energies averaging 0.025eV. This is advantageous for neutron capture reactions since capture cross sections generally increase as neutron energy decreases, with certain resonance regions exhibiting strong peaks in neutron capture probability. The higher probability for capture of thermal neutrons is due to their low energy, causing them to preferentially capture in the nucleus rather than scatter away or cause ejection of another nucleon, as is more probable for more energetic neutrons. Neutrons that are captured in the nucleus cause the isotope to transition to a heavier state, thus changing the mass number of the element and shifting the isotope towards a higher neutron to proton ratio. This can be repeated as the nucleus captures additional neutrons and transitions further to heavier isotopes.

When discussing neutron interactions, "cross section" becomes a dominant term used to reference the probability that certain interactions will take place. The probability of neutron capture resulting in the emission of a proton, for example, would be presented as the (n,p) cross section in units of barns with one barn equal to an area of $10^{-24}cm^2$. This cross sectional area definition is the projected area of the nucleus for a particular reaction. In reality this is not a physical area since the probability of an interaction can vary greatly with the velocity of the neutron. But reaction cross sections in units of barns are proportional to probability and are used for the calculation of interaction probabilities ranging from millibarns (mb) to megabarns (Mb) [55]. Neutron cross sections are both calculated using theory and measured in the lab for various materials and continually refined by experimenters with results compiled into several international databases. Accurate cross sections are essential to working with and understanding neutron reactions.

The technique of converting In-115 to In-116 investigated here could rely on a reactor neutron flux, but treatments would become prohibitively expensive and complicated since treatments using the short 14 second half-life would be required to take place immediately adjacent to a reactor. Testing has been performed with three types of neutron sources that could potentially be used in a clinical setting including a fixed neutron emitting radioisotope, a pulsed fusion neutron emitting source, and a high energy X-Ray source used to produce photoneutrons.

Activation of In-115 was first tested with a neutron emitting radioisotope source that produces neutrons continuously without the use of accelerators. This semi-permanent neutron source (Pu-Be) is a mix of two metals, plutonium and beryllium. Pu-Be sources produce neutrons when the beryllium metal is exposed to an alpha decay source, Pu in this design. Plutonium-239, with a half-life of 24,000 years, decays primarily through the emission of alpha particles and offers an extremely long useful lifetime. Similar sources of neutrons use other alpha emitting isotopes like Polonium-210 or Americium-241, an isotope commonly found in household smoke detectors. High energy alphas from this decay remove a neutron from the beryllium atom, the (α,n) reaction, resulting in neutrons of a broad spectrum with an average energy of 4.5MeV. While useful as a continuous source of neutrons, this type of neutron source is not practical for clinical use due to the low neutron production efficiency and output, on the order of 10^7 neutrons per second for a typical 2 Curie source. The high expense and overhead of a permanently radioactive source utilizing the (α,n) reaction on Beryllium relegates these (α,n) neutron sources to the research lab.

Pulsed neutron sources are more practical than (α,n) sources for use in a clinical application. Commercially available pulsed sources, often referred to as "sting tubes", produce neutrons from the fusion reaction of the two heavy isotopes of hydrogen, deuterium and tritium. These sources are commonly used in the oil and mineral industries for exploration purposes, produce higher neutron outputs than (α,n) sources and can only produce radiation when powered on. A typical deuterium fueled sting tube produces on the order of 1.5×10^7 neutrons/sec/cm^2 while a deuterium and tritium fueled tube produces approximately eighty times more neutrons, up to 1.2×10^9 neutrons/sec/cm^2, due to the higher fusion cross section for deuterium and tritium gases [33]. The commercial availability and competitive price of these sources makes neutron sting tubes a potential candidate for use in this application.

The third potential neutron source for providing sufficient In-115 activation are high-energy X-Ray producing linear accelerators, or LINACS, that are commonly used in external beam cancer therapy. In addition to electrons and X-Rays, these accelerators can be utilized as a source of neutrons to provide the required activation of the indium based treatment material. Rather than use the high energy X-Rays produced by the accelerator for dose delivery to tumors, secondary photo-neutrons produced through photonuclear interaction of the high energy X-Rays in the accelerator collimator or a specially designed X-Ray target can be used to irradiate the activation material. These neutrons are typically an unwanted side effect in EBT accelerators, and studies have shown that significant neutron fields can be produced in the accelerator head. Liu determined that a

Varian 2100 Clinac, a common accelerator used for EBT, produces upwards of $1x10^{12}$ neutrons at the collimator per Gy of dose delivered with an average energy of 0.49MeV when the collimator jaws are fully closed and the Clinac is operated with an electron energy of 20 MV [37]. Typical clinical units can produce 6 Gy/min of photon dose, corresponding to a production capability of $1x10^{11}$ neutrons/sec. With the collimator fully closed, the high energy X-Rays impinge directly on the high-Z collimator producing photo-neutrons that suffer very little attenuation and exit the collimator while the source X-Rays are almost fully absorbed. Since the binding energy for nucleons decreases as the nucleus becomes heavier, high-Z materials exhibit lower photonuclear thresholds, making them ideal for the production of neutrons by high energy X-Rays. Tungsten, a typical shielding material used in the collimator of a Clinac, will start producing photoneutrons when the X-Ray energy exceeds 6.2MeV, the threshold in tungsten for the Giant Dipole Resonance (GDR) reaction. A modern 2100C Clinac can operate at 20 to 22MeV X-Ray energy easily exceeding this minimum reaction energy. These standard clinical accelerators can produce $1x10^{11}$ neutrons per second by simply closing the collimator jaws with no alteration of the accelerator, providing a substantial neutron field for potential activation of isotopes on site.

When restricted to lower energy accelerators where the threshold for the GDR reaction in the heavy shielding materials like tungsten is not reached, other materials can be placed in the accelerator beam to produce photo-neutrons. Beryllium can be used as an excellent photo-neutron source due to a loosely bound neutron in the nucleus with a threshold binding energy for photo-neutron emission with gammas above 1.7 MeV yielding 2 alpha particles and a neutron as

$$ {}^{9}_{4}Be + \gamma \rightarrow 2 * {}^{4}_{2}He + n $$

3.1

With a threshold of 1.7MeV, the use of beryllium as a source of photo-neutrons in a medium energy accelerator of 6 MV becomes viable as a source of photo-neutrons with more than 2/3 of the emitted X-Rays from the accelerator exceeding the threshold. The use of a 6MV accelerator is investigated here with a beryllium target along with the application of moderating material to further favor the production of neutrons of the ideal energy for activation of indium. These optimizations are examined in the concluding chapters of this work.

3.2 Beta Emission by Radioactive Decay and Associated Radiation

Beta particles are high energy electrons emitted directly from the unstable nucleus of an atom, as opposed to electrons that exist in the electron orbital cloud. This emission of a beta particle occurs when a neutron in the nucleus transitions to a proton or when a proton transitions to a neutron. The charge of the emitted beta particle will be negative during neutron conversion to a proton, known as beta minus decay, or positive during proton conversion to a neutron, known as beta plus decay. Beta plus decay emits a positron, a particle with the same mass as an electron but opposite charge, an anti-particle of the electron. These positrons will annihilate with their electron pairs and emit a pair of gamma-rays. Positron emission is used in diagnostic imaging since detection of the annihilation gamma-rays can be used to locate their origin in the body, a process used in positron emission topography, or PET imaging.

Beta minus decay is most prevalent when an atom contains excess neutrons, with a neutron decaying to move the atom to a more stable state. Atoms can gain an excess neutron through neutron capture, or contain an excess number of neutrons as a result of decay from a heavier element. To move the new unstable isotope back to a more stable neutron to proton ratio, the emission of the beta particle allows the nucleus to gain a proton by conversion of a neutron. In contrast, isotopes that are lacking neutrons can also move to a stable proton to neutron ratio through the emission of a positron as a result of a proton transitioning it into a neutron. This transition can also be achieved through the capture of an electron by a proton, a process known as electron capture. Positron emission is less frequent than electron capture due to energy requirements since the mass of the resulting neutron is higher than the sum of the emitted positron and resulting proton. This excess mass must come from energy in the nucleus as it transitions to a more stable nucleus that has lower total energy.

In the treatment method examined here, positrons are not considered as a potential dose delivery mechanism due to the non-beneficial production of annihilation radiation produced when the positron comes to a stop in tissue. The pair of 511 keV gammas produced in the annihilation of a positron and electron result in unwanted dose to the patient and isotopes that produce this decay radiation are therefore avoided. Throughout this text it should be assumed that references to beta decay are describing the emission of negatively charged electrons rather than positrons. This process of beta decay can be written schematically as

$$ {}_{Z}^{A}X \rightarrow {}_{Z+1}^{\;\;A}Y + \beta^{-} + \bar{\nu} \qquad 3.2 $$

with X and Y the nuclear species, or indium and tin respectively in this study, the negative beta particle $\beta^-$and $\bar{\nu}$ the associated anti-neutrino. The parent isotope X gains in number of protons Z during conversion of a neutron. This process for In-116 decay and beta emission to tin (Sn-116) is represented as

$$ {}^{116}_{49}In \rightarrow {}^{116}_{50}Sn + \beta^- + \bar{\nu} \qquad 3.3 $$

While the process of beta decay generally has a high available energy, up to 10MeV, beta particles are not mono-energetic. The coincident emission of an antineutrino shares the decay energy in a three body reaction, producing a spectrum of beta particle energies rather than a single peak energy as observed with gamma rays. This spectrum is illustrated below in Figure 3.1 for the first metastable state of In-116. A beta particle end point energy of 3.274 MeV corresponds to the total maximum energy, or Q-value, of the decay. This energy is shared by the products of decay in equation 3.3. Products include the daughter isotope tin, the decay beta particle and an anti-neutrino. The heavy daughter nucleus is given negligible kinetic energy, leaving the Q-value to be split among the antineutrino, which does not produce measureable interactions in tissue, and the beta particle. Because of this distribution, mono-energetic emission of beta particles is never possible and dose calculations must account for both maximum beta energies and average energy. In addition to simple sharing of kinetic energy, beta decay energy spectra must also account for energy lost by the beta particle to Coulombic attraction from the positively charged nucleus. The negatively charged beta particle loses some energy during emission and escape from the nucleus, resulting in a drop in emission probability at lower energies. With this effect taken into account, a spectrum for In-116 can be calculated as illustrated in Figure 3.1.

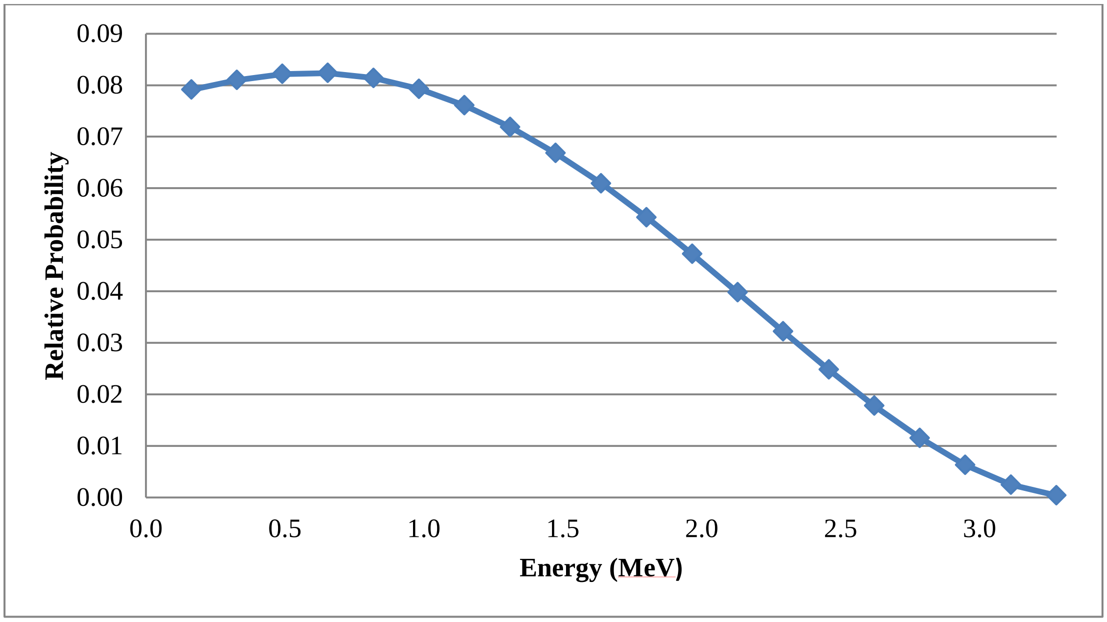

Figure 3.1 In-116 beta decay energy spectrum with Coulombic effects accounted for.

This spreading of beta particle energy into a spectrum results in an average electron energy of slightly more than one-third the endpoint energy, as illustrated previously. Therefore In-116 exhibits an average electron decay energy of 1.365 MeV. This difference between the maximum possible end point energy and the average energy of observed betas limits the number of isotopes that are potential candidates for effective treatment of tumors due to the relatively short range of beta particles in tissue. With a requirement to treat tissue to a depth of several millimeters, only beta emission with end point energies greater than 2 to 3 MeV can be considered for reaching shallow tumors due to the average beta energy.

Beta decay, by either emission of negatively charged electrons or positively charged positrons, is a precursor to gamma emission by the daughter nucleus and these gamma-rays can cause unwanted tissue dose even if the beta decay process fits the criteria for useful average energy and half-life. Gamma-ray emission is the result of an energetic nucleus transitioning to a stable ground state through the emission of photons. A nucleus can be left in an excited state after almost any decay, or it can be bumped into an excited state through absorption of energy. Following beta decay, the daughter nucleus is often left in an excited state and must emit one or more gamma-rays to reach a stable ground energy level. Oftentimes these gamma-rays can be quite energetic, resulting in dose to tissue beyond the treatment volume. Therefore it is beneficial to use isotopes that beta decay into relatively stable daughter nuclei resulting in the emission of few or very low energy gamma-rays.

3.3 Radiation Dose Therapy and Tissue Interaction

In the arsenal of tools that are used to fight cancer, radiation can be an effective method for stopping the spread of cancerous tumors. Energy that is deposited in matter when radiation interacts with the electrons and nuclei of atoms can be used to damage or kill tumor cells. By targeting tumors or lesions with radiation, treatments can sever the DNA strands of cancer cells and stop their spread by inducing cellular death or preventing further division. Current therapy methods utilize several types of radiation including gamma-rays, electrons, protons, neutrons and even more exotic particles like muons. The effectiveness of each type varies with the specific treatment required, but in general the goal of these therapy methods is to deliver as much energy as possible to the target tumor or lesion while sparing healthy surrounding tissue.

The current method investigated here utilizes electrons as a primary method for delivering radiation dose to tissue. Electrons are unique among radiation therapy methods due to their small size and negative charge. The charged nature of electrons means that they interact with the electron clouds of atoms and thus are continuously experiencing the Coulombic effects of the material they pass through. This gives electrons a finite range in materials as they are continuously slowing down, and thus depositing energy, along their entire track length. Gamma-rays, on the other hand, are energetic photons that only interact probabilistically with atoms and have the potential to pass through material without stopping or interacting. Because of this, gamma and X-rays tend to have much longer ranges in materials than electrons and can reach deeper tumors. Conversely, this penetrating nature can cause issues if the tumor is in a shallow area as the gamma-rays will continue through the target tissue and deeper into healthy tissue where they can deliver unwanted radiation dose. High energy X-Ray therapy, in fact, often results in skin side effects at both the entrance and exit side as the X-Rays penetrate the entire body. For this reason, electrons are often chosen instead of X-Rays for shallow treatment areas that are close to the surface, on the order of several centimeters deep.

Current therapy methods that utilize electrons produce them through the use of an accelerator that can provide high energy particles at relativistic speeds. These electrons are rated typically in electron volts (eV), with one eV equal to the kinetic energy that an electron would possess if accelerated across a potential difference of one volt.

Accelerators can produce electrons with energies into the several million electron volt (MeV) range with a 20 MeV accelerator in common clinical usage. With the rest mass of an electron being only 511 keV, electrons with kinetic energy higher than approximately 5 keV are considered relativistic and can no longer be treated with classical mechanics. This 5 keV threshold arises from the rule of thumb that relativistic treatment must be used when relativistic momentum differs from classical momentum by more than 1%. This can be seen by comparing the classical momentum equation 3.4, with momentum p, rest mass of the electron m_e and velocity v to the relativistic momentum equation 3.5, with the addition of the speed of light c:

$$p = m_e v \tag{3.4}$$

$$p = \frac{m_e v}{\sqrt{1 - \frac{v^2}{c^2}}} \tag{3.5}$$

As velocity v exceeds 0.14c, or 14% the speed of light, the relativistic momentum begins to differ from classical mechanics by more than 1% and we must begin to consider the particles relativistic. Equation 3.5 can be expanded on to determine the kinetic energy of a relativistic particle as calculated in equation 3.6:

$$KE = m_e c^2 \left[\frac{1}{\sqrt{1 - \frac{v^2}{c^2}}} - 1 \right] \tag{3.6}$$

With a speed of 0.14c, the kinetic energy of an electron (m_ec^2 equivalent rest mass of 0.511 MeV) that we must begin to consider relativistic effects is calculated to be 5.08 keV. This implies that electrons that are dealt with clinically are relativistic in nature as their energy easily exceeds several hundred keV in order to reach useful depths in tissue.

Electrons entering tissue begin depositing kinetic energy through several interaction methods including direct elastic and inelastic collisions resulting in ionization of atoms, and the emission of bremsstrahlung X-Rays or braking radiation, if they change direction rapidly. However these X-Rays are exceedingly rare in tissue due to the low-Z value. The fraction of decay beta energy lost to bremsstrahlung is proportional to the energy of the beta and the Z of the material according to:

$$fraction_{Bremm} = 3.5x10^{-4}Z * E_{\beta} \qquad 3.7$$

with E_β the beta end-point or maximum energy. Tissue, with a total Z of roughly 10 and an effective Z of about 7.4 leads to a 3MeV beta endpoint decay losing only 0.78% of kinetic energy to X-Rays. Therefore production of bremsstrahlung X-Rays only becomes an issue with higher Z materials and high energy electrons.

How X-Rays and gammas interaction with tissue is dependent on the photon energy with low energy photons depositing a majority of their energy through photoelectric absorption, transitioning to Compton scattering and eventually pair production at higher energies. Diagnostic X-Rays do not typically exceed 120keV, or an average of 40kV, so that a majority of interactions remain in the photoelectric and Compton scattering range. Therapeutic use of X-Rays must operate at higher energies in order to reach a sufficient depth and produce interactions in tissue mostly through Compton scattering. Operating a therapeutic X-Ray beam at energies above 24MeV leads to an increasing amount of pair production, greatly reducing local dose deposition, and so therapeutic X-Ray sources typically do not exceed 20MeV.

The biological effects of radiation are largely due to the presence of oxygen and hydrogen in the body and their effects on deoxyribonucleic acid (DNA) strands when ionized rather than the actual energy deposited by incident radiation. The capability of radiation to ionize these elements is the basis for the distinction between classifying radiation as ionizing and non-ionizing radiation, and their associated effects on DNA. While energetic electrons, photons and neutrons can carry significant kinetic energy, their ability to actually heat living organisms is very limited. For example an electron carrying 1 million electron volts (1 MeV) of kinetic energy, if fully stopped in just a gram of water, would deposit just $1.602\text{x}10^{-13}$ joules of energy in the form of heat. In Kilocalories this would be the equivalent of only $3.829\text{x}10^{-17}$ Kcal and thus require $2.612\text{x}10^{16}$ electrons to raise the temperature of the water by only 1 degree centigrade. Clearly the damaging effects of ionizing radiation on tissue are not due to heating alone.

Instead, the major biological effects of ionizing radiation in living cells are due to the damage caused to DNA by ionized hydrogen and oxygen. Since water makes up the majority of living tissue, there is an abundant volume of these atoms available for electrons produced by incident radiation to interact with. Radiation is considered ionizing when it possesses enough energy to knock electrons free from atoms and therefore break chemical bonds. The threshold for this is generally considered to be above 10eV based on the binding energy of the outer shell electrons in atoms of interest, with hydrogen the primary reference. For the major components of tissue, these binding energies for hydrogen and oxygen are 13.6eV and 41.6eV, respectively [46]. Of particular interest for biological effects, the energy required to break water molecules and liberate a hydrogen ion is slightly higher than a single hydrogen electron ionization at 16eV [47]. Thus X-Rays and radiation particles are always considered to be ionizing as they typically exceed this energy.

Radiation is a very general term for several types of phenomena that carry energy, from photons all the way to neutrons and heavy charged particles. Distinguishing between ionizing and non-ionizing radiation allows us to determine which types of radiation can directly damage living cells. Radiation that does not possess enough energy to remove electrons from their shells, below 10eV, is considered non-ionizing radiation. Longer wavelength radiation such as microwave radiation, radio waves, infrared and visible light are all examples of non-ionizing radiation. These do not carry sufficient energy to dislodge electrons in hydrogen and oxygen and therefore can only damage living tissue through heating and thermal effects. An exception to the inability of non-ionizing radiation to effect tissue is ultra-violet light, with a wavelength in between visible light and X-Rays. While considered non-ionizing since a typical UV photon does not carry sufficient energy to ionize atoms, UV radiation still damages DNA by directly exciting the DNA molecules causing errors and unwanted bonds. This makes UV radiation a major cause of skin cancer though not a viable treatment method for cancers due to its very shallow range in tissue.

Ionizing radiation rarely damages cellular DNA by direct impingement due to the small size of the DNA structure relative to the cell volume. While direct damage does occasionally happen and results in severing of the DNA strand, the more typical reaction is indirect damage to the DNA through the production of ionized hydrogen and oxygen when water molecules are disassociated by the radiation. Energetic electrons are created along the path of the incident radiation, whether it be beta particles gamma rays or other ionizing radiation. These newly created electrons stream through cells producing free radicals, H+ and OH-, by ionizing water molecules along their track length. Most of these hydrogen and hydroxide ions recombine quickly, but those that do not can reach the DNA of the cell and cause damage to the strands.

Damage to the DNA double helix strands are categorized by the severity of the breaks, a single strand break (SSB) or a double strand break (DSB), with the amount of damage from a particular radiation referred to as relative biological effectiveness (RBE) [45]. Each strand in the double helix structure of DNA consists of nucleotides that match a single counterpart nucleotide type on the other strand. Replication of DNA occurs when the strands are split from one another and copied based on this pairing of nucleotides. This means that in the case of a SSB, repairs can typically be made when only a single strand of the double helix is damaged by a radiation created free radical. A DSB with damage to both strands however is significantly more difficult to repair as the split can sever the helix completely. If the strand cannot be recombined, the cell will typically die or suffer mutations during replication.

While all DNA damage is caused by both ionization of water in the cells or direct severing of the DNA by radiation, the efficiency of DNA damage by each type of ionizing radiation varies. Two types of radiation depositing equal amounts of energy in a segment of tissue do not lead to identical outcomes for the tissue. Simple energy deposition in a material, or the number of Joules (J) deposited per Kilogram (kg), is quantified in terms of gray (Gy) with one Gy=1 J/kg. Therefore two types of ionizing radiation with the same kinetic energy that are fully absorbed in a material will deposit the same energy in terms of Gy. However, since cell damage is primarily caused by the secondary reactions in the material such as water ionization and hydrolization, two different types of radiation can result in differing amounts of cell damaging reactions. An electron and a neutron with the same kinetic energy, for example, will differ greatly in the amount of cell damage produced due to how quickly and how locally their energy is deposited.

These differences in the relative biological factor (RBE) are the basis for the quality factor, or QF, which is used to normalize different ionizing radiation types to one another using the dose unit sievert (Sv) and the direct linear conversion of Sv = Gy x QF. Quality factors for various types of ionizing radiation are presented in Table 3-1 based on United States NRC 20.1004.

Table 3-1. Quality Factors for Ionizing Radiation

Radiation Type	**Quality Factor**
X-Rays, Gammas, Electrons	1
Alpha Particles, heavy particles	20
Neutrons (various energies)	10
Protons	10

Radiation with a higher QF results in a higher number of SSB and DSB damage to DNA relative to the energy deposition. This damage to the DNA is what causes cells to die or to cease cell division, and when dealing with cancerous tissue, this cell death or halting of division of the cancerous cells is the objective for control of a tumor. Radiation therapy for control of a tumor is achieved through targeted application to cancerous cells to produce cell death, or enough damage to cancer cell DNA that they cease to divide and halt reproduction. Radiation must be carefully targeted at the cancerous cells and avoid healthy cells as much as possible, since healthy tissue is just as sensitive to radiation damage. Since cell death from DNA damage occurs when the cell attempts to divide, the effectiveness of radiation as a cancer treatment is related to how quickly the cells are programmed to divide. Because of this, cells that are slowly dividing or mature and fully differentiated tend to be resistant to cell death by radiation damage, in contrast to quickly dividing cells which are the most susceptible to death by radiation damage.

3.4 Radiation Transport and Simulation / MCNP

Therapy methods with electrons have been modeled extensively through the years by computer codes considered to be the gold standards for electron simulation for medical physics such as EGS (Electron Gamma Shower) that can quickly and accurately predict the dose that an electron beam will produce. The treatment method being investigated here, however, involves far more complexity than a mono-energetic electron beam incident on a volume of tissue. Rather than production of mono-energetic electrons in an accelerator typically found in the clinic, this method instead utilizes secondary radiation that is produced through the decay of a temporarily radioactive material produced through neutron activation. Additionally, the electrons to be utilized here are distinctly non mono-energetic and not limited to a collimated beam, but rather are emitted in a spectrum of energies from a volume of material. The use of a neutron source to activate an isotope to produce beta decay radiation requires a neutron transport code to predict both the effectiveness of the activation process, or how much of the desired isotope is actually produced, in addition to calculating the dose that is expected from the radioactive isotope. The Monte-Carlo radiation transport code MCNP, developed at Los Alamos National Laboratories (LANL), is used in this investigation due to a comprehensive library of materials with neutron and photon data based on the ENDF B-VI library of cross-sections, a wide range of available particles and energies, and the ability to utilize physics models when ENDF libraries are not available.

MCNP is the latest generation of Monte Carlo transport codes that have been in development at LANL for almost 60 years. The Monte-Carlo method of radiation transport involves transporting one particle at a time through materials configured in geometries specified by the user. MCNP requires the user to build an “input deck” containing the sizes and locations of shapes along with their material composition. A three dimensional model of the desired simulation is constructed, and CAD interfaces are available, allowing users to simulate almost any problem involving radiation transport, from nuclear reactors to planetary scale simulations. In addition to materials and geometries, the user also inputs the type of radiation source or sources and their location. An illustration of the conceptual Monte-Carlo method transport of photons in MCNP is presented in Figure 3.2. Particles are transported statistically from the source in random directions through materials where the physics of each interaction is predicted using tabulated experimental data or physics models. An individual particle is started at the source and followed until it interacts with an atom in some way, where secondary particles or radiation emission is produced, with the original and any secondary particles tracked until they are finally absorbed or when it reaches an area where it is not necessary to track anymore, such as a problem boundary.

.

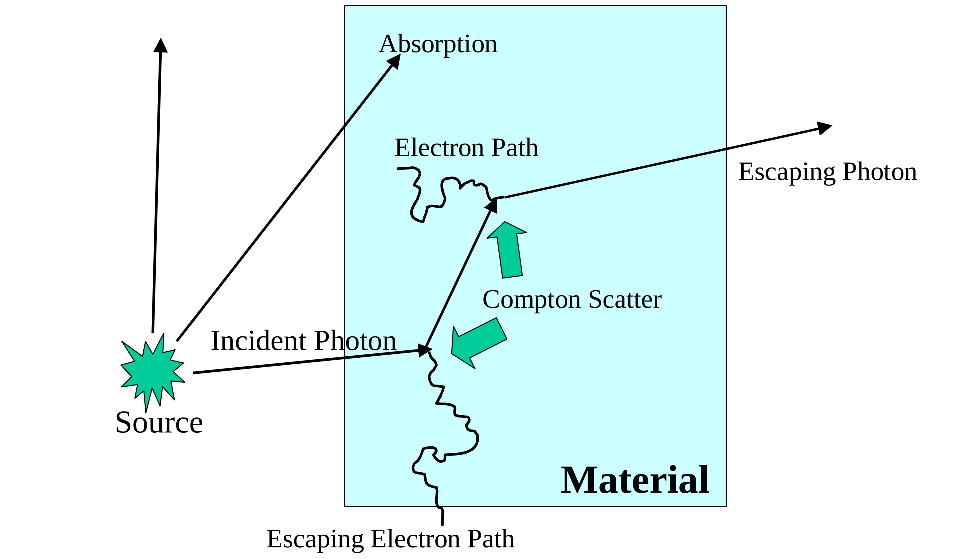

Figure 3.2 Example of MCNP Transport of Radiation Through Materials

The probability of an interaction with materials as the tracked particles travel is referred to as a cross section, described previously. These cross sections are stored in a library for every material in the problem and each interaction of a particle is assigned a reaction based on the cross section probability. Cross section libraries are experimentally obtained values, and if cross sections are for some reason not available for a particular material, then MCNP uses physics models based on theory. Because of this, it is always preferable to have access to cross section data libraries for all materials in a Monte Carlo simulation. Transport of these particles is repeated as many times as necessary to produce statistically reliable predictions in the simulation.

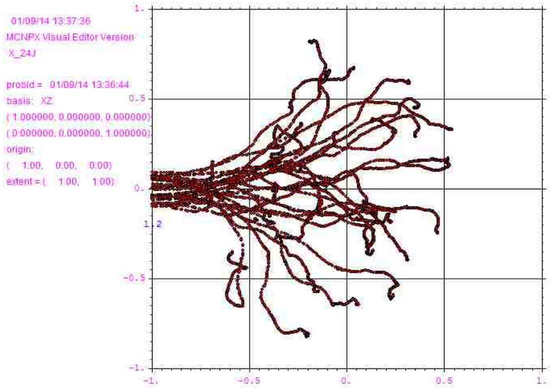

Figure 3.3 Individual electron tracks in an MCNP volume of tissue.

Extremely complex geometries and the transport of billions of particle tracks, often referred to as histories, can be tracked as the memory capacity of computers has continually expanded. Electrons can be very computationally intensive to track, due to their short path lengths between interactions and even a single electron can take a spurious path through a material, as illustrated in Figure 3.3. Entire computer clusters are often dedicated to radiation transport problems as a linear speed up is possible as more processors are utilized on a problem. By transporting a sufficient numbers of particles, MCNP is able to predict how a real system will behave. These features make Monte Carlo methods far superior to analytical calculations and predictions for the effects of radiation in the current work.

3.5 Radiation Detectors

Quantifying the amount of radiation that would be delivered by a source to a patient requires an accurate method of detection. Detection of radiation requires physical interaction of the particle in a detector to produce an effect that can be measured, such as the depositing of energy in a gas or solid material. The earliest detectors used gasses to visualize electrons as they ionized the gas inside evacuated chambers. As discussed previously, physical mediums like film, being reactive to both light and radiation, were used to inadvertently discover radiation and eventually to harness it for applications like medical imaging. Early solid materials relied on the emission of light during radiation interactions in plastics and crystals, a process known as scintillation. Advancements in semiconductor manufacturing have expanded the detection of radiation beyond just gases or scintillation and allowed direct conversion of radiation to electrons in a material, allowing more precise energy information to be extracted. Even with advances in solid material detectors, gas filled detectors are still commonly used with the type of detector chosen depending on the goal of the measurement.

To determine dose, or total energy delivered, a gas is often used in an ion chamber with an applied potential. As a particle crosses the ion chamber, it interacts in the wall or occasionally the fill gas and strips electrons along its path. These electrons then travel along the electric field lines in the chamber along the anode and cathode and produce a current. When this applied electric field is large enough due to a sufficiently high voltage, a cascade of electrons forms as the stripped electrons accelerate through the gas and release additional electrons from the ionized gas. This cascade results in a pulse of current, which is how proportional counters and Geiger-Mueller (GM) counters function. Ion chambers have been a staple in modern medical physics and are used to quantify total dose delivered. They are often placed inside tissue equivalent phantoms to determine dose at various depths. Because ion chambers rely on a gaseous medium, they typically don't provide good energy resolution since high energy radiation can pass through the entire gas volume without depositing all of its energy. Pressurizing the gas is used to increase the density of gas molecules and therefore both the probability of radiation interaction and the electrons available for cascade reactions, but even highly pressurized chambers cannot compete with the density of a solid material. In a solid material, radiation can often be fully stopped in a small volume of material with all kinetic energy collected. Due to the availability of two excellent solid state detector materials, ion chambers were not used in this application but would be a viable method of dose measurement.

Solid material detectors, often referred to as solid-state detectors, have made use of advances in semiconductor manufacturing techniques. Materials like high purity silicon and germanium have led to detectors that can provide more precise energy measurements than gas filled detectors. This advantage is primarily due to the fact that radiation can come to a full stop in a solid detector, rapidly depositing all of its kinetic energy in a small volume and not require a cascade of electrons through a gas to amplify the current and corresponding signal. In solid materials, the electrons produced in the material migrate along electric field lines but do not produce cascades in the process. Since the energy of the incident particle is so quickly deposited, the electrons and "holes" produced along the path of the particle are typically sufficient to measure at the anode and cathode after use of a pre-amp.

Two types of solid detectors were utilized in this experiment, high purity germanium (HPGe) and Cadmium Zinc Telluride (CZT), with both functioning on the same principle of electron-hole pair production from incident radiation. As a particle travels through a material ionizing atoms and releasing electrons along the way, the freed electron travels along the electric field lines to the positive cathode side of the detector while the "hole," or space the electron previously occupied in an atoms electron shell, also migrates along the field lines in the opposite direction to the anode as electrons cascade from atom to atom filling the travelling hole. To start this process, an electron must be removed from orbit by the incident radiation, with the goal of removal of as many electrons as possible in order to provide sufficient counting statistics. In order for this to happen, the electron binding energy must be low enough to allow a sufficient number of electron-hole pairs to be created from a single radiation event inside the detector. A material with a high electron binding energy will result in very few electron-hole pairs and therefore little to no signal. Because semiconductors have binding energies that are higher than metals but significantly less than insulators, they have become a popular choice for radiation detectors. A metal cannot be used for radiation detection, despite small binding energies, since the atoms freely conduct electrons even at room temperature which are then capable of moving along an applied electric field even with no radiation interaction. Insulators exhibit the opposite quality with electrons that are too tightly bound to be liberated in sufficient quantity and cannot travel towards a positive cathode.

Semiconductors are an ideal choice for a solid material to be used in radiation detection since the electrons are not free to travel at room temperature, like metals, while also not being as tightly bound as insulators. This binding energy of the electrons can be referred to as the bandgap energy, or the energy required to move electrons into a conduction band. For CZT, the bandgap energy is 1.57eV at room temperature and HPGe is 0.67eV [56]. This low bandgap energy for HPGe means that HPGe must be cooled so that electrons at room temperature do not spontaneously enter the conduction band. CZT, with a higher band gap, does not require cooling which is a significant benefit. Energy resolution is another component of detector choice with HPGe offering superior energy resolution due to low energy requirement per electron hole (e-h) pair. HPGe requires 2.96eV per e-h pair whereas CZT requires 4.64eV. This means that almost twice as many e-h pairs are created per eV in the HPGe compared to CZT. Additionally, manufacturing techniques allow much larger crystals of HPGe to be manufactured, on the order of 100cm^3 in volume or 3 to 4 cm thick, allowing full absorption of higher energy gamma-rays [57]. CZT detectors are typically only available in volumes on the order of 3cm^3 with thicknesses of a few millimeters, limiting energy gammas with thicknesses on the order of millimeters.

3.6 Fluid Flow in the System

The amount of radioactive material reaching the detection or treatment site depends both on the amount of initial activation and the flow characteristics of the fluid transporting the materials. Rather than a solid material being repeatedly transferred between two points, the indium isotopes are in a heterogeneous liquid mixture and can diffuse within the fluid. Movement in the fluid of the activated indium by diffusion, advection, and possible turbulence or non-laminar flow can spread the radioactive material along the tubing during flow causing some material to arrive in advance of the main activated bolus while some lags behind. Diffusion refers to the movement of atoms within the liquid in axial and radial directions along the flow path. Advection is the transport of the atoms along the flow path from mass transfer due to inertial forces. This relation between spreading of the activated material by diffusion and transport by advection must be accounted for when determining both dose to be delivered and when quantifying initial activation when used as a detector.

The rate of diffusion of elements within the eutectic mixture can be estimated using a diffusion coefficient, determined by the Stokes-Einstein equation for liquids with a low Reynolds number [48]

$$D = \frac{kT}{6\pi\mu r} \tag{3.8}$$

With D the diffusion coefficient, k the Boltzmann constant, T the temperature of the liquid metal, r the radius of the atom and μ the dynamic viscosity. To examine the relative importance of diffusion in the flow of the activated material, the relationship between the rate of diffusion and advection can be compared using the dimensionless Peclet number:

$$Pe = \frac{LU}{D} \tag{3.9}$$

with L the characteristic length of the duct, U the mean velocity of flow and the product of the two quantifying the advection properties of the fluid. This relation between advection and diffusion means that liquids with a high Peclet number will have transport of materials in the fluid dominated by inertial forces over diffusion. High Peclet number flow results in fluids that have very little diffusion between the laminae of fluid in the flow and this relationship becomes important when determining whether flow can be modeled using "segregated" flow. This chemical engineering terminology refers to problems involving laminar flow in the transport of a reacting fluid [49].

A complete model of this system capable of predicting the amount of activated material at any point in the loop involves accounting for movement of the In-116 through both diffusion and advection, in addition to creation of the In-116 through activation and loss to radioactive decay. These elements can be represented in a general form by the equation

$$D\nabla^2 - \vec{V} \cdot \vec{c} - \lambda c + \emptyset c \sigma_a = \frac{\partial c}{\partial t} \tag{3.10}$$

with diffusion D, fluid velocity V, the neutron flux $\emptyset$ that the fluid is exposed to, the radioactive decay constant of the isotope λ, the neutron activation cross-section σ_a for the isotope, and the concentration c of the isotope of interest in the liquid. Equation 3.10 can be rewritten for flow in a circular pipe with the Laplacian expanded into cylindrical coordinates for one-dimensional flow as

$$D\left[\frac{1}{\mathrm{r}}\frac{\partial}{\partial \mathrm{r}}\left(\mathrm{r}\frac{\partial \mathrm{N}}{\partial \mathrm{r}}\right) + \frac{\partial^2 \mathrm{N}}{\partial \mathrm{z}^2}\right] - u\frac{\partial N}{\partial z} - \lambda N + \emptyset N \sigma_a = \frac{\partial N}{\partial t} \tag{3.11}$$

with radius r, velocity u and number density of the radioactive isotope N [50].

A radial velocity profile u of the liquid metal as a function of radius r under laminar flow can be represented by the equation

$$u(r) = 2\bar{u}\left(1 - \frac{r^2}{r_o^2}\right) \qquad 3.12$$

with r_o the outer wall radius [52] and is valid for Reynolds numbers < 2300. Based on equation 3.12, the velocity of the fluid stagnates to zero at the walls as radius r approaches r_o and reaches twice the average velocity at the centerline for r=0. Accounting for this flow at centerline traveling at twice the average speed is important when dealing with radioactive isotopes that are decaying during movement through the loop. This becomes even more critical when dealing with a short-lived isotope like In-116 with a half-life of 14.1 seconds. The effect of radial diffusion and the validity of a segregated flow model can also be examined with the radial Peclet number. This radial Peclet number, Pe_{radial} in equation 3.13, can be used to determine the relation between diffusion and advection radially in the tube:

$$Pe = \frac{L\bar{u}}{D} \qquad Pe_{axial} = Pe\left(\frac{L}{r_o}\right)^2 \qquad Pe_{radial} = \frac{Pe}{2} \qquad 3.13$$

Fluids exhibiting high axial Peclet and low radial Peclet numbers can be modeled with well-segregated flow and we can assume very little diffusion between layers.

The portion of equation 3.11 covering radioactive activation and decay,

$$-\lambda N + \emptyset N \sigma_a = \frac{\partial N}{\partial t} \tag{3.14}$$

governs the rate at which the activity of the isotope increases or decreases due to neutron activation and decay. Activation or creation of the radioisotope is driven by the product of the activation cross section σ_a, the value of which is dependent on the incident neutron energies, and the flux ϕ or number of neutrons intersecting the fluid. Decay of the activated material, occurring continuously after activation, is driven by the half-life or time required for the isotope to decay by half. Half-life of the material is accounted for with the time constant λ which is natural log 2 divided by the half-life.

Equation 3.11, the overall equation modeling the complete flow, activation and decay system was solved using finite difference approximations for the derivatives for one-dimensional laminar flow in a circular pipe. An implicit solution using a numerical time iteration method was solved at every time step using inversion of a matrix. An implicit method was chosen due to stability of the solutions and the ready availability of computing resources. The iterative method chosen to accomplish this was the Gauss-Seidel method. Gauss-Seidel was used in the modeling of the system due to improved convergence speed over the Jacobi methodology for matrix solutions [51]. Application of this modeling method and predictions for fluid flow and activity of the In-116 isotope at the detector are discussed in detail in the proceeding chapter.

CHAPTER 4

MODELING

Modeling of the system consisted of fluid flow and material transport predictions for the entire system in addition to activation and radiation transport modeling to optimize irradiation setups and predict dose output. The system as tested consists of two main components that are critical to the effectiveness of the process, the activation cell and the irradiator cell. Additional features include the pumping mechanism and tubing as a transport vessel. The activation cell and the irradiator cell were modeled in MCNP radiation transport simulations with five neutron activation sources to predict the production efficiency of the radioactive isotope and to predict the dose to be delivered to tissue with each. Monte Carlo models of the actual radiation sources were also necessary to provide an accurate "source term" for the activation cell models. The pumping mechanism and tubing were used in analytical predictions of fluid flow properties of the system to predict the arrival time, increase in dose over time and duration of dose delivery.

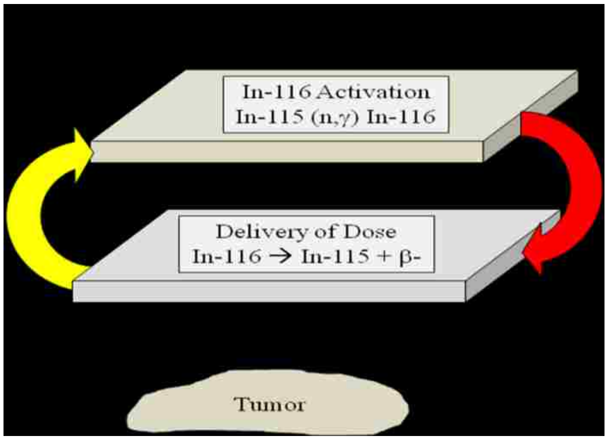

Figure 4.1 Conceptual Illustration of source term, activation, transport and application.

4.1 Modeling of Activation Cell

Two main components of the system, the activation cell and the applicator cell, were modeled in MCNP. The activation cell is the first step in the dose delivery process where the stable element, In-115, is activated to In-116 through neutron capture. Activating as much In-115 as possible in the shortest amount of time is the primary goal in this cell. Since In-115 exhibits substantial resonances for neutron capture at slow to thermal energies, an optimized cell geometry was used depending on what neutron source was used. The neutron capture cross section for indium-115 is shown in Figure 4.2 with peak capture resonances appearing repeatedly across a neutron energy spectrum. These resonance regions are areas where the incident neutron energy matches binding energies in the nucleus and result in an orders of magnitude increase in capture probability for a particular energy. Therefore an activation cell that first moderates incident neutrons towards these resonant energies will produce a greatly increased amount of In-116 compared to a high energy, mono-energetic source.

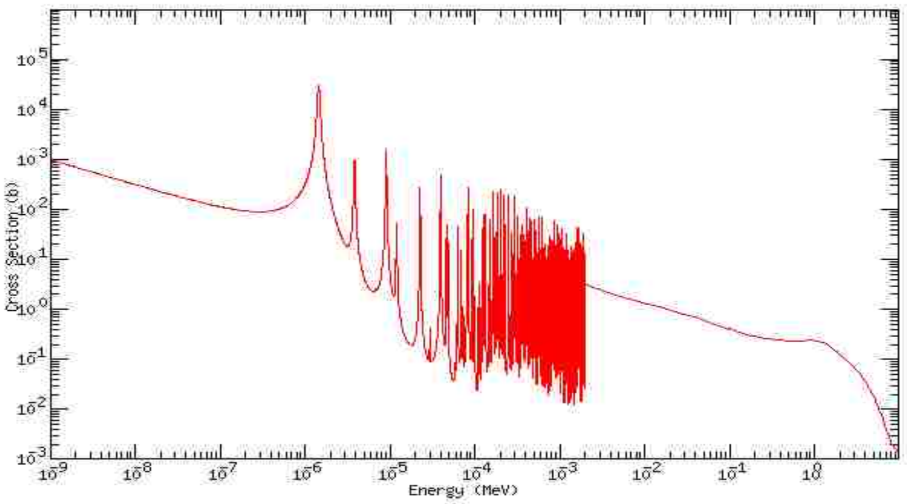

Figure 4.2. Neutron capture cross section for In-115.

The amount of In-116 created in the activation cell is critical to the effectiveness of the overall system. The activation cell must position the eutectic mixture in the neutron field while providing sufficient moderation of the neutrons to optimize the (n,gamma) capture on In-115. This moderation is dependent on the particular neutron energies incident on the applicator. In this work, ideal moderation materials and geometries are investigated for the five potential sources of neutrons consisting of a broad spectrum Pu-Be source, mono-energetic deuterium fusion neutron source, and 6MV, 15MV and 20MV X-Ray photo-neutron sources. Due to the significantly varying activation cross section based on neutron energy exhibited in Figure 4.2, a simple average neutron energy assumption is not sufficient since individual neutron sources can produce substantially different neutron energies. An accurate radiation transport model that can estimate all neutron energies and their magnitudes, or fluences, is necessary to obtain a more reliable activation prediction.

The activation cell must also contain a sufficient volume of the eutectic mixture to deliver the desired dose once reaching the applicator. Since In-116 decays with a 14.1 second half-life, the mixture is not continuously pumped between activator and applicator cells and the mixture instead remains stationary in the neutron field long enough to reach secular equilibrium. This equilibrium is the point at which production of the In-116 is equivalent to the decay and further time under irradiation results in negligible increases in the quantity of In-116. This equilibrium between In-116 production and decay over time during neutron irradiation can be represented by the equation

$$\frac{\partial N_{In116}}{\partial t} = -\lambda N_{In116} + \emptyset N_{In115}\sigma_a \qquad 4.1$$

which can be seen as a component of the previous equation 3.11 with neutron flux ϕ, activation cross section σ_a, and decay constant λ. The decay constant for In-116 is equal to $0.693 / t_{1/2}$ or $0.0491\ \text{sec}^{-1}$. Solving for In-116 atoms as a function of time gives

$$N_{In116}(t) = \emptyset N_{In115}\sigma_a * \frac{1 - e^{-\lambda t}}{\lambda} \qquad 4.2$$

With a constant activation rate, and assuming that the number of In-115 target atoms stays constant, the number of In-116 atoms gradually reaches a plateau after 4 to 5 half lives with equilibrium between decay and production. Figure 4.3 can be applied to any isotope based on only the decay half-life. Short lived isotopes will quickly reach equilibrium while longer lived isotopes will require long irradiations to reach their plateau.

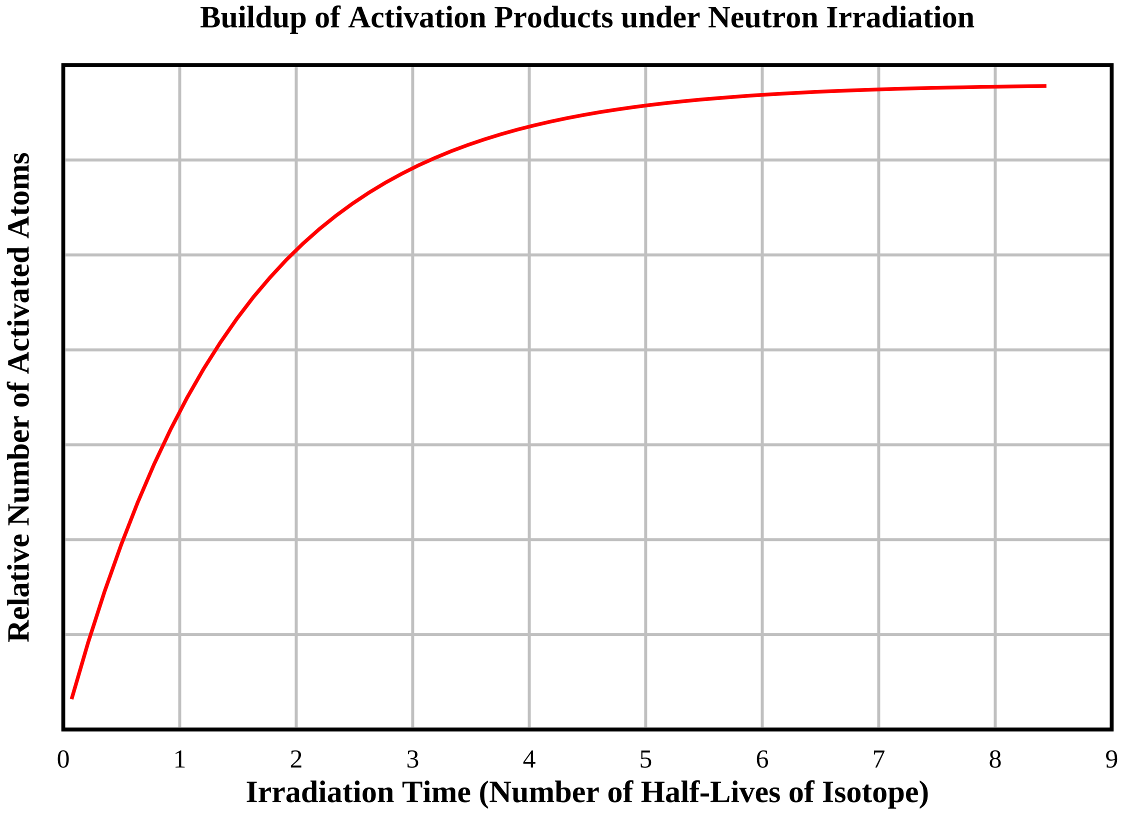

Figure 4.3. Calculated In-116 growth curve for exposure to a continuous neutron source.

Remaining in the neutron field beyond this point of equilibrium introduces unwanted additional neutron activation products with longer half-lives into the material as these longer lived isotopes start to build up. Of particular interest is the first meta-stable state In-116m1 with a half-life 54.3 minutes and a decay process involving high energy gamma-rays, which can present an unwanted dose component. While creation of this isotope is difficult to avoid, resulting dose from the decay of In-116m1 can be minimized by limiting the time of exposure to the activated indium. The rationale for exposing the indium to a neutron activation field for no longer than about 4 half-lives also applies during the dwell time that the indium remains over the treatment area. A dwell time in the applicator of 4 half-lives, or about one minute, delivers 94% of the decay betas from In-116 while minimizing dose from longer lived activation products. The impact of additional isotopes on dose, measurements of this metastable state and techniques to minimize both production and resultant extra dose are discussed in more detail in proceeding chapters.

Equation 4.2 is applied whenever the source of neutrons is a continuous irradiation over time. The five neutron sources modeled here consisted of four continuous sources and one pulsed source, the dense plasma focus (DPF). The DPF produces all emitted neutrons within 100 to 200 nanoseconds, producing all activations at once and requiring only a decay correction as the material travels to the detector/applicator.

Moderation needs for the activator cell depended on the source of neutrons utilized. Due to the broad energy spectrum of the Pu-Be source, and the housing of the source in a large neutron moderating paraffin filled drum, a moderator was not anticipated to be needed. Other sources, however did require moderators for optimizing In-116 production. The monoenergetic DPF source produces 2.45MeV neutrons by deuterium-deuterium fusion and therefore requires moderation. The Varian M6 produces a broad spectrum of photoneutrons and also benefits from moderation.

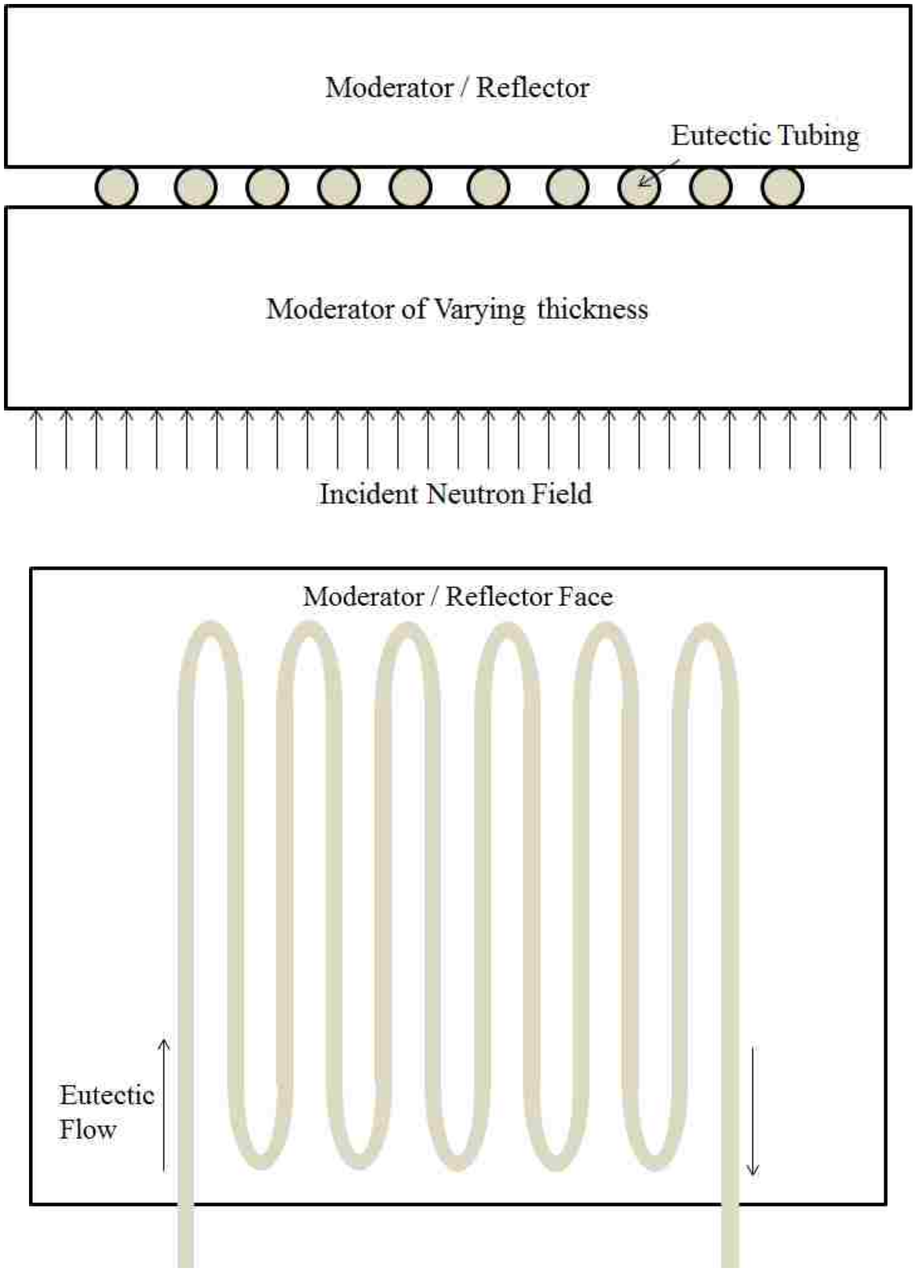

Figure 4.4. Conceptual activator cell radiator flow design (bottom) for modeling utilizing varying moderator and reflector thicknesses (cross section top).

Figure 4.5. Physical polyethylene pieces used for DPF and Varian M6 moderating and reflectors.

Since activation does not require the decay betas to pass through any materials or exit the tubing, the activator cell simply followed a radiator design that allowed 1cc of eutectic in 1/16” ID Teflon tubing to be exposed to the neutron moderation area. This radiator design was used for all sources except for the Pu-Be source which utilized a cork screw pattern in order to fit the dimensions of the irradiation port.

4.2 Applicator Cell

At the opposite end of the process where the resulting radioactive isotope, In-116, is placed near the target tissue region during decay, the main goal is to allow as many beta particles to exit the applicator as possible and requires a thin window material to avoid attenuation of the electrons. On this side of the process the primary goal was designing a non-metallic cell that would maintain non-turbulent flow and efficiently deliver the activated fluid to a treatment area. While liquid metal like GaInSn is convenient for transport by tubing and pumps, it also has a significant self-shielding effect on the emitted beta particles. Because of this self-shielding, an applicator is most effective when it spreads the radioactive In-116 over a broad area while minimizing thickness of the liquid metal to allow beta particles to escape the mixture. A design is presented in this work that minimizes turbulent flow and spreads the eutectic over a thin and broad surface area.

Decay betas from In-116 possess an average energy of 1.365 MeV and have a range of several millimeters in tissue, but are severely self-attenuated within the eutectic mixture itself. The continuous slowing down approximation (CSDA) range, which provides an average range for elections and accounts for deviations made during their track length, is only about 1.5 millimeters, or about 1/16", in GaInSn for a 1.365 MeV beta. This means that even in the case of a large volume of eutectic, only beta particles from the outer 1 to 2 millimeters of the fluid will escape and deposit dose in the adjacent tissue. Therefore the ideal applicator spreads the mixture out at the application site to utilize the maximum surface area possible while minimizing self-attenuation of the betas within the eutectic by not becoming thicker than the CSDA range of the electrons.

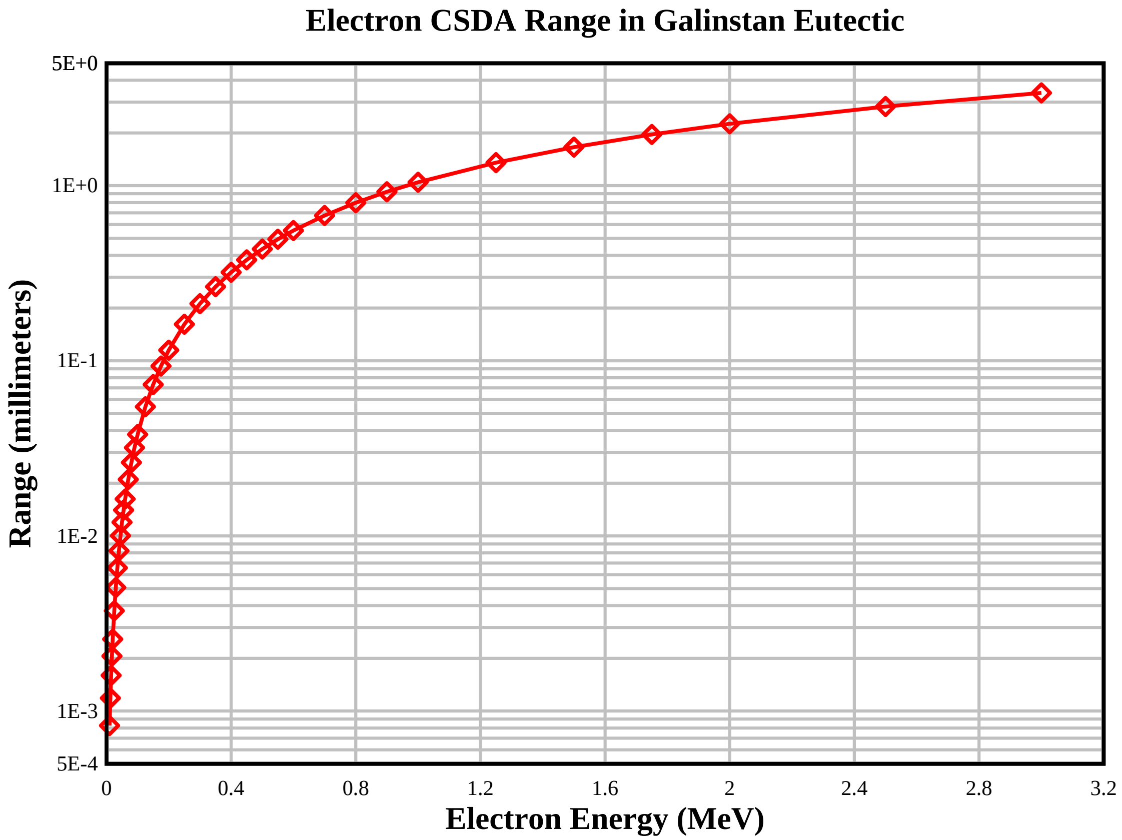

Figure 4.6. Calculated electron CSDA range in GaInSn for energies of interest.

Given the CSDA range for an average In-116 decay beta of 1.5mm or ~1/16" based on Figure 4.6, the applicator should not be thicker than 1/16". Despite remaining no thicker than the CSDA range, self-attenuation and energy loss is unavoidable. MCNP models show that In-116 betas still suffer significant attenuation and some energy loss during emission from the eutectic. Figure 4.7 illustrates the resultant MCNP simulated emission spectrum from one side of a 1/16" thick cell compared to the original decay spectrum in solid. .

.

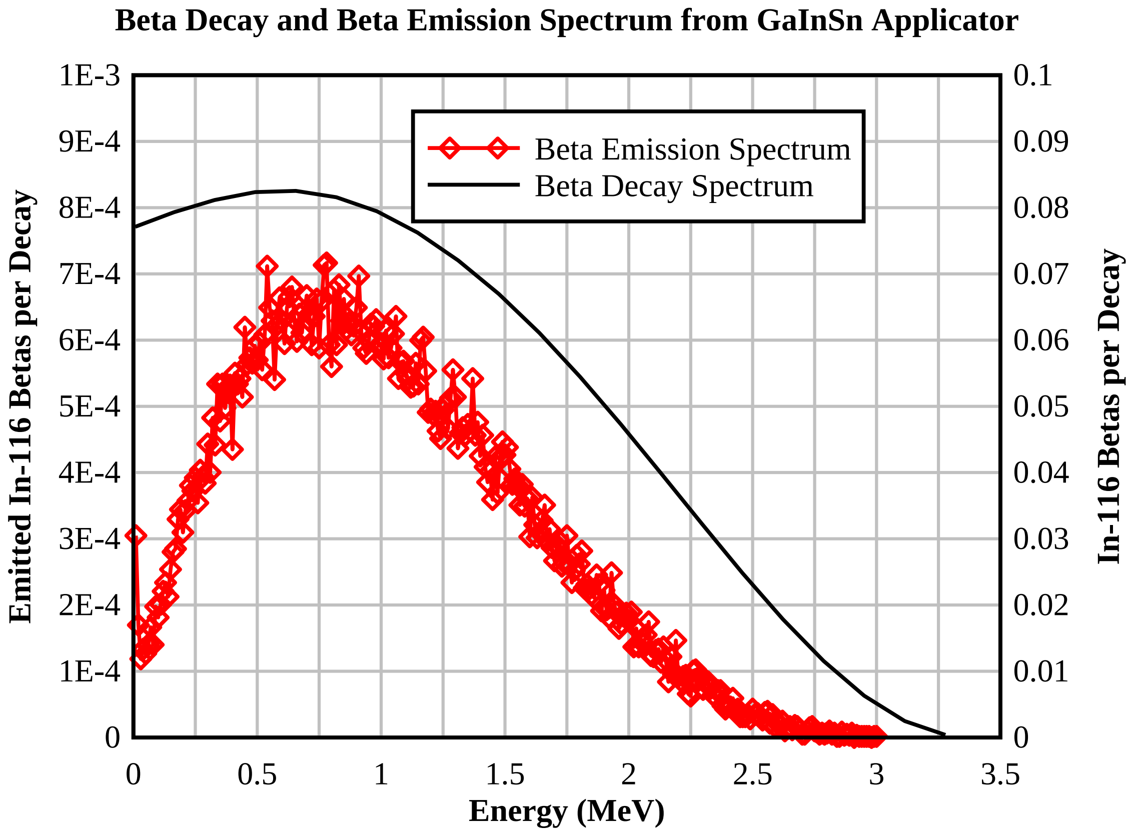

Figure 4.7. Emitted MCNP calculated decay spectrum from GaInSn cell and original decay spectrum.

Note in Figure 4.7 the emitted spectrum scale on left axis and original decay spectrum scale on right. This spectrum not only shows a loss of high energy betas but attenuation in emission magnitude as well. The integral of the emission spectrum (solid line) is 1.0 with the plot a probability of electron energy per decay. Integrating the emitted spectrum (data points) results in a total of 0.094, meaning only 9.4% of betas emitted within the GaInSn cell exit the surface.

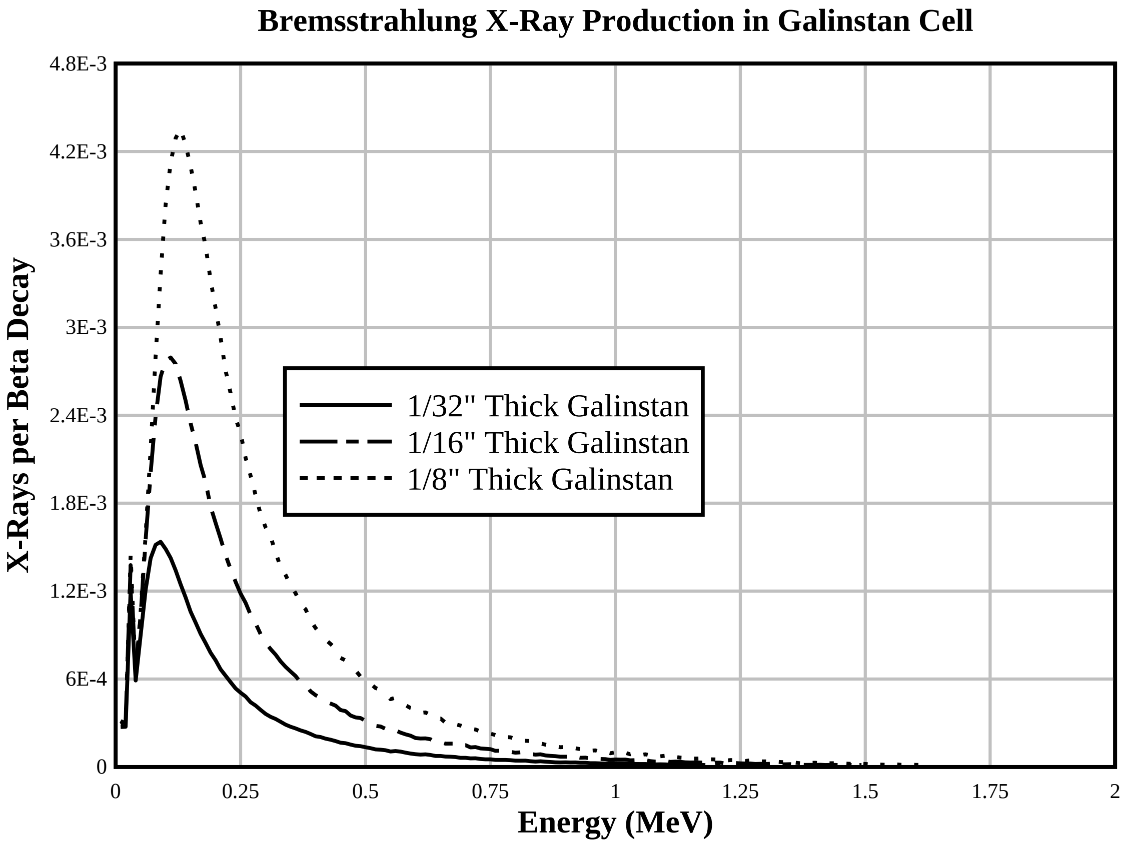

Figure 4.8. X-Ray spectrum generated by decay electrons in the GaInSn cell.

An additional reason to avoid an irradiation cell thicker than 1 CSDA length is the unnecessary generation of bremsstrahlung X-Ray radiation by the decaying betas. A GaInSn cell made to be as thin as possible reduces total decays in the volume and electron path length. X-rays can easily exit a thick GaInSn cell and produce unwanted dose while the associated decay electrons do not. Due to the range of In-116 decay betas, maximizing beta dose and minimizing X-Ray dose, an applicator cell thickness of 1/16" was chosen for this work. As shown in Figure 4.8, doubling the cell thickness also doubles the number of X-Rays exiting the cell, primarily due to the fact that twice as much GaInSn is present for the same surface area and the X-Rays are minimally self-attenuated in the eutectic.

In addition to self-attenuation in the eutectic, a closed loop system requires that the mixture be re-circulated back to the irradiator cell and not come into contact with the treatment surface or the detector used here. While the GaInSn mixture is considered non-toxic in humans based on the MSDS, intentional or accidental contact with skin or treatment areas is prohibited in a sterile environment. Additionally, loss of the mixture between irradiation cycles would be undesirable. A thin window is therefore used in the applicator cell to allow passage of the betas out of the eutectic and into the CZT detector. A 0.5mm styrene barrier is used as a window in this work, producing negligible attenuation of the beta particles while containing the eutectic mixture. The corrosive nature of the GaInSn to metals is once again of concern as the applicator must use non-metallic components. Based on this requirement, models and physical prototypes utilize plastics like ABS and PLA for the activation and applicator cells which are fabricated on 3D deposition and SLA printers.

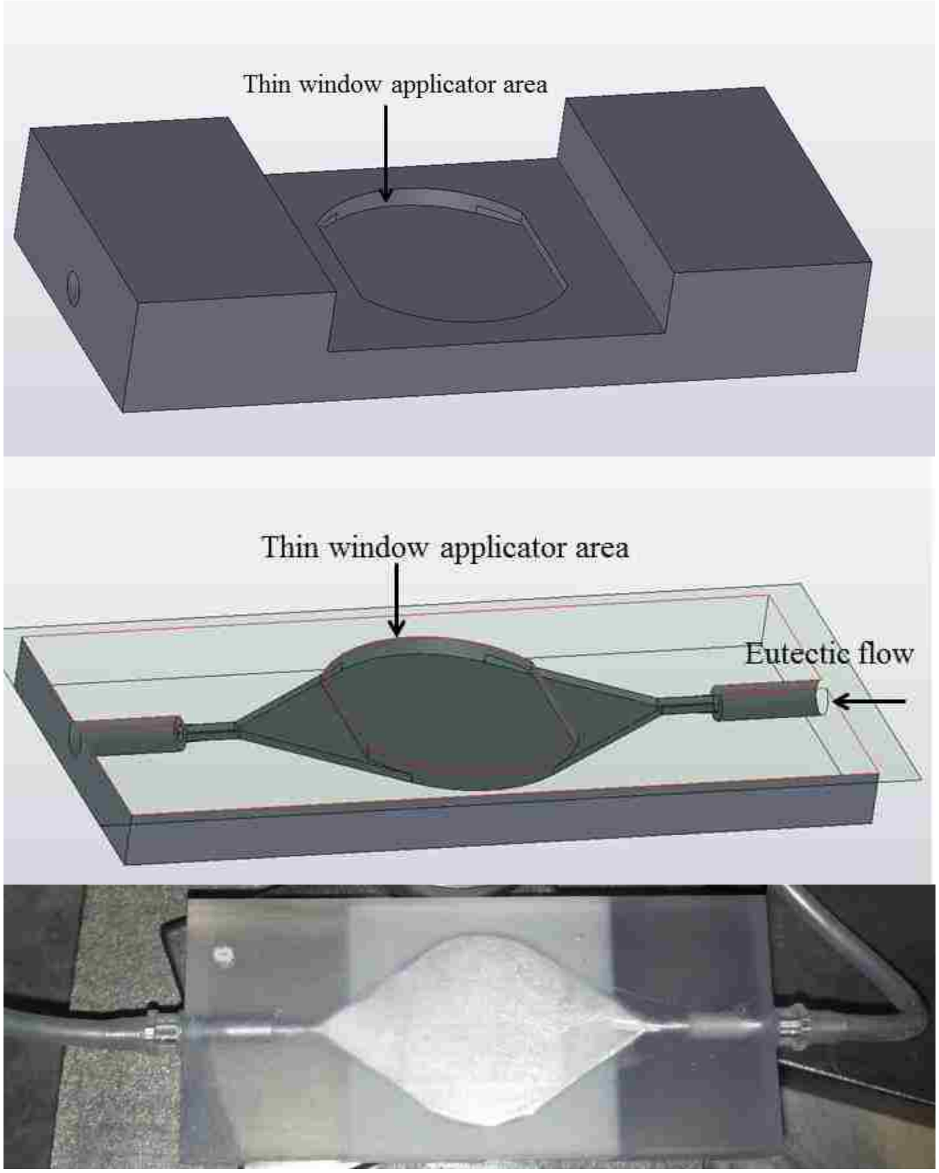

Figure 4.9 CAD model showing flow transition to thin applicator window area and applicator cell printed in clear plastic showing eutectic flow.

The ultimate goal of modeling the activation and applicator cells is to establish a reliable model to predict dose and allow for optimizations. In order to effectively compare models of In-115 activation to physical experimental results of detected betas, several factors must be accounted for including 1) self-attenuation of the beta particles in the GaInSn, 2) spectral changes due to scattering and absorption in the GaInSn as shown previously in Figure 4.7, 3) backscatter of betas from the CZT preventing detection, 4) geometrical effects like $1/R^2$ reduction from distance and differences between detector area and emission area, 5) correcting for any attenuation by barriers or membranes and any occlusion of the detector face, and 6) decay correction for transit time of the pumped material. MCNP models were used to determine the following values in Table 4-1 for the CZT detector and applicator utilized here. These factors are applied to experimental data to compare to MCNP calculated activation amounts. Combining all values in Table 4-1 results in a correction factor of 3.2×10^{-3}. When using a photoneutron source, this factor becomes 2.46×10^{-3} based on reported differences of 30% overestimation in MCNP photoneutron calculations versus established benchmarks [63].

Table 4-1. Correction factors from model to experiment excluding decay corrections.

Model to Experiment Correction	**Betas detected per decay**
Beta fluence in CZT cell per decay (MCNP)	0.005
Barrier attenuation (MCNP)	0.89
Activation cell volume vs. Applicator volume	0.80
Detector Occlusion	0.90
Combined Correction Factor	3.2×10^{-3}

4.3 Monte Carlo Modeling of Neutron Activation Sources

Optimizing In-116 production and designing an ideal moderator and activation cell requires an accurate neutron source term. In-115 activation techniques would ideally use a neutron source with pure 1 to 2 eV neutrons to match the resonance peak in the neutron capture cross section. However real neutron sources produce a non-ideal spectrum of orders of magnitude higher energy and these neutrons need to be slowed down, or moderated, to become more effective at producing In-116. Small changes in neutron energy can result in widely varying interaction probability, making average energy assumptions inaccurate. Activation models therefore used neutron source terms produced by MCNP modeling to predict actual neutron spectrums and fluences from all three neutron sources studied here. Rather than simply use a pure Pu-Be neutron spectrum source term as shown in Figure 4.10, MCNP models used this term combined with a model of the physical drum and shield to determine the actual spectrum encountered by the eutectic. In the case of the DPF neutron source, the 2.45 MeV monoenergetic point source at the pinch point is created very close to scattering media inside the source chamber and attenuated by surrounding vacuum hardware, resulting in a broadening of the neutron energy. The third neutron source, the Varian M6 accelerator, utilized a more complex MCNP model that produced neutrons through a process of electron bombardment of an X-Ray producing target, followed by photoneutron production in a beryllium target. Finally, for scaling purposes to predict clinical dosage, a Varian Clinac neutron source was used based on prior photoneutron production studies.

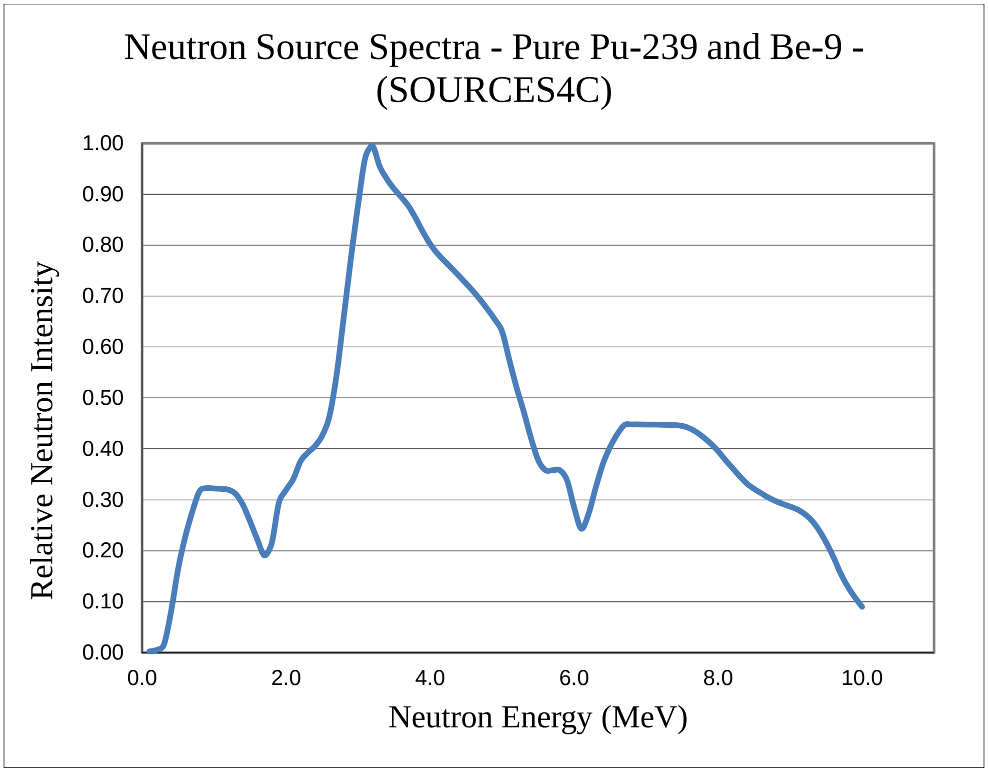

Figure 4.10. Calculated non-moderated Pu-Be Neutron Spectrum from Sources4C.

For the Pu-Be source, the neutron spectrum used for modeling is calculated using the code SOURCES4C to produce Figure 4.10 which assumes a pure plutonium and beryllium mixture. Pu-Be sources produce a relatively broad spectrum with peak neutron energy of 10MeV, an average energy of 4.8MeV, and source emission strength of 1.13×10^7 neutrons per second [44]. This source spectrum was placed inside an MCNP model of the physical source drum and associated paraffin shielding to calculate the moderated neutron spectrum. The MCNP model and actual source drum are shown in Figure 4.11. An access port to the source was included and measured 1.5 inches in diameter. This access port is where the eutectic mixture was pumped into the shielding and into close proximity with the Pu-Be source. Two configurations of the Pu-Be source can be used, to include a "source up" and a "source down" configuration. The source is normally located 3 inches below the access port but can be raised to provide a direct line of site down the access port. This change in configuration allows for two possible neutron spectrums at the activation point based on moderation by the paraffin and proximity to the source. Due to the significantly higher neutron fluence in the “source up” position, only that configuration was used for models. The resulting heavily moderated neutron source is presented in Figure 4.12, verifying that no additional moderator is needed at the activator cell point.

Figure 4.11 Pu-Be drum (left) and MCNP cross sectional model (right)

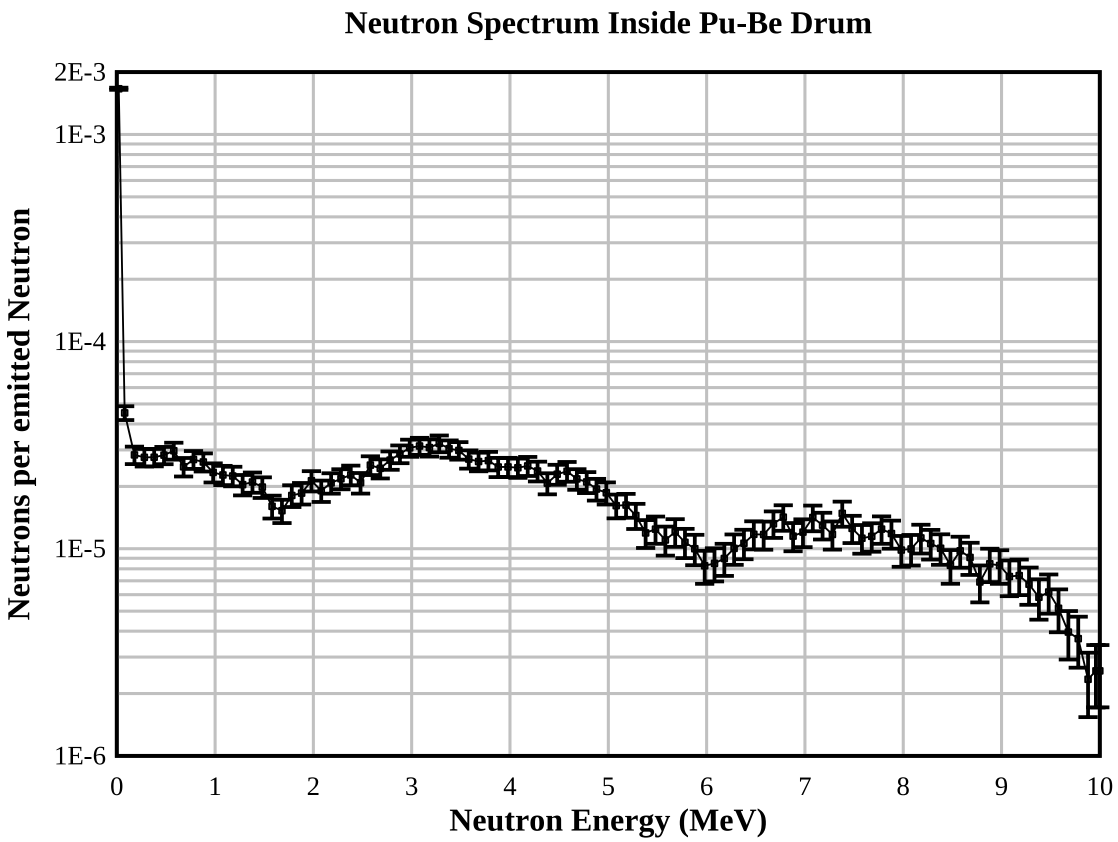

Figure 4.12 Resultant Pu-Be neutron spectrum at irradiation point inside drum.

With a 1cc volume of GaInSn placed in the Pu-Be irradiation port, MCNP models calculate an In-116 production rate of 1.4×10^{-4} activations per emitted neutron. With a Pu-Be steady neutron source strength of 1.1×10^{7} neutrons/second, we can expect a production rate of 1.6×10^{3} atoms/second. For a 60 second irradiation, we can decay correct using equation 4.2 with a resulting 3.0×10^{4} atoms of In-116 produced in the 1cc cell. This small amount of activations is insufficient for providing clinical dose and is difficult to detect after being pumped to the detector. For this reason, the Pu-Be source is only used for activation analysis to determine the composition of the GaInSn on the HPGe detector.

The DPF used in this work typically produces more than $1x10^{11}$ neutrons per pulse, emitted over a very short time frame of about 100 nanoseconds. The DPF source was modeled in MCNP to predict activation in the GaInSn for varying thicknesses of neutron moderators. Since the DPF produces mono-energetic 2.45 MeV neutrons, polyethylene moderators are required to slow neutrons down into an energy range where capture becomes more favorable. Varying thicknesses of moderators were modeled including the use of reflectors behind the GaInSn cell. The DPF model used in MCNP is shown in Figure 4.13

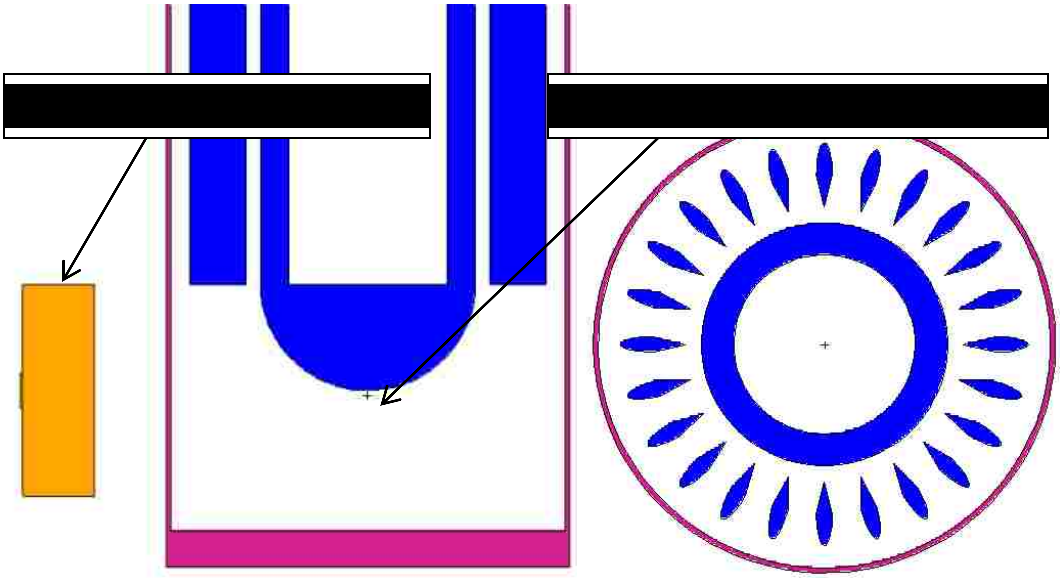

Figure 4.13. MCNP modeling geometry of DPF, neutron moderator and GaInSn cell. Moderator was modeled both in this configuration and flush with the outer DPF tube.

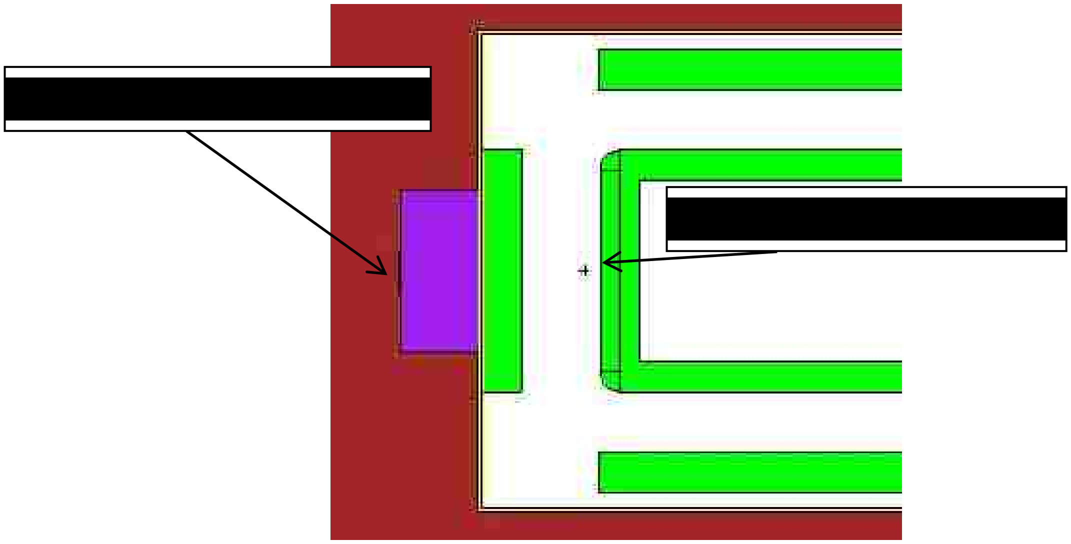

Figure 4.14. MCNP modeling geometry of “INNY” DPF, neutron moderator and GaInSn cell.

A sample moderated neutron output for a 2 inch moderator as shown in the above figures is presented in Figure 4.15 showing strong thermal production regions but also retaining a significant peak at 2.45 MeV, the energy of the primary fusion neutrons passing through the moderator. For In-116 production, ideal neutrons should be in the thermal to several eV range, meaning that these high-energy neutrons do not contribute to capture and need to be moderated as much as possible. Moderators studied here ranged from 0.5” to 3”. DPF neutron yields vary from shot to shot, rather than the continuous output exhibited by the fixed source Pu-Be or the M6 accelerator, and shot to shot yields are measured with various yield detectors. Therefore modeling outputs for dose are scaled to measured DPF output for each shot when calculating dose.

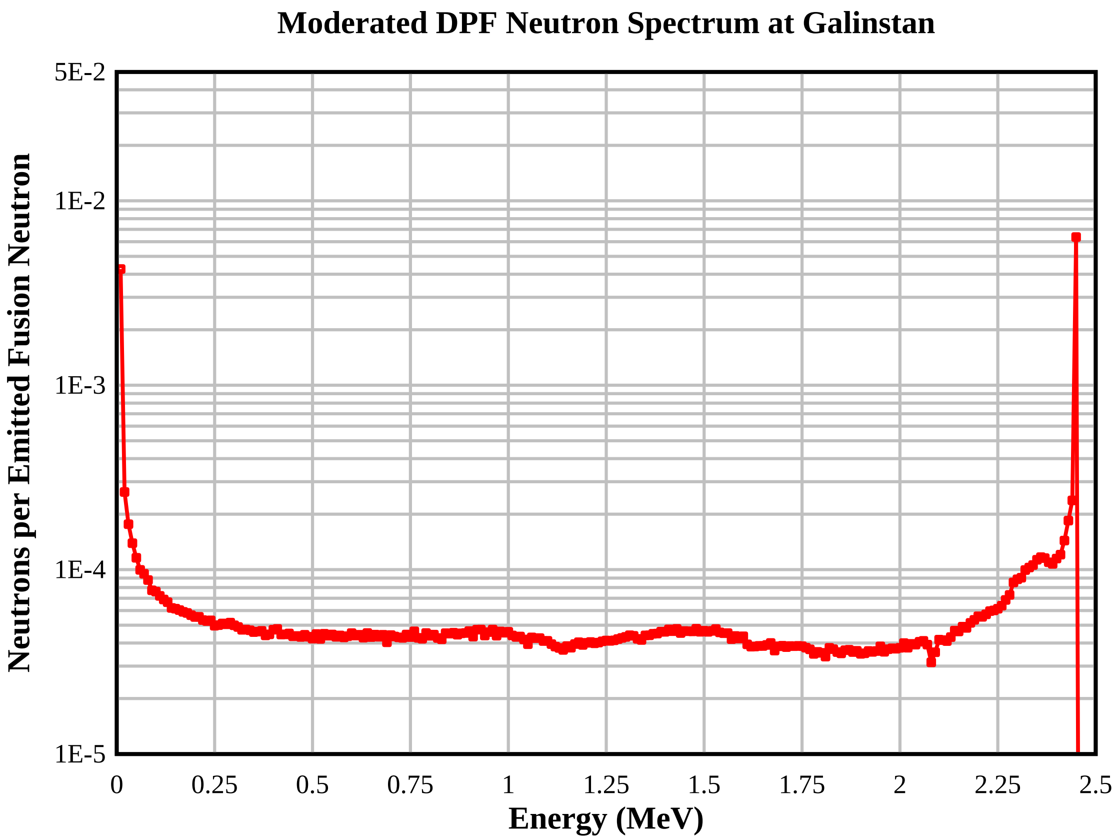

Figure 4.15. Calculated DPF neutron spectrum reaching GaInSn for a 2in moderator.

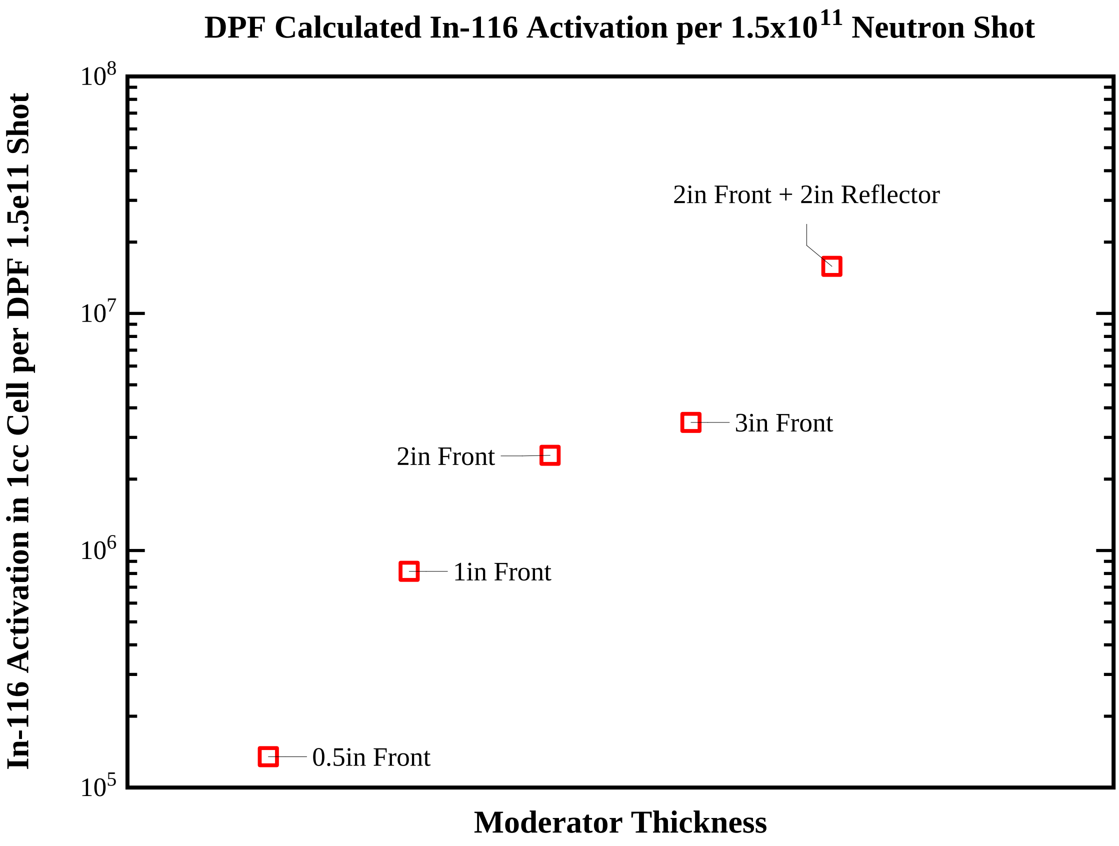

Figure 4.16. Calculated DPF In-116 activation in GaInSn target for varying moderator thicknesses assuming a single 1×10^{11} neutron pulse for all moderators.

From Figure 4.16 it is apparent that a reflector behind the front moderator and sandwiching the activation cell produces close to an order of magnitude more activations of In-116 per shot from the DPF. Moderator distance to the DPF tube was also decreased during experiments to be flush with the tube outer surface and activation models were run for these configurations as well. Additionally, a model of the activation cell in an "INNY" configuration (Figure 4.14) was modeled for comparison to experimental irradiations.

A model of the Varian M6 accelerator used at UNLV for these experiments and presented in Figure 4.17 was used to predict photoneutron production and moderation at the GaInSn to compare with experiments and optimize In-116 output [59]. Similar models were used for the M6 and the higher neutron output and higher energy K15 by swapping the target for a 9 and 15MeV compatible target in the model to scale up to predicted photoneutron yield.

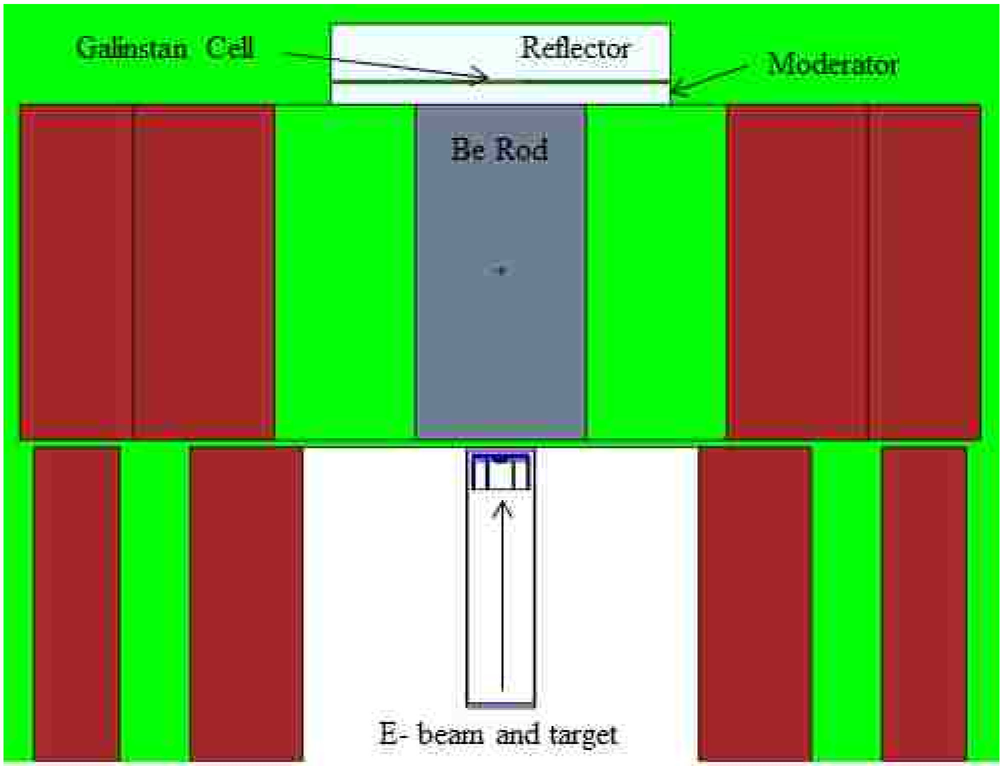

Figure 4.17. MCNP geometry for photoneutron production in an M6 accelerator.

Photoneutron production used a beryllium rod 3" in diameter, 6" in length placed directly on the exit of the uncollimated X-Ray target. Electron pulse rates and currents were used in the model to determine photoneutron output according to

Table 4-2. Resulting photoneutrons for a 3/8" front moderator and 1" rear reflector is presented in Figure 4.18 for a standard beam current. This spectrum was determined for every variation of moderator used in the experiments. Moderator thicknesses and sequences were varied and are presented in the results.

Table 4-2. Electron pulse frequency and magnitude for photoneutron models.

Model and E	Pulse Rate	e- / sec
M6 6MV	156.6Hz	3.14E+14
K15 9MV	220Hz	7.14E+14
K15 15MV	220Hz	6.73E+14

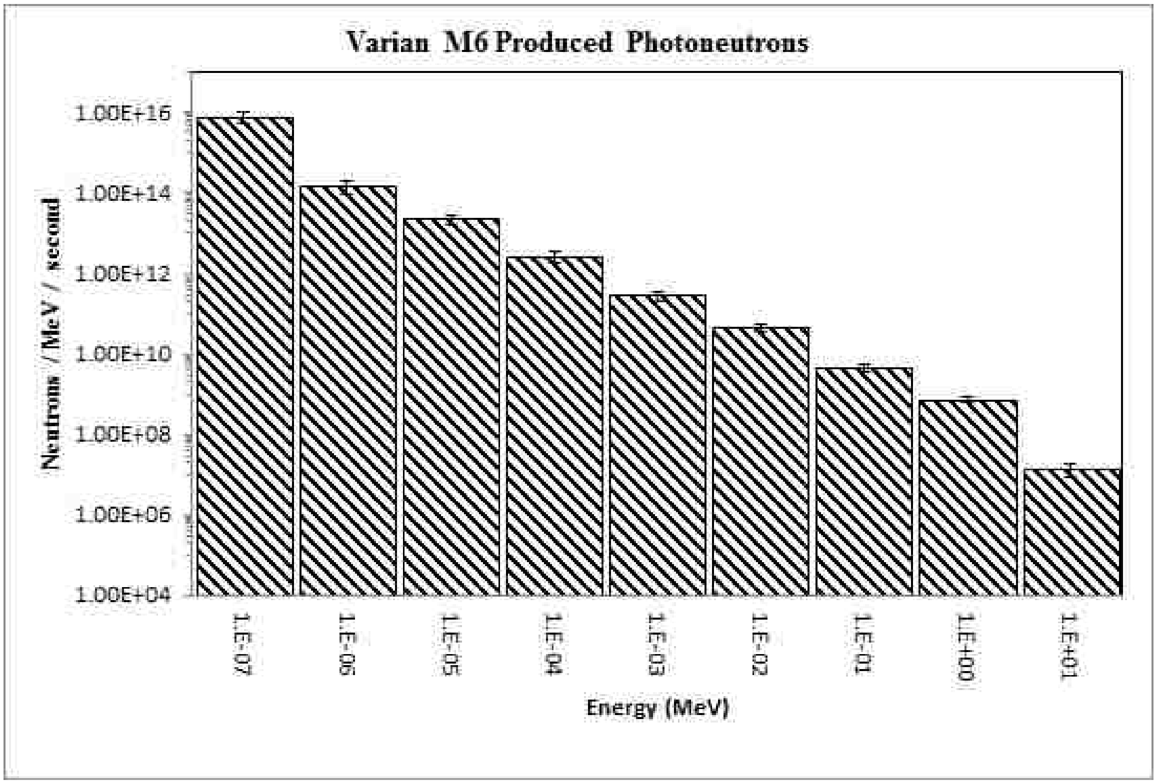

Figure 4.18. Photoneutron spectrum and fluence at the GaInSn target from a Varian M6 accelerator running at standard 156.6Hz rep rate.

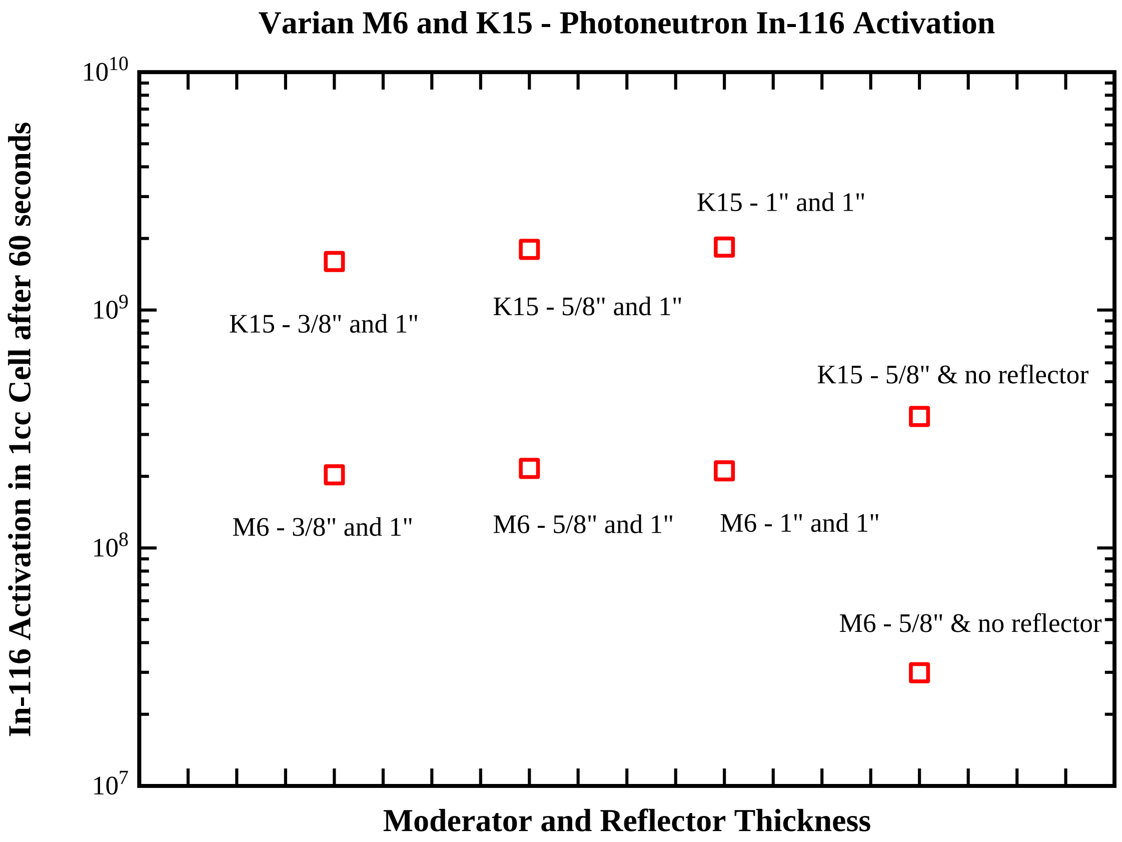

Figure 4.19. Photoneutron calculated activation of GaInSn target from a Varian M6 and K15 accelerator running at similar beam currents.

Predicted In-116 activation amounts are plotted in Figure 4.19 for the M6 accelerator with a GaInSn activation cell sandwiched between a moderator and reflector as shown in Figure 4.17. Results for a higher energy K15 is also presented showing the effect of the increased photoneutron production from 15MeV endpoint X-Rays. For comparison, the predicted activation shown from the M6 and K15 accelerators use similar machine currents of 6.28×10^{14} and 6.73×10^{14} electrons/second on the target, respectively. These currents are expected from accelerator rep-rates of 315Hz for the M6 and 220Hz for the K15.

A model of an ideal activation cell for a Varian Clinac was also determined based on predicted photo-neutron spectrums for a 20MeV accelerator. These accelerators are in widespread use in cancer treatment facilities and are a potential source of activation neutrons. While not designed with neutrons as a primary emission goal, they are capable of significant neutron production through X-Ray interactions in the tungsten and high-Z components of the accelerator head including the collimator, target, filters, jaws and MLCs. It was assumed that these accelerators were not modified in any way to optimize neutron output but instead relied on direct impingement of the X-Ray beam on the collimator and jaws, such as would be achieved by simply running the accelerator with the tungsten jaws and MLCs completely closed. Several studies have looked at photoneutron production in clinical linacs, all with similarly shaped outputs such as that from a 15MV unit in Figure 4.20.

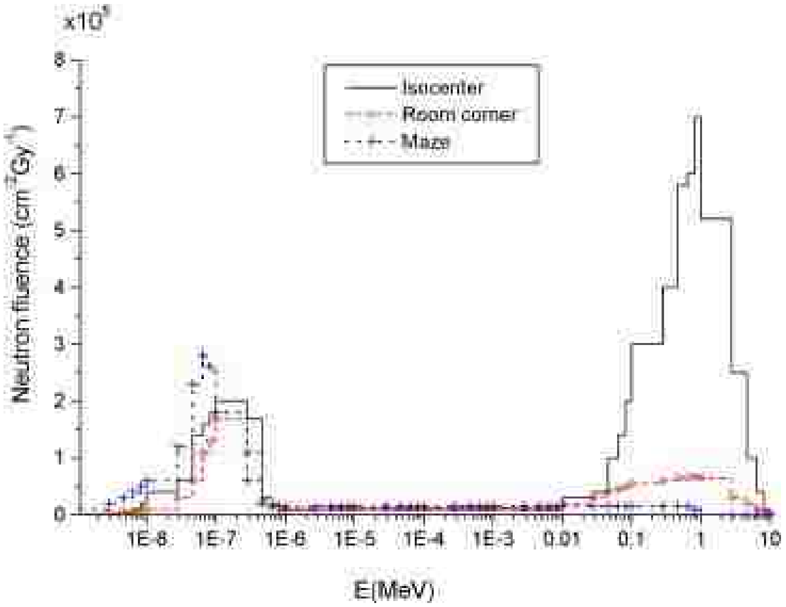

Figure 4.20. Photoneutron spectrum from a 15MeV Primus clinical linac. Reprinted with permission [60].

A photoneutron spectrum from an extremely common clinical unit in the U.S., the Varian Clinac 2100C, is presented in Figure 4.21. This spectrum is used in MCNP simulations according to the diagram in Figure 4.22 to calculate In-116 activation and predicted output. Studies show that a closed jaw Clinac can produce 1.2×10^{12} neutrons in the accelerator head per MU [62], or monitor unit, which is a scaling value for dose produced per minute at isocenter. A typical accelerator is capable of 600MU/min, meaning 7.2×10^{14} neutrons per minute can be produced in the accelerator head as a whole. This is a substantial neutron flux and provides the opportunity for thermalization and activation of the In-115 being studied here.

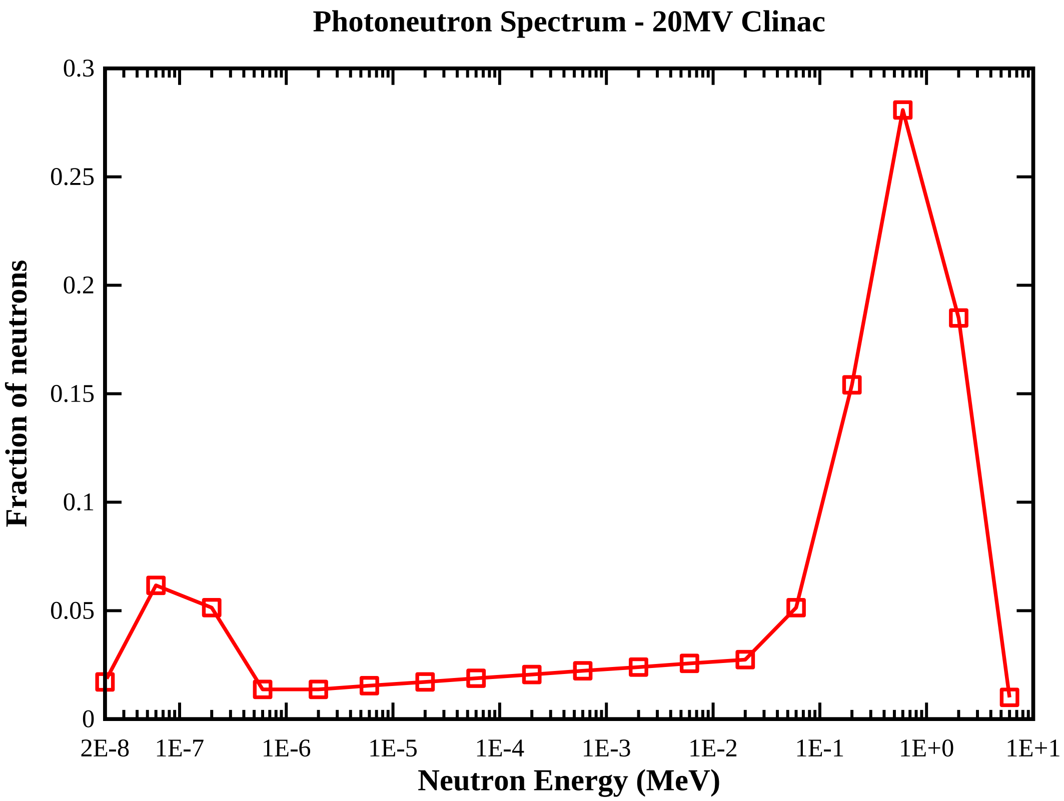

Figure 4.21. Clinac 2100 20MV photoneutron spectrum used in MCNP model for activation scaling, based on S.Ovalle studies [61].

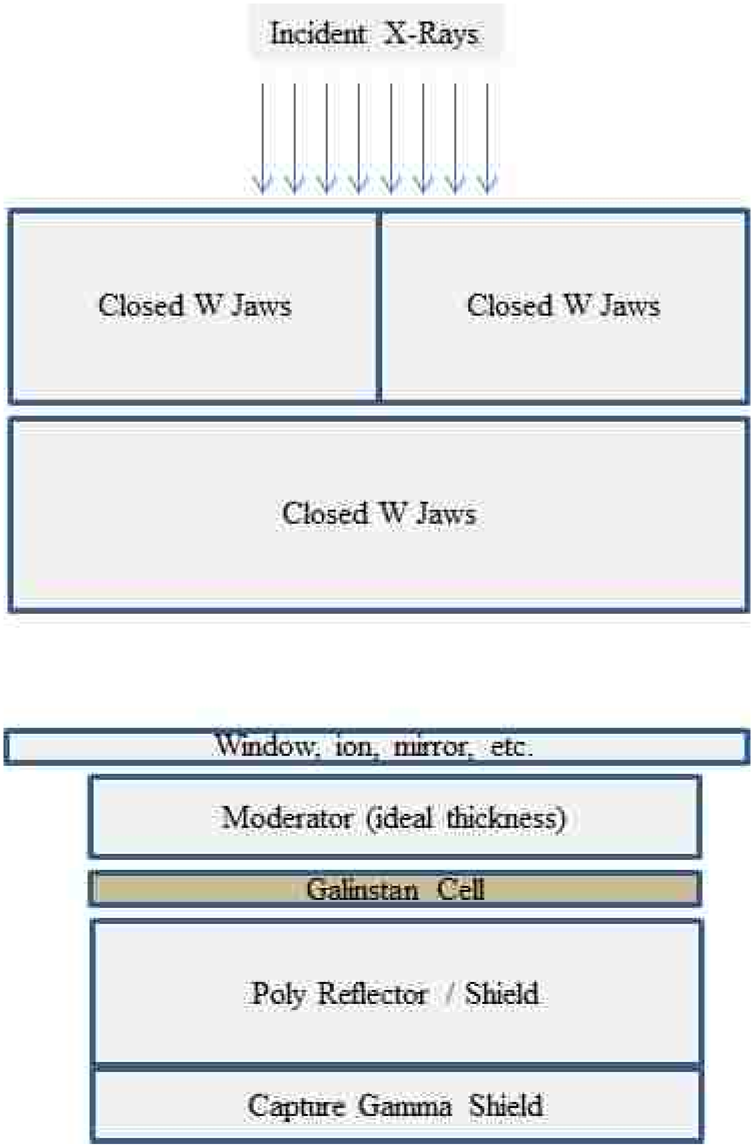

Figure 4.22. MCNP Model diagram for photoneutron production in a clinical Varian 2100C accelerator.

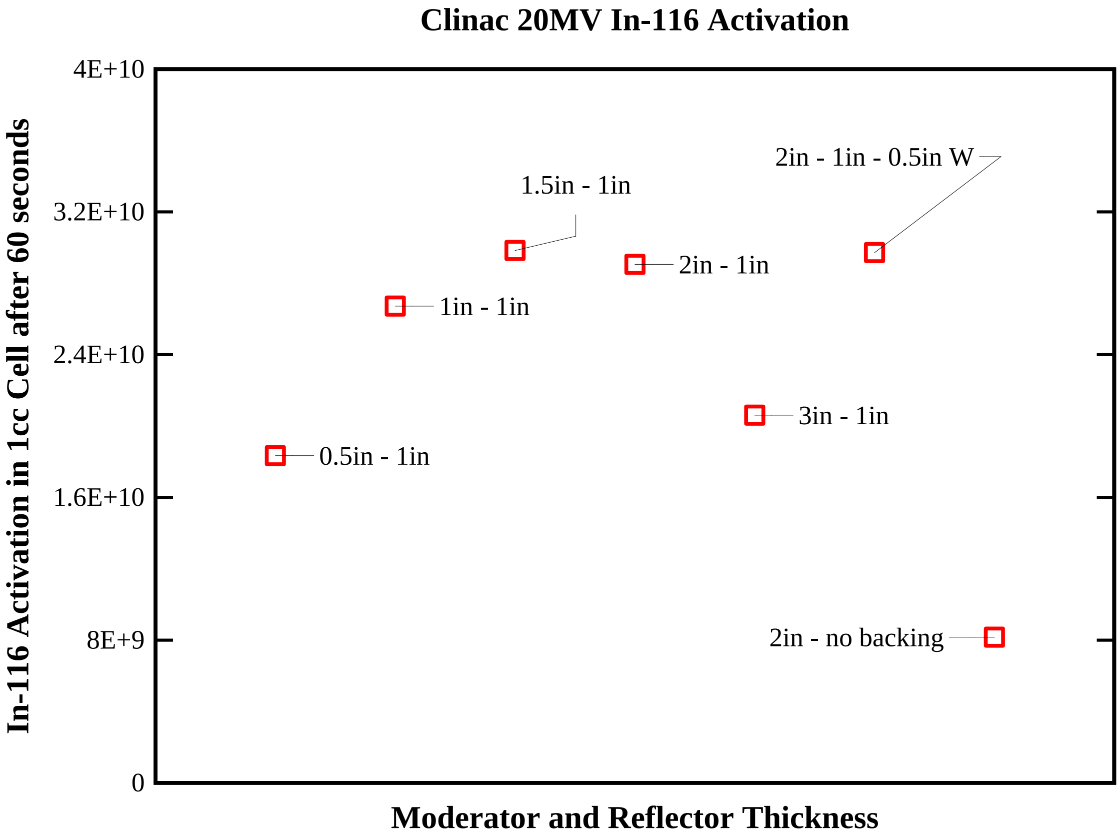

Figure 4.23. MCNP In-116 activation model results for various front moderator and rear reflector thicknesses.

A Clinac 2100C operating at a full current of 600MU/min, producing 7.2×10^{14} neutrons per minute with polyethylene moderators and reflectors sandwiched around a 1cc GaInSn activation cell will produce the most activation with 1.5" front poly and 1" reflector according to Figure 4.23. The importance of a reflector is apparent as removal results in a drop of 3.5x in activation. A tungsten backing to shield the room from capture gammas in the polyethylene has no effect on activation amounts but will help reduce excess gamma dose in the room.

4.4 Analytical Modeling and Prediction of Fluid Pumping System

Modeling was performed to predict the behavior of the activated material within the liquid transport mechanism using dimensions and conditions present in the experimental setups used for data collection. Fluid modeling was performed for both the continuous source of neutrons from the Pu-Be and X-Ray photo-neutron source along with the pulsed source from the DPF. With the use of a continuous source, the fluid must be held stagnant in the neutron field to achieve a steady state of activated material where decay is balanced with activation.

Based on the radial velocity profile of the liquid metal determined earlier, the following segmented flow can be modeled based on fluid flowing in laminae.

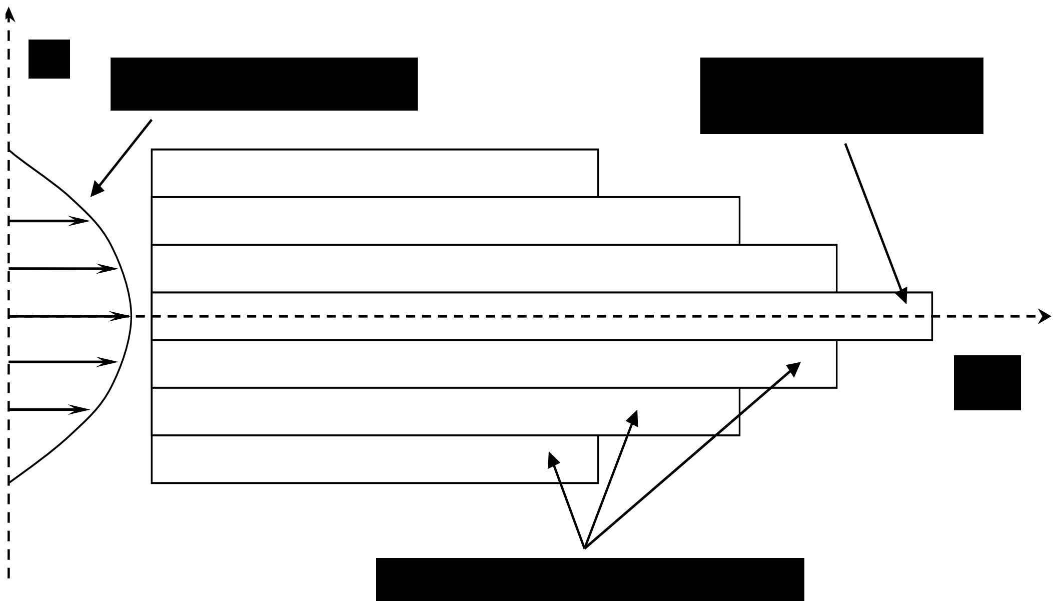

Figure 4.24. Segmented flow along the GaInSn transport tubing.

Models predict that segmented flow will exhibit a gradual rise in detected radiation at the detector as the radioactive material in the center of the tubing, at r=0, reaches the detection area with twice the average speed of the bulk fluid. The difference between assuming uniform flow and segmented flow is illustrated in Figure 4.25. This "early arrival" of radioactive material has implications for dose delivery as this material begins depositing dose before the expected arrival of an activated bolus.

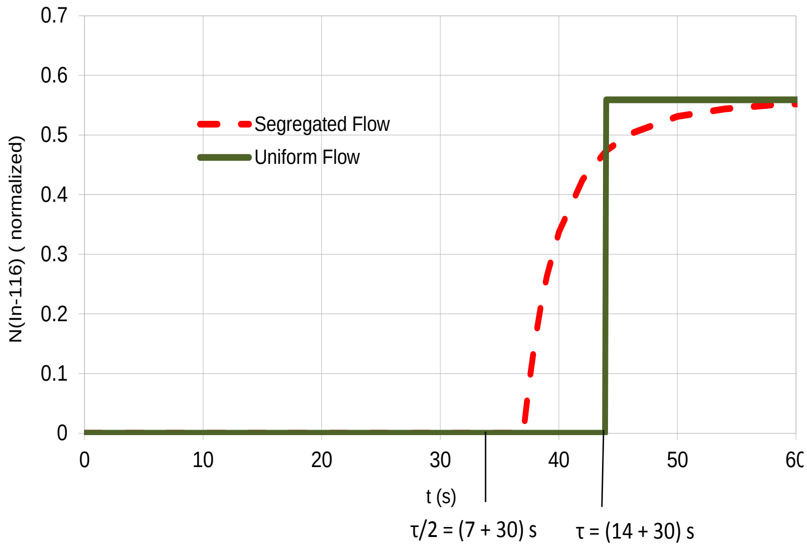

Figure 4.25. Segmented versus uniform flow along the GaInSn transport tubing.

For the geometries used here, the detector face is 27.5 inches from the center of activator volume. With a pumping speed of 1.8 inches per second, the expected arrival of the uniform flow bolus would be 15.3 seconds. However with segmented flow accounted for, the detector will begin to encounter In-116 decays at half this time, or 7.6 seconds with the bulk material peaking at 15.3 seconds. This characteristic is shown in the results.

CHAPTER 5

EXPERIMENTAL SETUP

The pumping, activation, and application system was tested on three substantially different types of neutron sources and utilized two types of radiation detectors for quantifying the amount of neutron activation in the indium. Each neutron source represented a potential option for neutrons in a clinical environment with varying effectiveness for activation of the indium isotope of interest. Containment of the GaInSn while still allowing detection of decay beta particles was a challenge that required several revisions of the application cell, with a final design being used on all three types of neutron sources.

5.1 Application Cell, Activation Area, and Pumping System

Due to the corrosive to metal nature of GaInSn, a transport system was required with no metallic components coming into contact with the eutectic. Silicon tubing was chosen to transport the eutectic between the activation site and irradiation site. In clinical applications, tubing durability and wall strength are important features, especially if small radius turns are required. Figure 5.1 outlines the main components of the system, referred to as the application cell, activation area and pumping system. The application cell must allow beta particles to escape the eutectic and enter the detector or patient treatment area. This component requires a thin exit window that contains the eutectic during circulation while still allowing passage of the beta radiation.

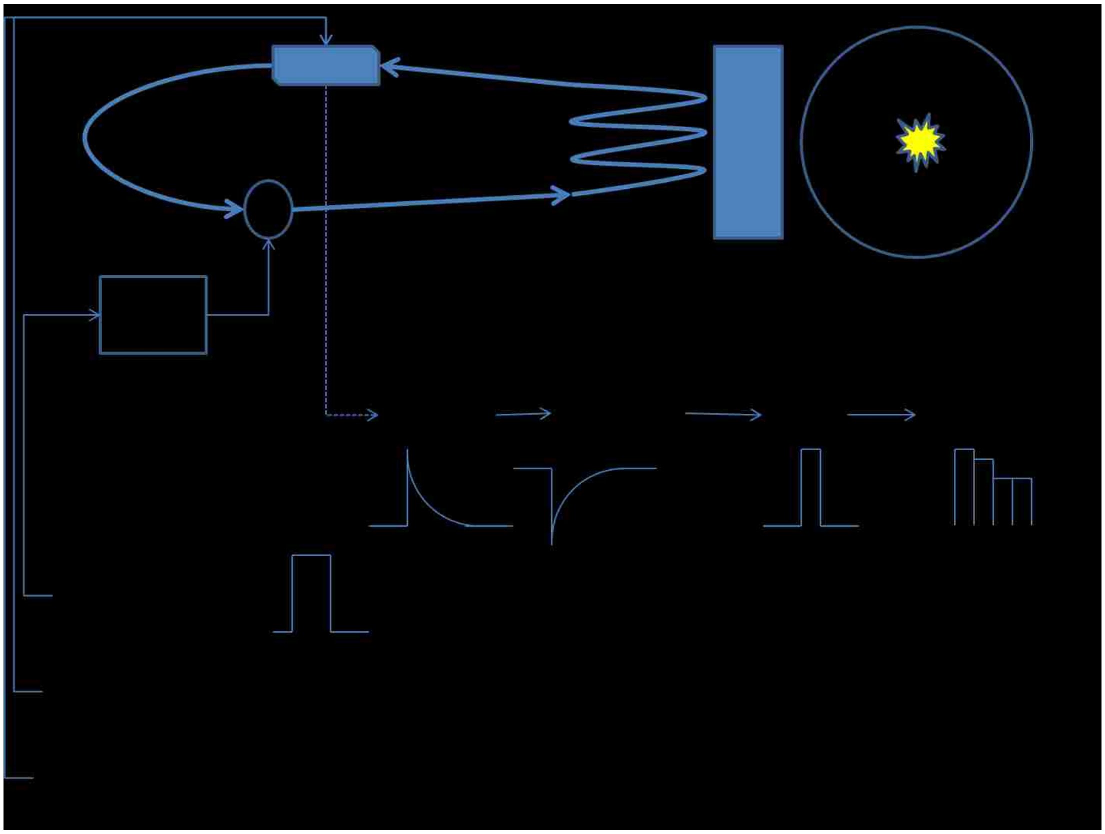

Figure 5.1. General overview of the pumping, detection and activation system and electronics used for all neutron sources.

The application cell components were constructed first in ABS plastic with fused deposition modeling (FDM) printing followed by a final design that utilized Accura® 60 plastic printed on a stereolithography (SLA) printer. SLA fabrication was used for applicator manufacturing due to tight tolerances required in the final print for passage of the liquid eutectic between tubing and applicator region. The semi-translucent property of the Accura® 60 plastic was convenient for visually ensuring that no air pockets formed in the applicator region.

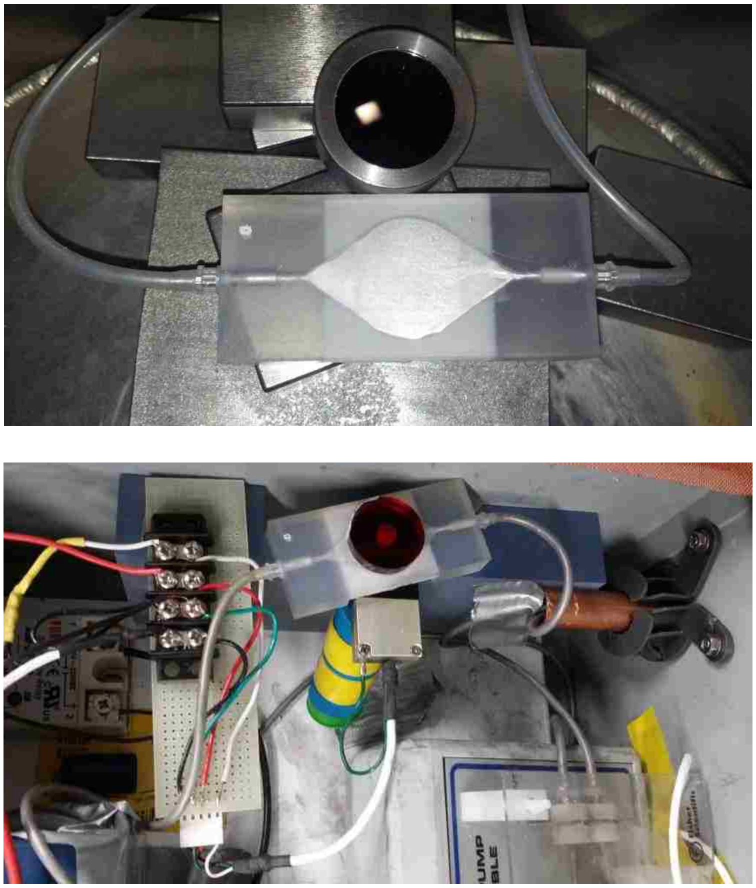

Figure 5.2. Application cell from back side showing spread of GaInSn, white styrene thin window facing down (top) and application cell inside Hoffman box with associated pumping system and electronics (bottom).

High corrosiveness of the eutectic with metals leaves only a few options for pumping and moving the material between activation site and treatment site. The material could be translated back and forth between the two sites using a plunger/piston style method or pumped in a closed continuous loop. The loop method was utilized in this work by using a peristaltic pump to squeeze the tubing and displace the fluid. This method works in much the same way that peristaltic pumps are used for laboratory fluids that must remain sterile or isolated inside tubing and how blood is moved in medical equipment. A peristaltic pumping method was chosen due to the ability to maintain a constant pumping rate that can be correlated to eutectic mass flow rate based on pump speed and the ability to maintain a closed loop system. Every revolution of the roller on the peristaltic delivers the same volume of material depending on tube diameter, with speed controller by a variable dial. A Fisher Scientific™ Variable-Flow Peristaltic Pump model 13-876-2 was used as pictured in Figure 5.3. These pumps utilize various rotary speeds and varying tube sizes to provide user selectable flow rates between 0.4 to 85mL/min. A narrower pumping volume speed is determined based on tube size selection. 1/16" ID tubing was used for a pumping volume speed of 3.0-12.0 mL/min depending on rheostat settings. Pumping speed rheostat setting was recorded for every irradiation and measurement to provide eutectic flow rates.

Figure 5.3 Fisher Scientific™ Variable-Flow Peristaltic Pump [58].

5.2 Radiation Detection System

Detection of decay radiation from the indium flowing through the applicator, both beta particles and gamma-rays, was performed with a High Purity Germanium (HPGe) detector manufactured by Ortec for spectral measurements of gamma radiation and by Cadmium Zinc Telluride (CZT) detectors by eV Products for dose measurement of the beta decay. The HPGe was utilized primarily for identification of any additional unwanted isotopes using specific decay gamma rays in a spectral analysis. The solid state HPGe detector is cooled with liquid nitrogen and offers very low electron hole (e-h) pair energy thresholds and excellent gamma-ray energy resolution can be achieved, allowing identification of activated isotopes within the eutectic. With a thin beryllium window to allow passage of the betas, the HPGe also offers complete beta absorption and excellent gamma-ray energy resolution. However since the HPGe was only used with the low activity Pu-Be source, beta dose was not quantified using this detector.

CZT type detectors were used primarily to detect beta particles while offering significantly lower gamma-ray background than HPGe. With a thickness of only 5mm the CZT has poor photon detection efficiency for higher energy gammas due to a small probability of interaction in the volume. Beta particles of the energy investigated here, on the other hand, are fully absorbed in the CZT and provide complete energy deposition with even a 3MeV beta stopping before a depth of 4mm in the detector. CZT also offered the advantage of no need for liquid nitrogen cooling and associated heat transfer components and electronics.

A third detector type, the silicon PIPS type detector, traditionally used for alpha and beta detection, was initially used with poor outcome due to the limitations of measuring beta particles with the high relative energy of the In-116 decays. 700 micron thick active depth PIPS were utilized but had insufficient active depth to fully stop the In-116 beta particles. This results in only partial charge collection of the betas. PIPS also lack the thickness and density to collect gamma-rays and therefore provided no useful purpose for In-116 measurement. While thicker depletion region PIPS are available, up to 1000um [55], cost and availability prevented their use in this work with CZT performing excellently in their place.

5.2a HPGe experimental setup

As part of the effort to measure any potential impurities or unknown isotopes that might lead to undesirable secondary decay radiation, an HPGe detector was used to measure activation of a eutectic sample after irradiation with the UNLV Pu-Be source. Energy spectrums from the In-116 decays were measured using a multi-channel analyzer mode on a portable Canberra Falcon-5000 HPGe detector. A 1 cc sample of the eutectic was irradiated in the Pu-Be access port for 1 hour to match the approximate amount of eutectic typically present during irradiation by the DPF and X-Ray photoneutron source. The 1 hour time of irradiation was chosen in order to allow sufficient buildup of any potential activation isotopes.

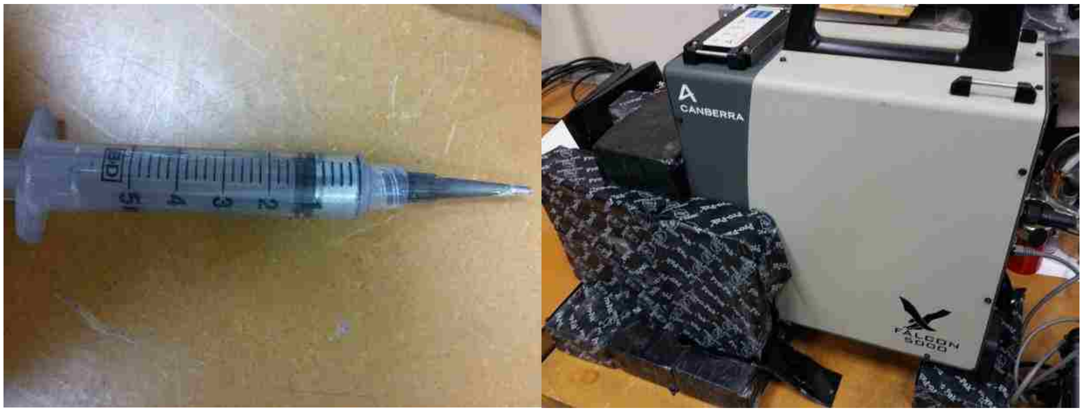

Figure 5.4 GaInSn sample irradiated on Pu-Be and shielded HPGe detector.

The HPGe was calibrated using a 4 point method with three gamma check sources according to Figure 5.5 with an excellent linear channel/energy response. The HPGe was operated at -3400V, x5 Gain, 1.9x fine gain, with a shaping function setting of 8.8us rise time, 1.2us flat top and auto base line restore.

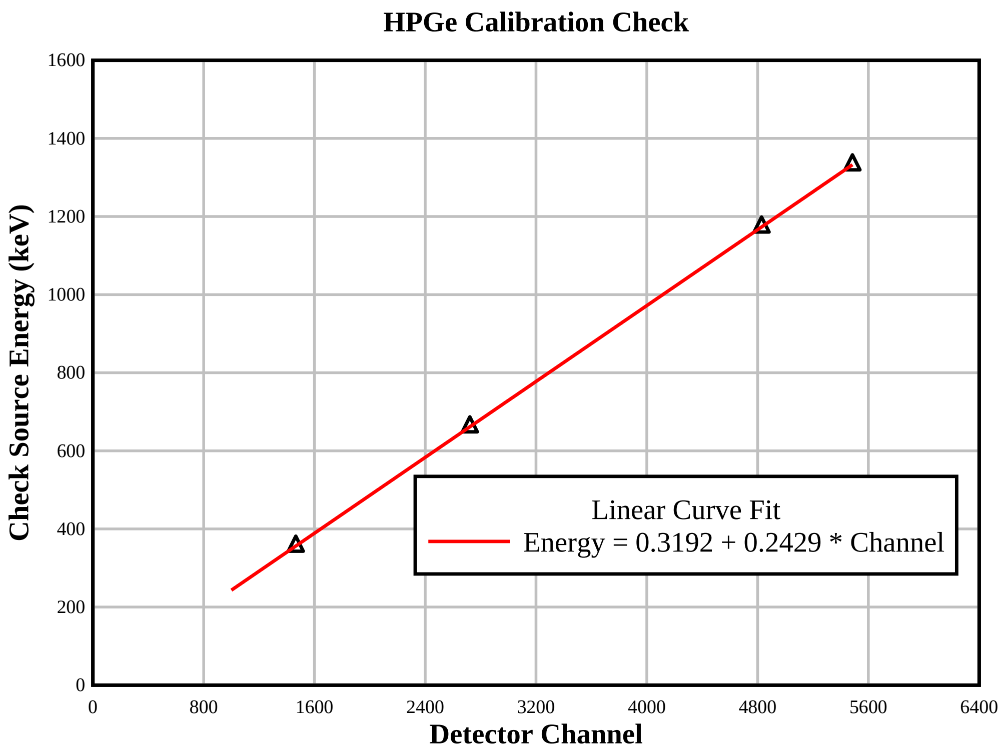

Figure 5.5. HPGe calibration curve fitting with Co-60, Cs-137 and Ba-133 sources.

5.2b CZT experimental setup:

Three identical CZT detectors, manufactured by eV Products, model number A4, were used in the course of the study to quantify beta decay. These detectors house onboard preamps and their solid aluminum housings pictured in Figure 5.6 were modified to allow passage of beta particles into the CZT crystals by opening a hole in the aluminum and plastic housing. Since the eutectic is contained in the applicator cell behind a thin styrene layer, the CZT was exposed to the air with the applicator facing the detector. The active detection region consisted of four 5x5x5mm^3 crystals for a total surface area of 1cm^2 and thickness of 5mm. This surface area and thickness is important for calculating the beta fluence intersecting the detector and for calculating the equivalent dose that would be delivered to tissue. All beta measurements were performed with a detector bias potential of +63V to +75V depending on the power source and preamp potential of +12V to +17V.

Figure 5.6 CZT detector with preamp electronics (left) and active 10mmx10mm CZT face (left highlighted).

5.3 Data Acquisition Procedure

Data collection for both dose measurement and isotope identification was accomplished using a pulse counting technique commonly referred to as a multi-channel scalar (MCS) method, in addition to a pulse height measuring technique called pulse height analysis (PHA). PHA is often performed using a multi-channel analyzer (MCA) mode to keep track of the height of voltage pulses from the radiation detector. In general, MCS mode counts total pulses over time increments to track trends, while MCA mode builds a spectrum of the number of pulses of certain heights. As discussed earlier, a radiation detector utilizes the charge deposited by an interacting particle to produce a current across a material with an applied voltage. Detectors utilize materials as varied as air or gasses mixed to produce desired characteristics, to materials such as pure semiconductors. This work utilized the CZT and HPGe semiconductor materials which rely on the release of electron-hole pairs that then migrate through the material along the applied voltage fields to the anode and cathode, producing a pulse with a height corresponding to the particle energy.

In MCA counting modes the height of these pulses is measured and the total particle energy deposited in the detector is then known. Individual pulse heights can then be binned together according to voltage magnitude to produce an energy spectrum. This energy spectrum is a pulse height histogram with bins equivalent to the frequency of pulses with the same heights, and thus energy, together along the abscissa. This energy spectrum can be used to identify a particular isotope or isotopes as the source of the radiation. In contrast to MCA mode, in MCS mode the frequency of all pulses during a specified time window can be measured to produce a time history of interactions. In this mode, a pulse height window is sometimes used as a discriminator to count pulses of certain energies during a window of time. MCS mode counting produces time decay plots which can be used to identify the half-lives of the parent isotopes. Experiments here utilized MCA mode for HPGe spectral analysis and MCS mode for half-life decay fitting and for total dose/activation measurement.

While the energy deposited in a detector by very slow count rate isotopes could be measured directly by an oscilloscope, the effects of pulse pile up require the use of hardware or software capable of dealing with radiation pulses that begin to pile on top of each other. This effect is due to the capacitive nature of a radiation detector and the decay tail that occurs as the electron-hole pairs move towards the anode and cathode, respectively. After a single radiation interaction produces one pulse which then begins to decay, another pulse arrives before the capacitive decay has finished and stacks on the tail, causing that pulse to register an artificially large pulse height. This false pulse height is compounded when the count rate becomes so high that the detector can saturate and no longer register events. When saturation occurs, the detector is essentially "dead" and thus the frequency of this period is referred to as the detector dead time.

Pulse pile up is primarily dealt with using pulse shaping techniques by analog circuitry techniques or more recently digital pulse shaping. Dead time is a function of detector characteristics, such as electron-hole mobility and applied bias voltage. Dead time in this work was not a significant issue due to the low to moderate count rates observed in the detector. Pulse shaping was accomplished with digital analysis in the MCA and MCS software Genie 2000 by Canberra, and MCS-32 by Ortec. Data acquisition utilized the Canberra DSA-1000 which provides both MCS and MCA acquisition modes and digitizes the pulses for pulse shaping in the software along with Ortec Easy-MCA's. Pulse pile-up was prevented through the use of either amplifiers with built in shaping or constant fraction discriminators.

MCS mode retains time information for the detector and is therefore extremely useful when determining parent isotopes based on half-life using decay of activity. While it is now possible with newer digitizer software to retain both time and energy history for an individual event, the limitations of a CZT detector and broad beta energy make energy information unreliable in this case. MCS mode data collection used 100 millisecond time bins with all pulses within a selected energy window binned into a histogram. 100ms time bins allowed excellent resolution for dealing with isotope half-life values in the 2 to

60 second range. MCS data collection also allows for analysis of fluid pumping characteristics as arrival times of activated material are observed. Equipment used to collect and analyze output from the CZT detector for the three types of neutron irradiation are listed in Table 5-1. Differing hardware and software combinations are not expected to change the quality of data collection from each type of neutron source.

Table 5-1. Pulse shaping and data collection modules for experimental runs.

Pu-Be Irradiations
Ortec Inverter NIM module
Ortec NIM module 584 Constant Fraction
Canberra DSA-1000 MCA / MCS
DPF Irradiations
Ortec Inverter NIM module
Ortec NIM module 584 Constant Fraction
Ortec MCS-32
Varian M6 Irradiations
Ortec NIM module 682 Spectroscopy Amplifier
Ortec MCS-32

5.4a Neutron Activation Sources: Dense Plasma Focus

Activation of the GaInSn mixture with a pulsed Dense Plasma Focus (DPF) neutron source presented several challenges to successful data collection versus a static and continuous neutron source such as the Pu-Be or Clinac. Due to the extremely short pulsed nature of the source, all activation takes place within the pulse time length of the machine which is about 100ns in this particular case. Near instantaneous activation eliminates the need to pump and stop the fluid near the source long enough to saturate and reach equilibrium, as would be required with a continuous source. However this exceptionally high yield of neutrons in a short time period requires a high current input from a large capacitor bank over a short period of time. This creates significant electromagnetic interference (EMI) that can disable or damage electronics in the vicinity of the device. Since the fluid must be pumped quickly from the activation cell to the applicator cell after activation, placing the detection and pumping assembly at an EMI safe distance from the DPF was not an option. Due to this challenge, the detector electronics were EMI shielded and turned off as an additional precaution during actual firing of the DPF.

To accomplish this, a metal Hoffman style box was used to house the entire experimental assembly, including the pump, detector electronics, applicator and triggering relays. Power for the pump was provided by a battery inside the enclosure and voltage for the detector was applied externally over a BNC cable from a remote power supply that was off during shots. Communication with the MCS card was provided over a 100ft BNC cable to a monitoring PC. A trigger was also run to the enclosure to turn on the pump. This allowed all electronics to be shielded from the EMI and remain off during a shot while enabling them to be quickly turned on immediately after neutrons were produced and the GaInSn was activated.

During all DPF shots, multiple independent neutron yield measurement systems are operated to determine the number of neutrons emitted with every pulse. The DPF can vary in output over several orders of magnitude, so shot-to-shot yield measurement is important. For these runs, independent DPF neutron yields from a beryllium activation detector are reported for comparison to In-116 activation results. The beryllium detector has an expected uncertainty of ~10% in yield reporting.

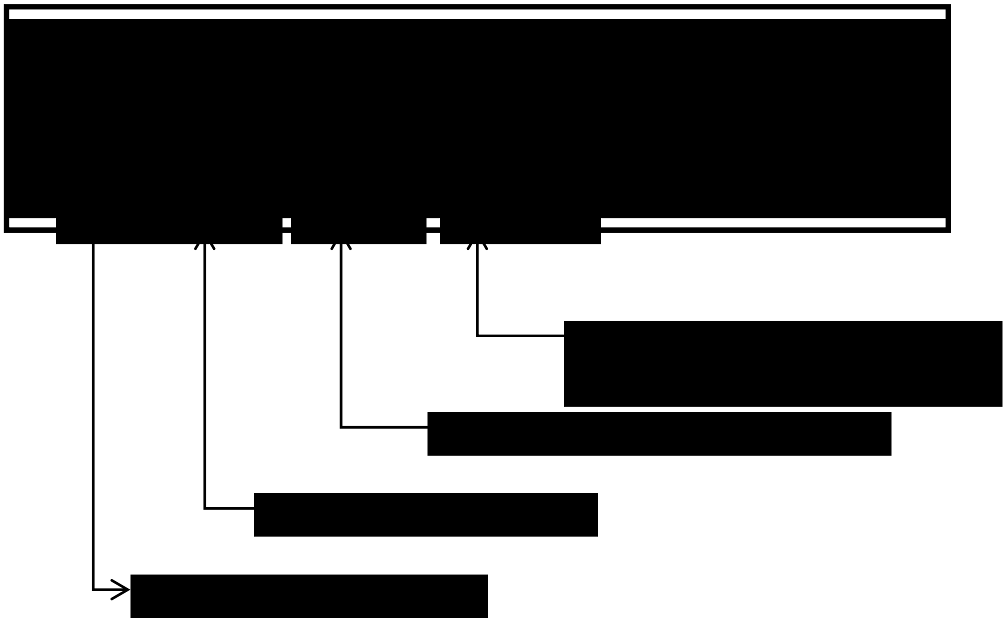

Figure 5.7 External inputs and outputs to detection and pumping Hoffman box.

Figure 5.8 Irradiation setup with pump and detector, transport line to moderating material and DPF neutron source (left) and close up of transport tubing on moderator (right).

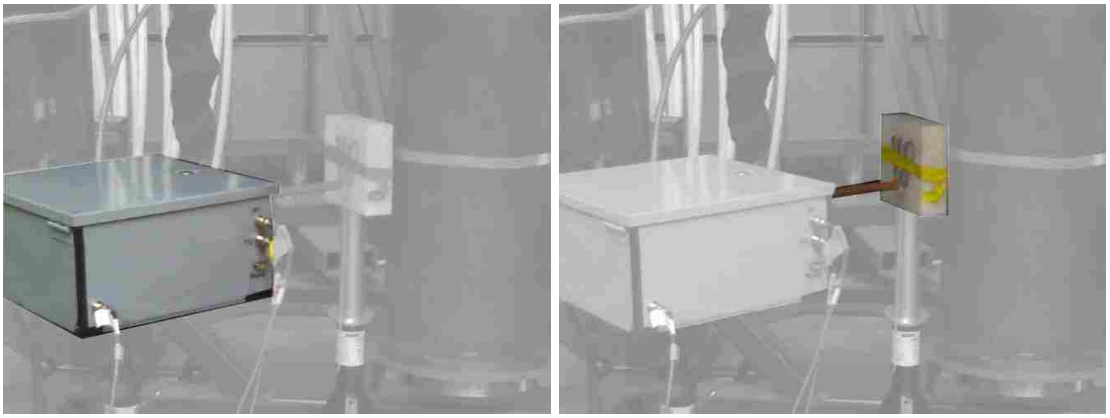

Figure 5.9 Hoffman box containing pump and detector (highlighted left), transport line to moderating material and DPF neutron source (highlighted right).

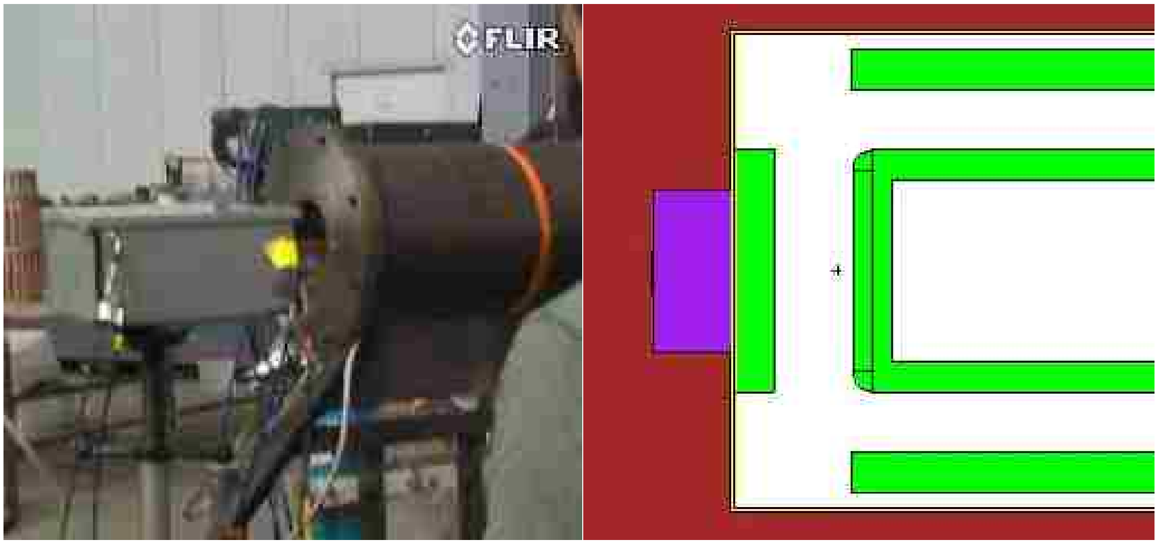

Figure 5.10 The pumping system was also placed in the DPF tube turned horizontal to the ground to reduce distance from the pinch point, an “INNY” configuration.

This same irradiation, pumping and detection setup in an EMI shielded Hoffman was used for both the Pu-Be and photo-neutron sources as well since it provided a compact and portable method of irradiation and counting of the In-116 decay.

5.4b Neutron Activation Sources: Plutonium Beryllium (Pu-Be)

With a significantly lower neutron yield than a DPF, the Pu-Be source was used primarily for spectral measurements and initial feasibility studies since low activation amounts make this not suitable for providing clinical doses. Spectral measurements as discussed earlier examined the gamma decay lines of the material and can provide information on particular isotopes in the activated material. Spectral analysis is important for determining the amount of unwanted or potentially dose modifying materials that can build up with repeated irradiations.

Without a need for EMI shielding, the system could be run with continuous power and monitoring of the detector. A pumping scheme to follow predicted optimal flow and stop times to maximize activation was used as illustrated in Figure 5.11.

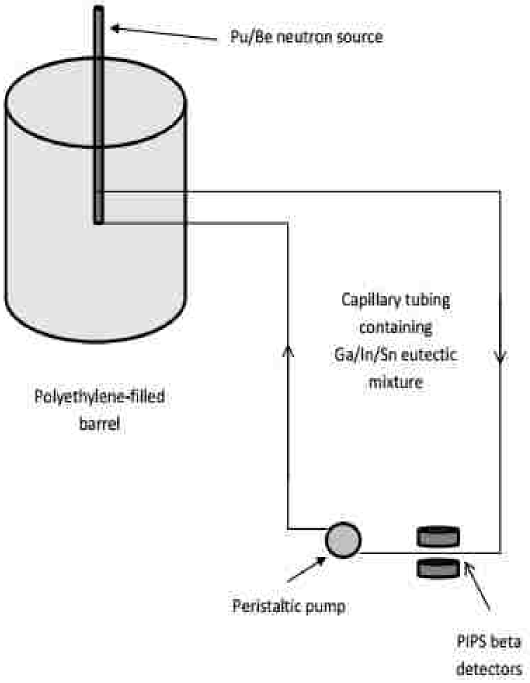

Figure 5.11. Flow Scheme Used for transport of GaInSn through a Pu-Be source.

The GaInSn mixture was pumped into an access port on the side of the PuBe source shielding drum. Models determined that proximity to the source was more effective for activation than adding moderator between the GaInSn and the Pu-Be material. Since the shield drum consisting of paraffin wax poured into steel acts as a large moderator, it was not necessary to remove the Pu-Be source and the access port acted as an effective scattering and moderating material. As indicated by the models the area in the access port of highest neutron activation effectiveness, a combination of fluence scattered neutron energy, was immediately adjacent to the Pu-Be source in a raised position. Therefore the eutectic transport tubing extends all the way from outside the port to the source. In addition to active pumping, a static volume of GaInSn was also irradiated in the Pu-Be source for 1 hour to build up any potential contaminants or unknown isotopes and subsequently analyzed on the shielded HPGe detector discussed previously.

5.4c Neutron Activation Sources: Photo-neutrons from Varian X-Ray Source

While not typically intended as a source of neutrons, high energy X-Ray producing accelerators do produce neutrons as a secondary, and often unwanted, form of radiation. These photo-neutrons are produced in the accelerator components and shielding through photonuclear interaction of the X-Rays. These photo-neutrons can become a significant source of extra dose around an accelerator as X-Ray energies exceed 9MV and are typically shielded with polyethylene. Accelerator designers take steps to minimize neutron production in accelerators above 9MV by changing both target materials and shielding materials to elements that have a higher photo-neutron threshold.

The accelerator available for these experiments, however, operated at 6MV with photo-neutron production not a typical concern. Since it was desirable to produce neutrons, a material with a lower photo-neutron threshold was used to increase production beyond what would typically be generated in the accelerator target or shielding. Neutron output from these X-Ray sources can be increased significantly by using target materials in the beam with low thresholds to produce photo-neutrons with beryllium being chosen for these experiments. A high output Varian 6MV accelerator was used with a Be target measuring 3" diameter x 6" long. Additional activation capability for the In-115 was provided by slowing the photo-neutrons with polyethylene moderation materials, moving the neutrons into an energy range with more favorable cross section for the In-115(n,γ)In-116 reaction.

Figure 5.12 Irradiation setup for the Varian M6 photoneutron source.

The above figure shows a GaInSn irradiation configuration on the M6 accelerator with a polyethylene front (top piece) and poly reflector (bottom piece). The eutectic enters the area between the poly pieces through tubing inside the copper shielding from the left and returns through the same port. Polyethylene in experiments and modeling predictions were varied according to Table 5-2 to alter the photoneutron spectrum.

Table 5-2. Polyethylene reflector and moderator configurations used with the M6.

Configuration #	**Front Moderator**	**Reflector**
M6-1	3/8” (0.953cm)	1” (2.54cm)
M6-2	5/8” (1.58cm)	none
M6-3	5/8” (1.58cm)	1” (2.54cm)
M6-4	1” (2.54cm)	1” (2.54cm)

CHAPTER 6

RESULTS

6.1 How Dose is Calculated and Presented

Since energy deposited by the electrons is measured in a detector medium that differs significantly from the composition of human tissue, an equivalent tissue dose must be calculated. This is typically done in the medical physics field through the use of ion chambers that are placed at various depths in a tissue equivalent material (TEM) or by using thin thermos-luminescent detectors (TLDs). Physical differences between the ion chamber and real tissue are then adjusted for through the use of correction factors and a depth dose profile can be made. In this particular case the electrons are of a low enough energy that very shallow depth dose profiles are produced, on the order of only a few millimeters deep. This makes physical measurements challenging compared to typical mono-energetic 6 MeV and higher accelerator electron beam depth dose profiles which instead have depth dose profiles of tens of centimeters. Because of the excellent capability for Monte-Carlo codes to predict electron behavior, a surface electron flux is measured here with the CZT detector for each neutron activation source, and a depth dose profile expected in tissue is then constructed by Monte-Carlo methods with MCNP. Physical validation of depth dose measurements would be required prior to clinical use in human medicine and these measurements would be done with repeated irradiation of TEM using stacked sub-millimeter thickness pieces of TEM material and a thin film at various depths. However with limits during certain experiments on the frequency of neutrons available for activation, this more exhaustive process is not feasible here and depth dose curves instead rely on surface dose and extrapolation to depth through Monte-Carlo modeling, a well established method for radiation interaction prediction. Figure 6.1 outlines the MCNP geometry used to determine dose at depth in tissue for the In-116 decay betas.

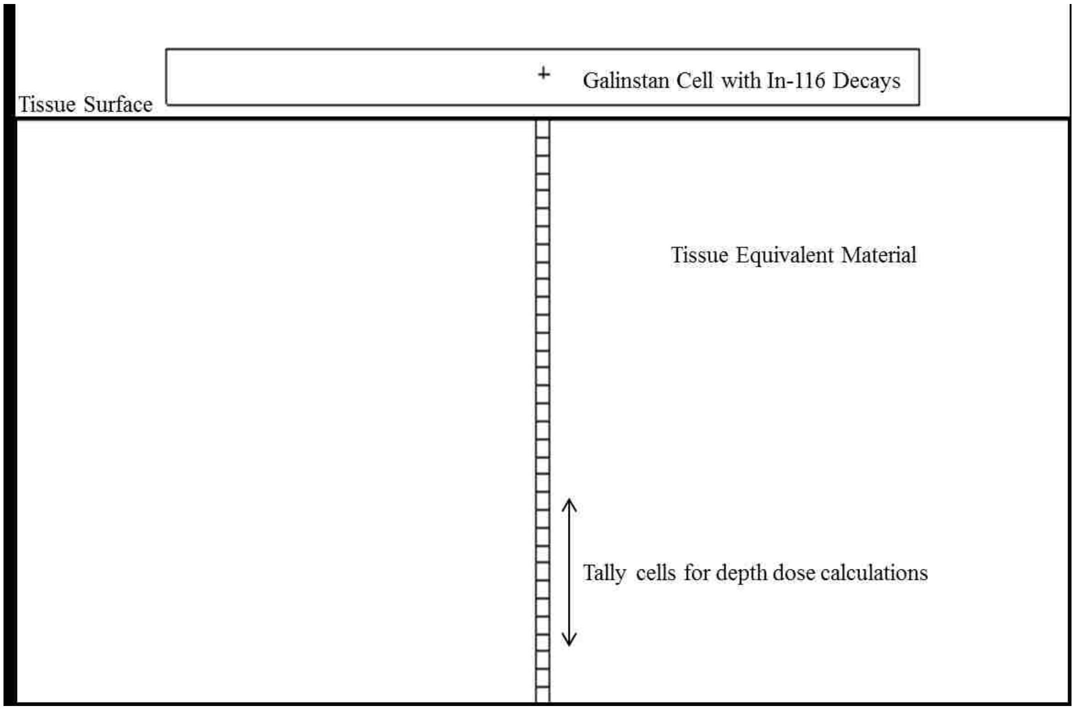

Figure 6.1. MCNP model geometry for determining PDD in tissue.

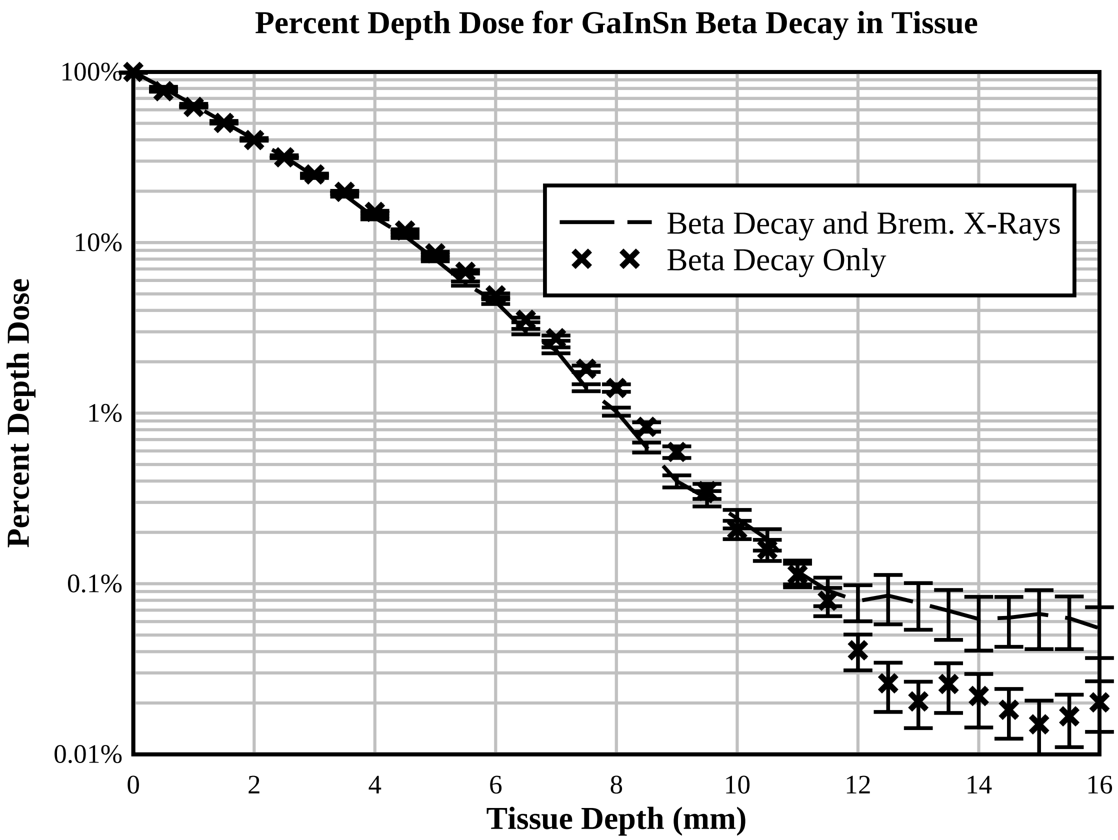

Figure 6.2. PDD for In-116 ground state decay betas in tissue with and without bremsstrahlung produced X-Rays.

The two dose curves above in Figure 6.2 show the minor contribution of X-Ray production in the GaInSn that only becomes apparent at depths greater than 12mm where the electron dose has essentially fallen off to zero. This sharp dose fall-off stands in contrast to the PDD for a current methodology for shallow tumor treatment marketed by Xoft Inc that utilizes 50kV X-Rays. As shown below in Figure 6.3, the competing Xoft X-Ray source continues to dose tissue for 10 of millimeters beyond where the In-116 decay dose essentially becomes zero. Ir-192, a standard brachytherapy technique utilizing gammas of 373 keV results in a similar PDD plot as the Xoft system.

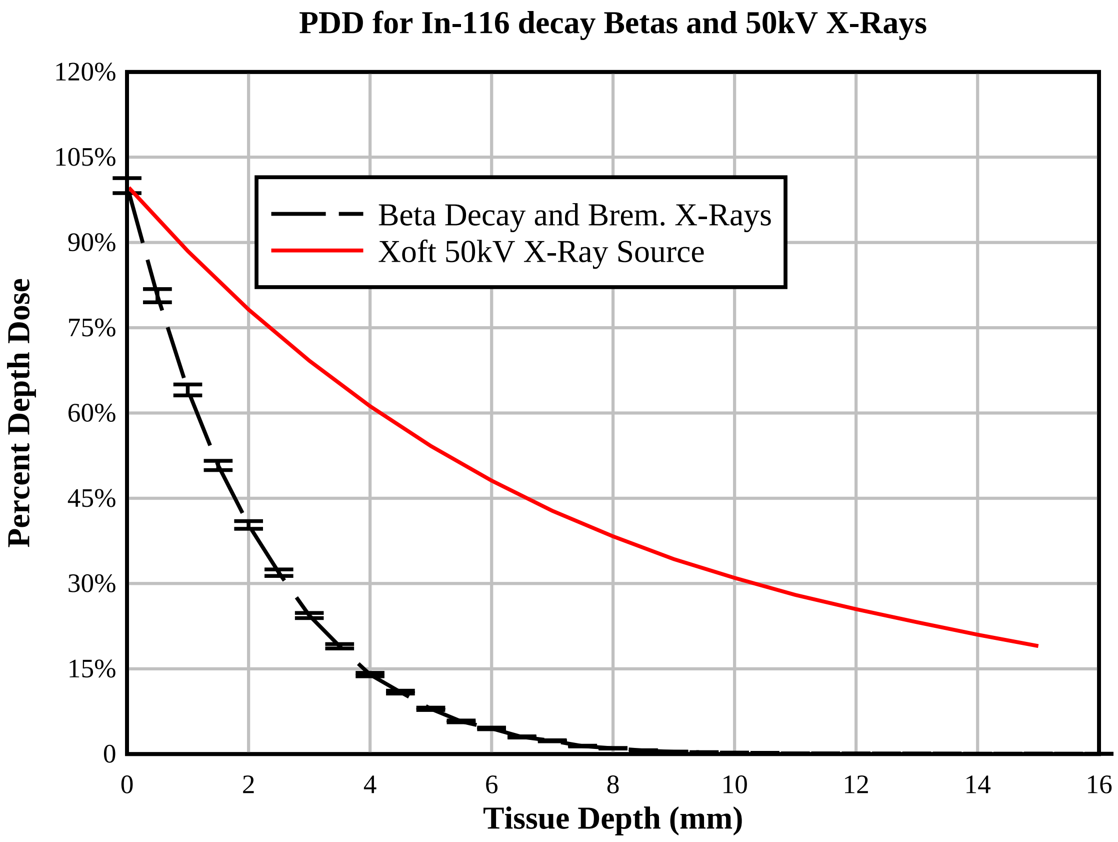

Figure 6.3. PDD for In-116 decay in tissue compared to the Xoft 50kV X-Ray source.

Percent depth doses of interest for the GaInSn decay betas are provided in Table 6-1. It is apparent that this method is most applicable to shallow lesions no deeper than 3mm, beyond which the dose falls off dramatically. Potential treatable lesions with betas that can reach this depth, such as certain types of skin cancers and corneal lesions, are discussed in the conclusions.

Table 6-1. PDD in tissue from In-116 decay in a 1/16" thick GaInSn applicator.

Depth	**PDD**
0.25mm	90%
0.5 mm	80%
1.0 mm	64%
2.0 mm	40%
3.0 mm	25%
5.0 mm	8%
10 mm	0.20%

With percent depth dose profiles established for the In-116 decay betas, we must convert the betas detected by the CZT detector to an equivalent dose in tissue. The higher density CZT compared to tissue results in electrons quickly depositing their energy in a very shallow depth. 3MeV electrons have a CSDA range of 4mm in CZT, meaning that 4mm of CZT will fully stop any In-116 decay beta. Because of this, we can assume that electrons are 100% absorbed within the CZT crystal used in these experiments. With the energy of impinging betas on the CZT known based on isotope decay properties, a measure of beta count rate in the CZT can be directly converted to energy deposited and thus dose. Based on this assumption, dose to tissue can be calculated by counting the total number of beta particles impinging the CZT detector and the values in Table 6-1 can be used to calculate both total dose and a depth dose profile.

In addition to compensating for the path length differences in tissue, surface effects of the CZT detector versus those in tissue must be accounted for. Just as correction factors are used for gas filled ion chambers to equate their response to equivalent dose in tissue, a correction factor is used for the CZT crystals used here. The large density difference between CZT and tissue has a major effect on the number of electrons that scatter off the material and do not deposit energy. Because the CZT detector is a flat, uniform material, complicating factors that arise with the use of ion chambers such as circular geometries, wall thicknesses, gas densities, active and non-active regions and other factors did not need to be corrected for.

An increased percentage of electrons backscattering out of the CZT detector and not being recorded is expected compared to electrons impinging on tissue. A Monte-Carlo MCNP model of both a tissue equivalent (TEM) and CZT detector material volume with an In-116 beta spectrum impinging on the surface was quantify electrons that enter the tissue or CZT versus those that are backscattered to determine a backscatter ratio according to Figure 6.4, also presented previously for backscatter correction in model comparisons.

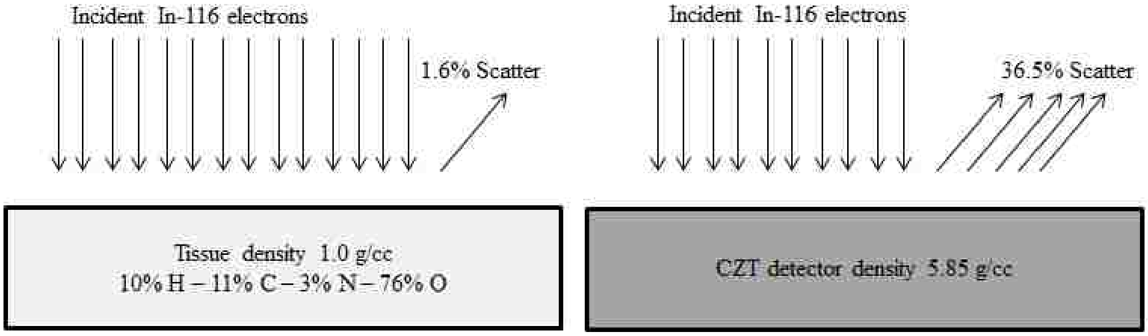

Figure 6.4. Electron backscatter geometries for tissue versus CZT detector.

The predicted backscatter percentage from CZT for In-116 decay betas is approximately 36.5% versus about 1.5% for tissue, meaning that 36.5% of the total electrons that reach the CZT detector are scattered away and deposit no energy. Therefore, to find equivalent counts in tissue based on measured counts, the CZT measured electron fluence must be multiplied by a backscatter factor, C_B, that accounts for the difference between these two scattering percentages with a value of C_B=1.6.

With an ultimate goal of delivering electron dose to tissue, results are presented in terms of gray (Gy) and one-hundredth of a gray (cGy), a standard metric unit used to quantify radiation energy deposition that does not account for differences in tissue damaging effectiveness between types of radiation. This effectiveness is the quality factor (QF) of radiation, a concept discussed previously. The sievert (Sv) is commonly used to correct for effectives in tissue, with 1 Sv equal to 1 Joule of energy deposited per kilogram of mass when the QF=1. The gray multiplied by the QF for a particular radiation type is equal to the Sv. A dose of 1 Gy with a QF=10 would be equivalent to 10 Sv, as would be calculated for alpha particles. For simplicity, since this work deals only with electrons that have unity quality factor, all doses will be presented in units of Gy or cGy and will inherently account for the electron dose quality factor of 1.

Decay activity of the GaInSn after neutron activation was measured in total electrons detected in the CZT per unit time, rather than energy deposition by individual electrons. As discussed previously, due to the natural spread in energy of beta decay particles, identifying the original isotopic source of an individual beta particle is impossible when that energy is measured independently of any other particle. When using a pulse counting technique with the CZT detector to determine dose, we must know the particle energy to determine actual dose. However this information is not present in a multichannel scalar collection mode. By counting total electrons over time, an activity decay plot is acquired which can be matched to the half-life of the original isotope. This activity decay plot can be curve fit with exponentials to correlate half-life values to known isotopes and identify the parent isotopes and the associated decay beta particles. With the parent isotopes known and total number and energy of electrons per unit time impacting the detector measured, the total decay energy deposited in the detector can be determined.

Since dose is energy deposited per unit mass that the radiation interacts with, the mass and therefore the volume in which the energy is deposited is inversely proportional to the total dose. In a high density CZT material, the electrons deposit energy quickly and in a shallow volume, leading to a high dose at the surface. In tissue, however, the electrons travel much further and spread the dose deposition over a certain depth. Dose in the CZT is therefore not equivalent to dose in tissue and results must account for increased electron path length in tissue. To accomplish this, the calculated percent depth dose tables above for tissue are created through Monte-Carlo models using thin layers of tissue to determine dose at incremental depths. Total dose at certain depths is determined by multiplying the PDD value by dose at the surface, or a depth of zero, which is considered to be 100% dose at a depth of 0mm. This surface dose is determined by extrapolating dose at a measured depth back to zero and provides a reference to determine dose at a depth of interest.

Total dose is simply the integral of dose over the total depth of penetration. A percent depth dose table is presented for each neutron activation method, Pu-Be, DPF and LINAC since electron decay energies can change based on parent isotopes and parent isotope compositions are dependent on activation neutron energies. Integral dose is then presented for each activation source and the various parameters that were investigated, including pumping times, activation times and source neutron intensities.

6.2 Activation and Dose Results From a Dense Plasma Focus Source

Activation testing with the Dense Plasma Focus (DPF) source was performed with 2 configurations of moderator along the outside of the tube (radial) and with moderator and activator cell placed axially to reduce distance from the pinch point to the eutectic. Unlike the Varian M6 which produces a volumetric source of photoneutrons along the path of the X-Ray beam in the beryllium, the DPF emits all neutrons from a small point source on the order of just a few cubic millimeters. Therefore the intensity of neutrons hitting the activator cell is a function of the $1/R^2$ drop off of neutron fluence as distance is increased. If the distance is doubled, the fluence drops by a factor of four, so proximity of the activator cell to the pinch point is critical for In-116 production..

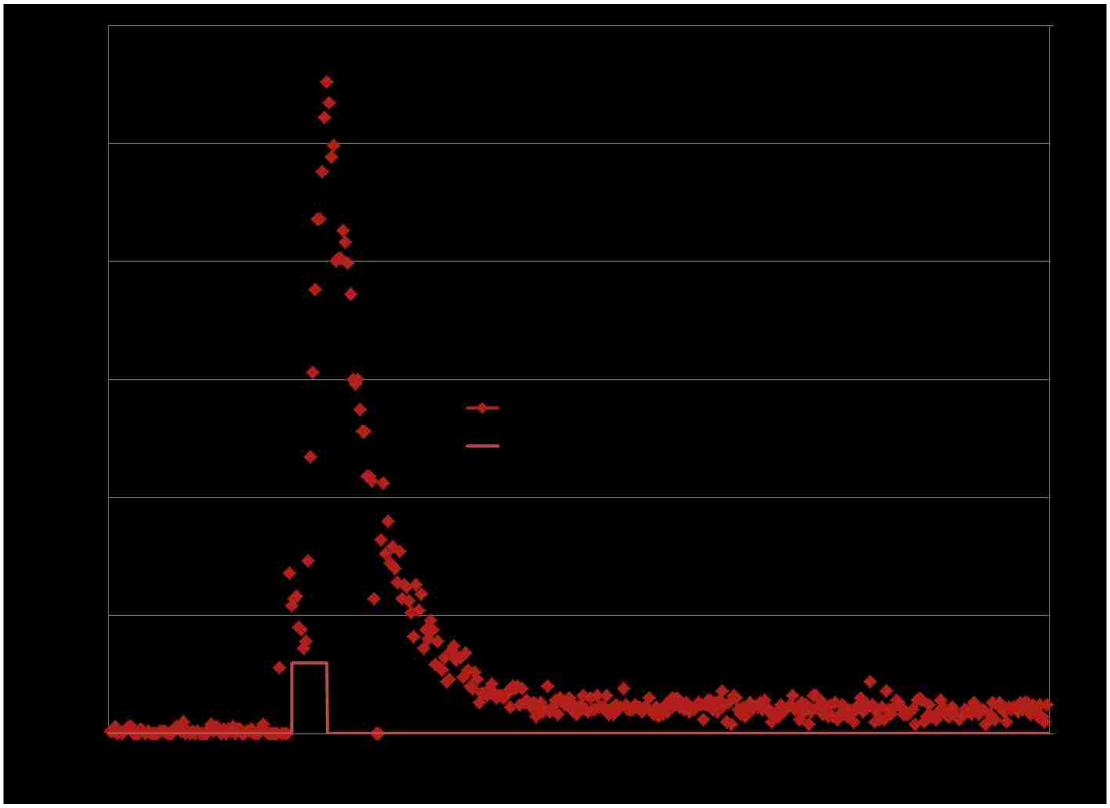

Figure 6.5. Decay data on CZT for a DPF shot followed by 15 seconds of pumping.

An example of beta decays detected on the CZT detector from the applicator cell is presented in Figure 6.5 for a single pulse of neutrons followed by 15 seconds of pumping the activated bolus to the detector. A decay line can be fit to the peak to confirm the detection of the 14.1 second ground state of In-116 as shown in Figure 6.6. Using this fit line, the total activation present in the activation cell during neutron irradiation can be determined using decay time correction and the time between the DPF "shot" and the peak of activity. The total activation in the irradiation cell is divided by the geometry-specific MCNP derived calibration factor to calculate a predicted neutron source strength. This neutron yield is compared to an independent yield detector in Table 6-2 and plotted in Figure 6.7 with good agreement.

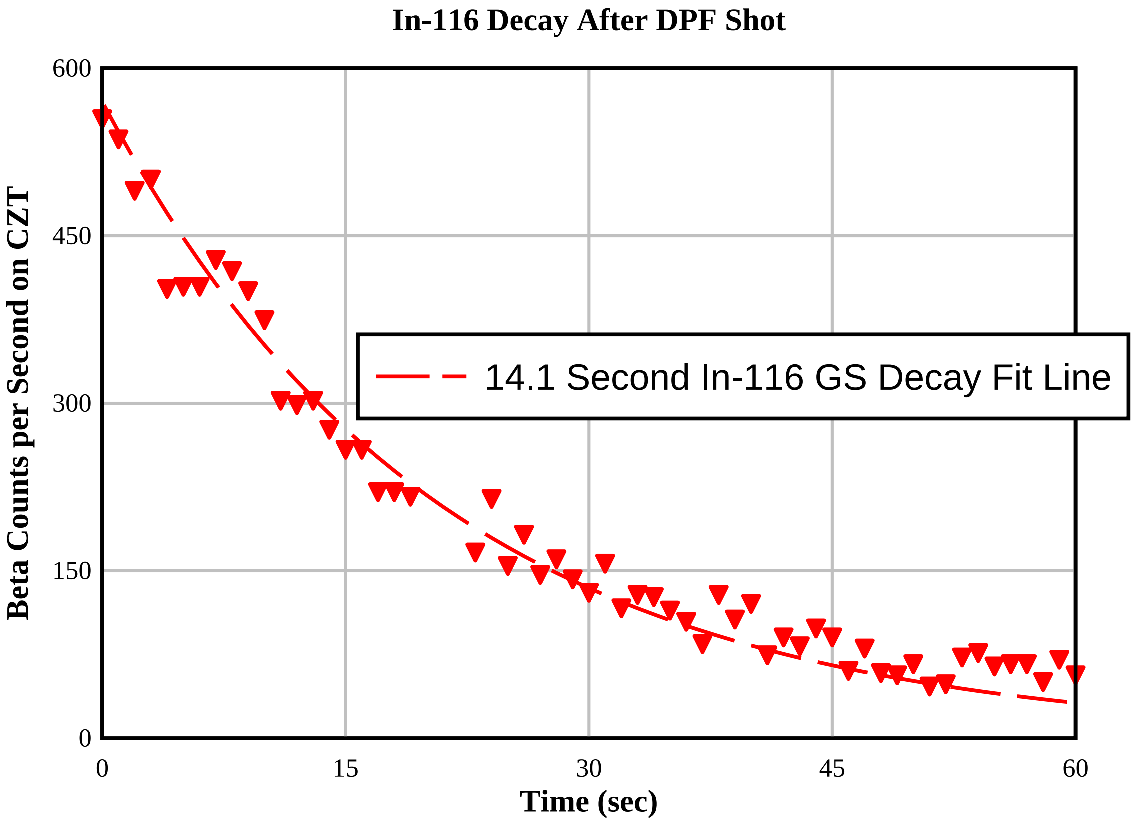

Figure 6.6. Decay data for a DPF irradiation .

Table 6-2. DPF predicted yields per shot based on CZT detector and models compared to independently measured DPF yields.

DPF Configuration	MCNP Cal Factor	Predicted Yield in neutrons/shot based on CZT counts	Be Rod Measured neutrons/shot	Models to Detected Ratio
Standard	1.7E-05	2.27E+11	2.18E+11	1.04
Flush	2.9E-05	3.03E+11	2.80E+11	1.08
Flush	2.9E-05	4.96E+11	4.63E+11	1.07
Flush	2.9E-05	1.84E+11	1.64E+11	1.12
INNY	5.0E-05	1.90E+11	1.50E+11	1.27
INNY	5.0E-05	1.56E+11	1.29E+11	1.21

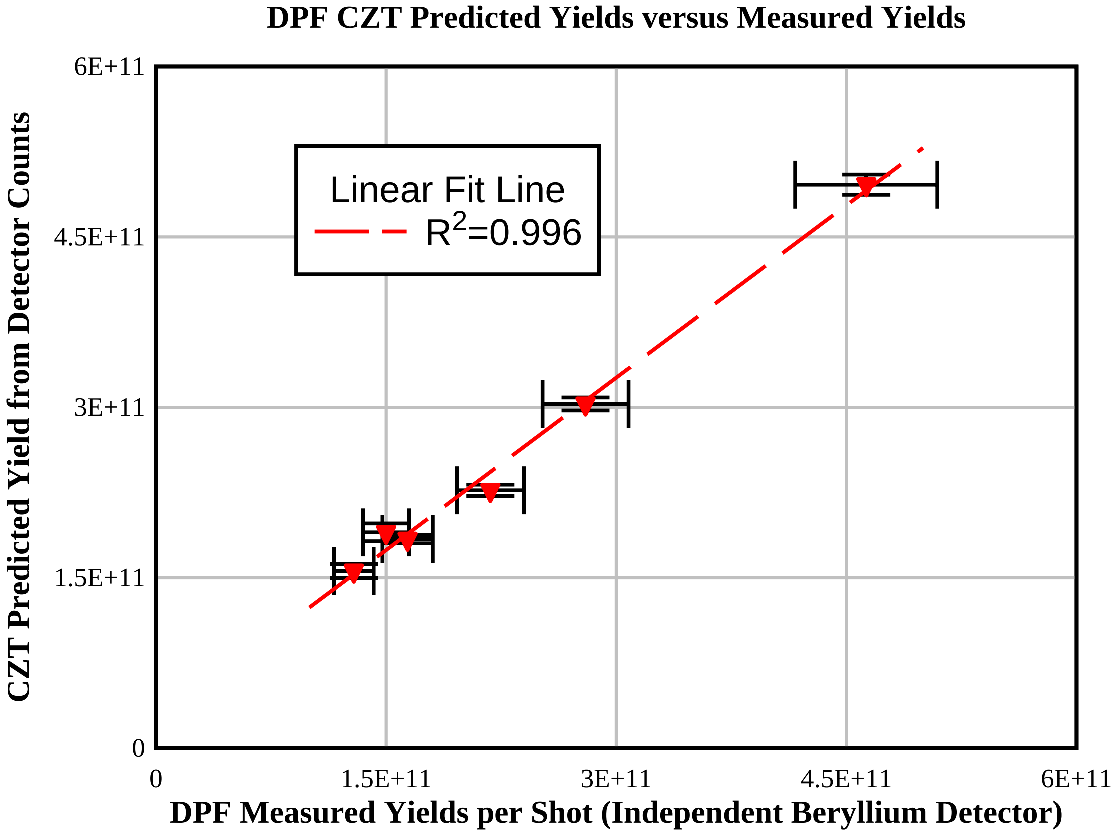

Figure 6.7. Predicted DPF yields from CZT detection of In-116 versus yield measured by independent detector showing good linear agreement.

While the decay beta measurements on the DPF showed excellent yield measurement capabilities compared to existing yield monitors, dose per shot was insufficient to be useful in a clinical setting. Results for 3 moderator configurations are presented in Table 6-3 along with optimized values. These optimized values would be the dose from increased activation achieved with the ideal moderator/reflector combination examined earlier of 2in front and 2in reflector. However even with an ideal moderator/reflector, the DPF is unable to produce sufficient activation for clinical use and the In-116 system can only be used as a neutron yield detector in this case.

Table 6-3. Dose per DPF shot in tissue at a depth of 0.5mm from In-116 decay.

Run #	**Detected counts**	**Associated In-116 Decays**	**Dose (cGy/shot)**	**Dose Rate Optimized (cGy/shot)**
2in standard	4436	1.39E+06	1.76E-03	1.11E-02
2in flush	10600	3.31E+06	4.21E-03	1.53E-02
2in flush	16702	5.22E+06	6.63E-03	2.42E-02
2in flush	7178	2.24E+06	2.85E-03	1.04E-02
INNY	12768	3.99E+06	5.07E-03	1.07E-02
INNY	9292	2.90E+06	3.69E-03	7.79E-03

6.3 Dose Results from X-Ray Photo-Neutron Source

Activation testing of In-115 was most successful with the Varian M6 X-Ray source and a beryllium photoneutron target due to the high constant flux of neutron available from this source. Raw data from one of these runs and an overall experimental timeline is presented in Figure 6.8. The ideal irradiation protocol involved 60 seconds of neutron irradiation in the M6 with detector electronics off, followed by pump start and the detector powered on. The activated In-116 bolus shows a clear arrival at the detector towards a peak value depending on pump speed

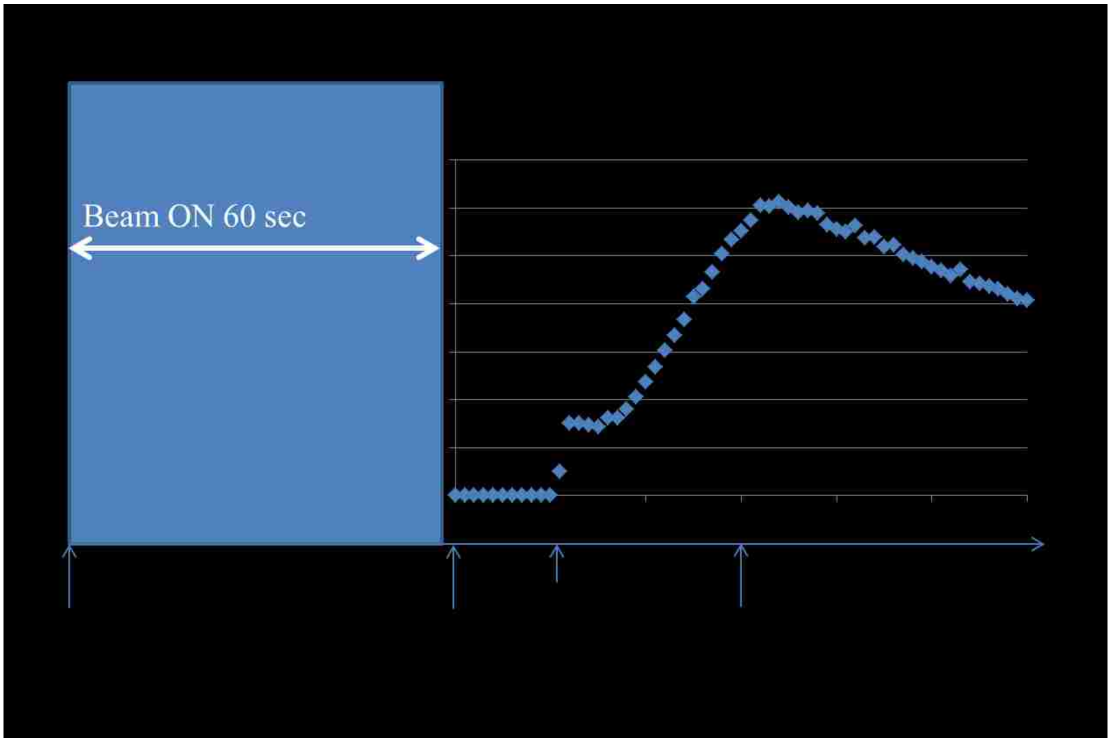

Figure 6.8. Irradiation protocol followed for data collection on 15 seconding pumping runs.

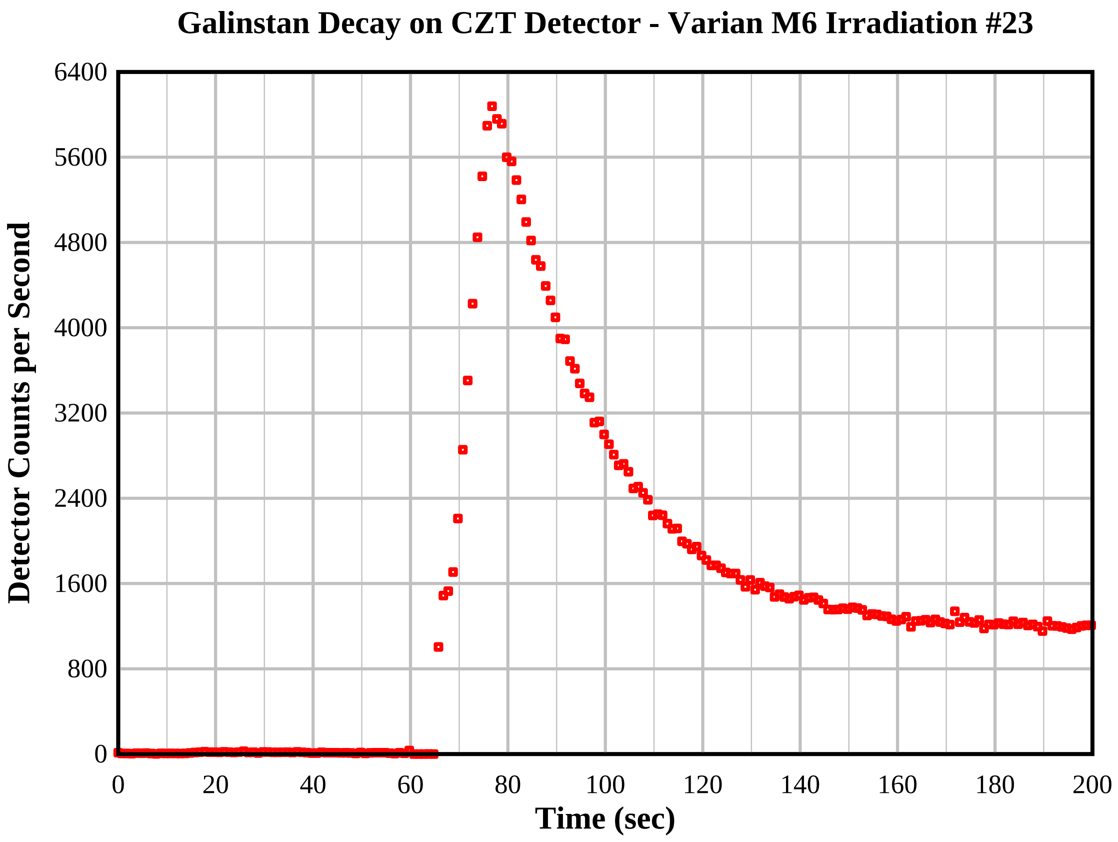

Figure 6.9. GaInSn decay on CZT detector for Varian M6 irradiation showing activated bolus arrival and subsequent decay on detector.

The figure above is a raw data set from a 60 second irradiation with 15 seconds of pumping. Since the m1 activation state becomes more prevalent as irradiations are repeated, this m1 background must be subtracted from each irradiation result to determine the contribution of the primary ground state decays. The background subtraction analysis was performed for all runs and is presented in detail for this irradiation run only, with a summary of the results given for subsequent runs.

Subtraction of the background m1 state component has an added benefit of confirming the isotopic composition of the decaying isotopes since unexpected components will appear with distinct decay half-lives. These decay fits can be used to confirm prior HPGe spectral analysis showing that the GaInSn is only exhibiting 2 decay components of In116, the 14.1 second ground state and the 54.3 minute m1 state.

The m1 state decay line is fit to the data from Figure 6.9 after allowing the 14.1 second ground state to decay sufficiently. The fit line data was chosen as 300 seconds to 2100 seconds with a fit line used assuming a single 54.3 minute decay half-life. This single decay component fit line for the ground and m1 states is calculated using equation 6.1 here:

$$A(t) = A_o * e^{-\frac{ln2}{t_{\frac{1}{2}}} * t} \tag{6.1}$$

with A_o the extrapolated decay activity at time zero, $t_{1/2}$ the half-life of the component and t the time in seconds. Using this fit line in Figure 6.10 below we see an excellent fit for the In-116 m1 state using a half-life of 54.3 minutes and an Ao of 1185, assuming that time zero occurs at the peak of the bolus arrival and start of decay at t=77 seconds previously in Figure 6.9.

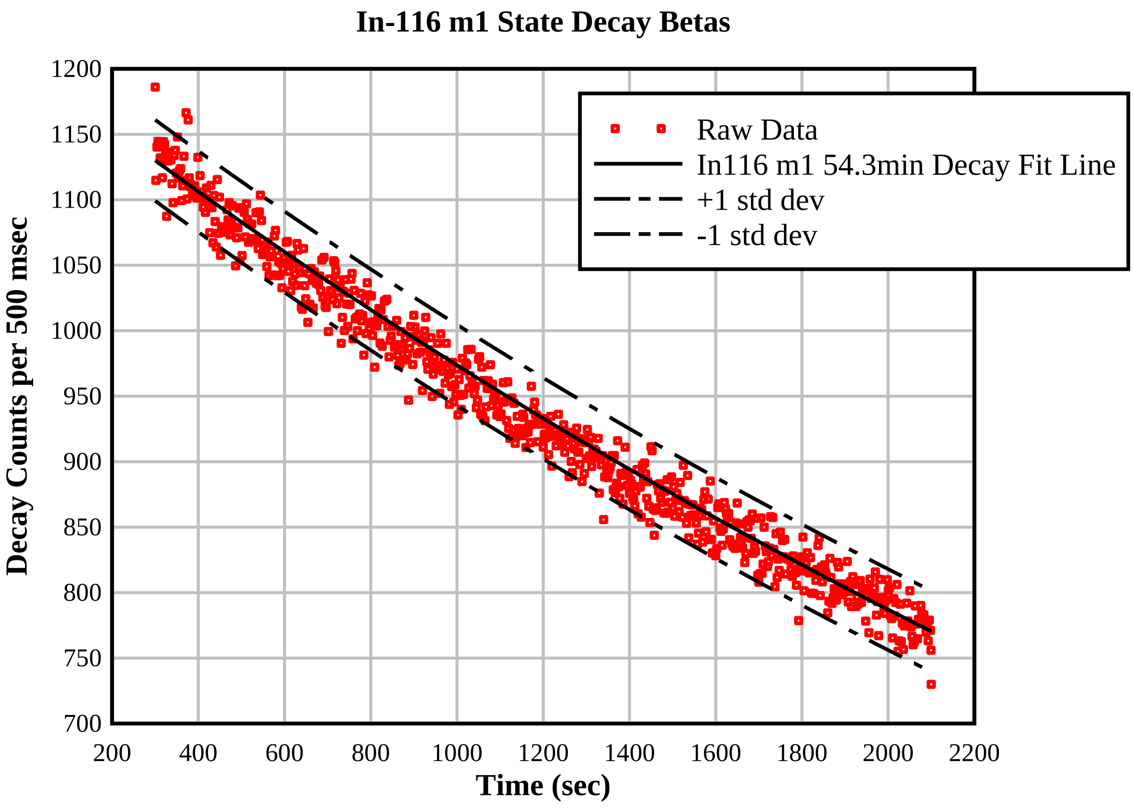

Figure 6.10. In-116 metastable state m1 54.3 minute decay fit line.

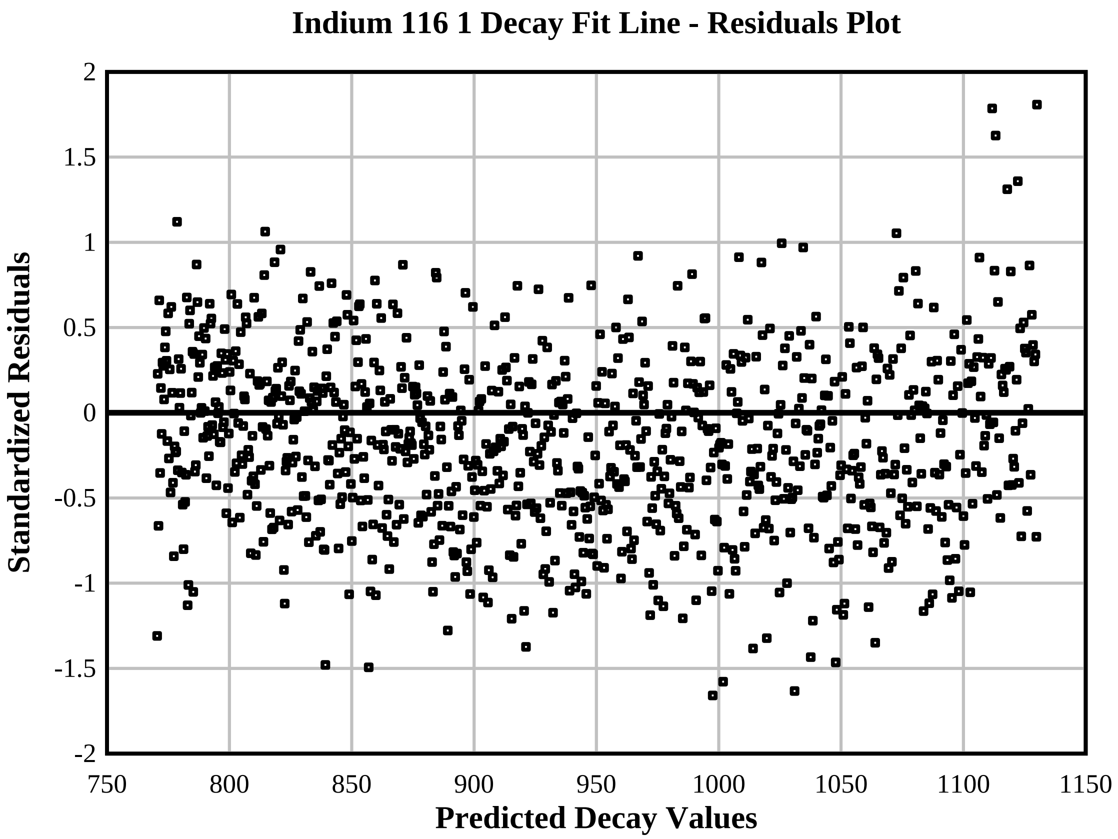

Figure 6.11. Residuals analysis for In-116 metastable state m1 54.3 minute decay fit showing good random residual spread.

Both Figures Figure 6.10 and Figure 6.11 show excellent fit to the m1 component of In-116 decay from 300 seconds to 2100 seconds. The residuals plot above is the difference between measured decay and the decay fit line using the In-116 m1 state. Random distribution of residuals means the fit line is sufficient. Using this m1 state fit line, the raw decay from the applicator cell after the M6 irradiation can be corrected to provide the In-116 ground state component only with a 14.1 second half-life.

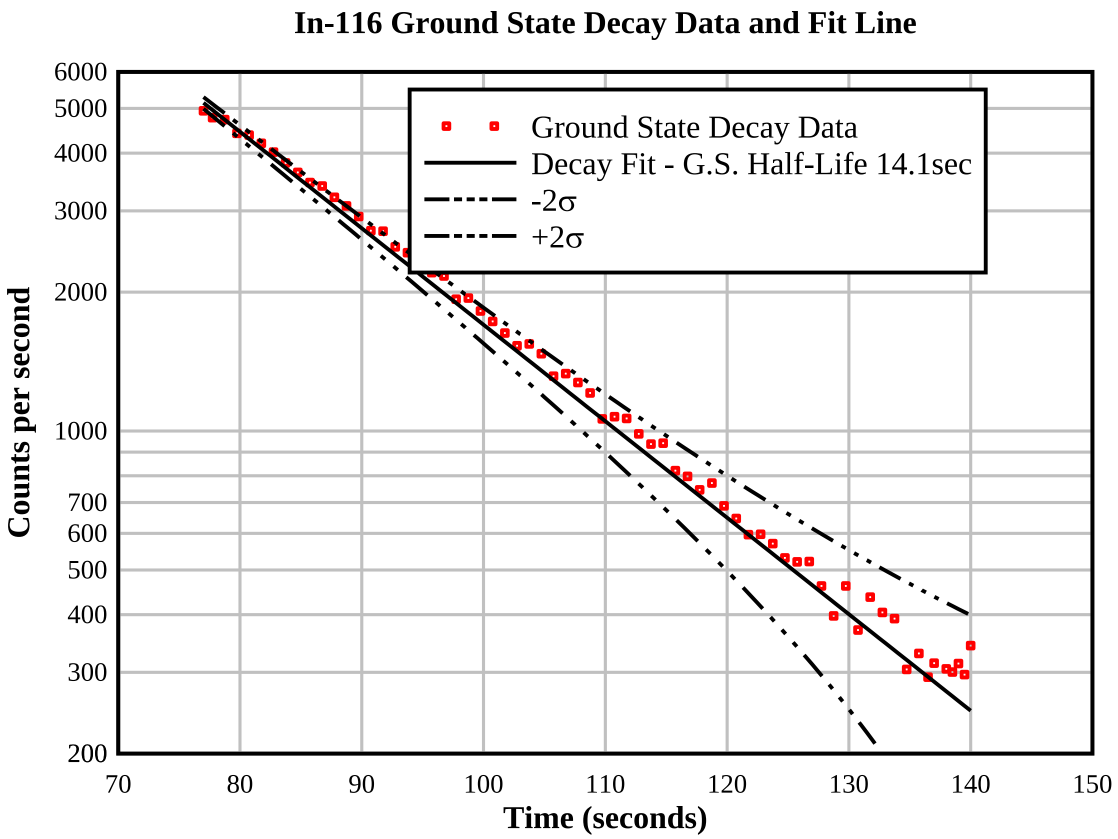

Figure 6.12. Decay fit line for In-116 ground state with m1 state subtracted.

It is apparent from the fit line data for the ground state and m1 In-116 decay states (14.1 seconds and 54.3 seconds, respectively) that no other isotopes are present in the GaInSn decay after irradiation as confirmed by the HPGe spectral analysis on the Pu-Be activated sample. Based on this, we can assume that all dose delivered to the detector or equivalent tissue is from these two decay states. Combining these fit lines and summing the expected decay values from both states with the experimental data gives an excellent fit to the observed GaInSn decays on the CZT detector as shown in Figure 6.13.

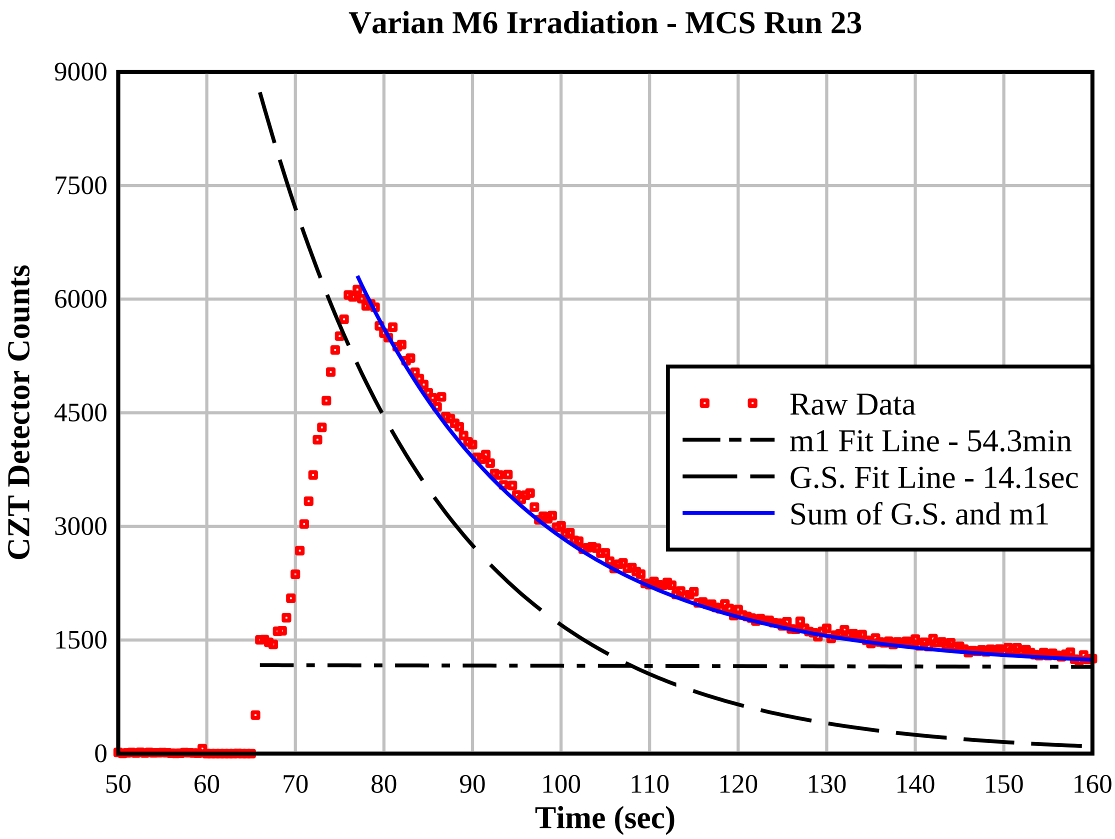

Figure 6.13. Detected GaInSn activity on CZT with ground and m1 component fits.

With confirmation that we can separate the decay into two components from In-116 ground state and m1, the contribution to dose from each metastable state can be evaluated. The above figure can be separated into CZT detector counts based on type of particle by breaking down the decay spectrum into ground state betas, m1 betas and gammas, and background. The same dataset used above with beam irradiation stopping at 60 seconds, pump turning on at 60 seconds, and peak arrival of the activated bolus at 77 seconds, is presented in Figure 6.14.

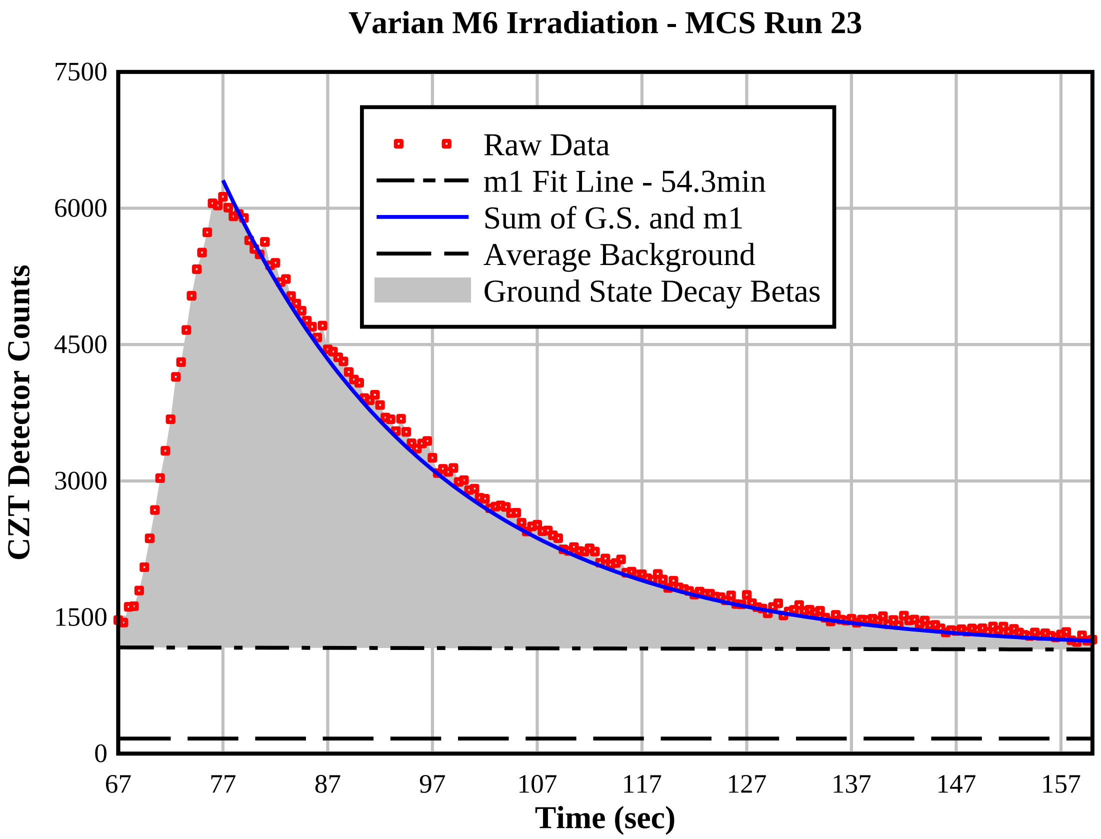

Figure 6.14. Three decay components of CZT detector counts from decaying GaInSn.

Due to the buildup of the m1 decay state, its contribution to dose must be evaluated. Since the m1 state decays primarily by low energy beta emission and higher energy gamma rays, it is not expected to contribute significantly to the shallow depths of the percent depth dose plots above. However, the gammas would present a longer tail as they penetrate deeper into tissue than the In-116 grounds state beta particles. A comparison of the decays of the ground state and m1 state is presented in Table 6-4. Note that the m2 state is included in the m1 cross section since it quickly decays (2 second half-life) to the m1 state.

Table 6-4. Decay properties of the ground state and m1 state of In-116.

	In-116 Ground State	**In-116 m1 metastable state**
Half-Life	14.1 seconds	54.3 minutes
Thermal σ	81 barns	121 barns (includes m2 state)
Decay Radiation (per decay)	β- 3.28 MeV (98.7%)	β- 0.604 MeV (10.3%) β- 0.876 MeV (32.5%) β- 1.01 MeV (54.2%)
	Gammas	Gammas
	No Significant Gamma emission	0.138 MeV (3.70%) 0.417 MeV (27.2%) 0.819 MeV (12.1%) 1.097 MeV (58.5%) 1.294 MeV (84.8%) 1.507 MeV (9.92%) 2.112 MeV (15.1%)

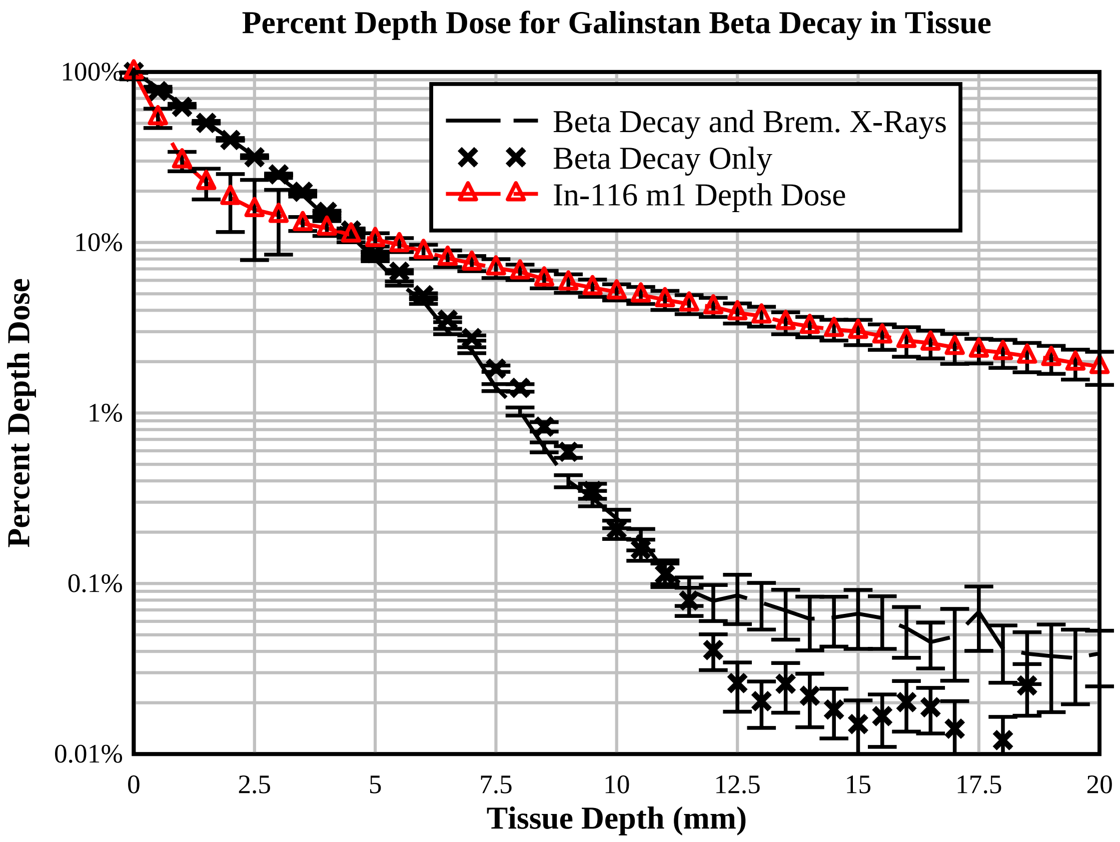

Figure 6.15. Comparison of PDD between In-116 ground state and m1 decay radiation.

While it appears that the m1 decay state significantly increases the PDD at depths, these two states occur with large differences in half-life and therefore cannot be summed into a single dose profile curve. Due to buildup during repeated irradiations, the activity of the m1 state can increase during decay over tissue. Therefore they must be evaluated separately with the doses for the ground state and m1 state calculated independently with each irradiation. Doses are presented here first for the ground state 14.1 second decay for all cases. Predicted m1 dose that would be delivered with continued irradiation is then presented.

Table 6-5. Detected decays compared to MCNP predicted activation and detection of In-116 for the same moderator configuration on the M6, 3/8" front and 1" reflector.

Run #	**M6 Pulse Rate (Hz)**	**Detected Decay Betas on CZT**	**MCNP In-116 in Cell**	**MCNP decay, transport and detection corrected**	**Models to Detected Ratio**
18	157	108634	1.02E+08	1.05E+05	0.96
19	157	110368	1.02E+08	1.05E+05	0.95
20	157	105789	1.02E+08	1.05E+05	0.99
21	157	109615	1.05E+08	1.08E+05	0.99
22	250	152081	1.62E+08	1.67E+05	1.10
23	315	198914	2.05E+08	2.10E+05	1.06

From Table 6-7 we see excellent agreement between MCNP predicted activation values and the ground state decay betas detected on the CZT. The third column is the total detected betas from the peak of the bolus arrival, approximately 77 seconds in these cases, with the m1 activity subtracted for each irradiation. The m1 background demonstrated continual increase during sequential runs as expected. The fourth column, MCNP predicted In-116 activations, is based on the 5/8" front and 1" reflector and the photoneutron production of the machine at a specific pulse rate and associated current. In the fifth column, total MCNP calculated production expected in the GaInSn cell over 60 seconds is corrected for decay in transit to the peak, 17 seconds, and multiplied by the detection efficiency factor 2.46×10^{-3} determined previously in Table 4-1. With good agreement between predicted decays and detected decays, we can expand the analysis to derive actual dose from both the measured M6 irradiations and scale that dose to that expected from a clinical accelerator.

Dose that would be expected in tissue utilizes all detected betas, including those in the rising portion of Figure 6.14. Through inverse application of the decay detection correction factor used to compare models to experiment for total activation, the total decays in the GaInSn cell can be determined through total area of the decay curve. This total area includes the rising slope of the arrival of the bolus during pumping in column two of Table 6-6 with associated total decays in the GaInSn cell in column three. Using these decay values, the percent depth dose models from section 6.1 can be used to determine the surface dose at 100% PDD. For the In-116 ground state decay, MCNP calculates $1.27\text{x}10^{-9}$ cGy delivered per decay in the first 0.5mm depth cell. This allows dose calculation in column 4 for one minute of decay.

Table 6-6. Dose results measured for M6 and scaled for K15 and Clinac.

Run #	**Detected counts**	**Associated In-116 Decays**	**M6 Dose (cGy/min)**	**K15 Dose (cGy/min)**	**Clinac Dose (cGy/min)**	**Clinac Dose (Gy/hr)**
18	206473	5.33E+07	6.78E-02	1.06	19.4	11.6
19	222051	5.52E+07	7.01E-02	1.10	20.1	12.0
20	215114	5.18E+07	6.58E-02	1.03	18.8	11.3
21	226442	5.31E+07	6.74E-02	1.06	18.6	11.2
22	300454	7.28E+07	9.25E-02	0.91	16.6	9.9
23	395178	9.70E+07	1.23E-01	0.96	17.5	10.5

Clinac scaling utilized the maximum activation efficiency case determined previously of 1.5" front moderator and 1" reflector near the closed jaws of the accelerator head and operating a maximum current of 600MU/min. It is apparent that HDR brachytherapy in the range of 12 Gy/hour is only possible through the use of a Clinac due to the significantly higher In-116 activation compared to the lower energy K15 and M6.

With a higher output from the Clinac, the contribution of the m1 state consisting of both low energy betas and gamma-rays must be accounted for. With optimized Clinac output, it was assumed that a single activator dwell over tissue was 60 seconds with a 15 second pumping time. Since one “bolus” can be activated while the other is decaying over tissue, the plot in Figure 6.16 presents pairs of dose representing the dose from each bolus. The integral dose over a 45 minute cycle is ony 37.6 cGy, meaning that m1 dose is negligible compared to the 900 cGy (9Gy) that would be delivered by a 12Gy/hr In-116 source in the same time period.

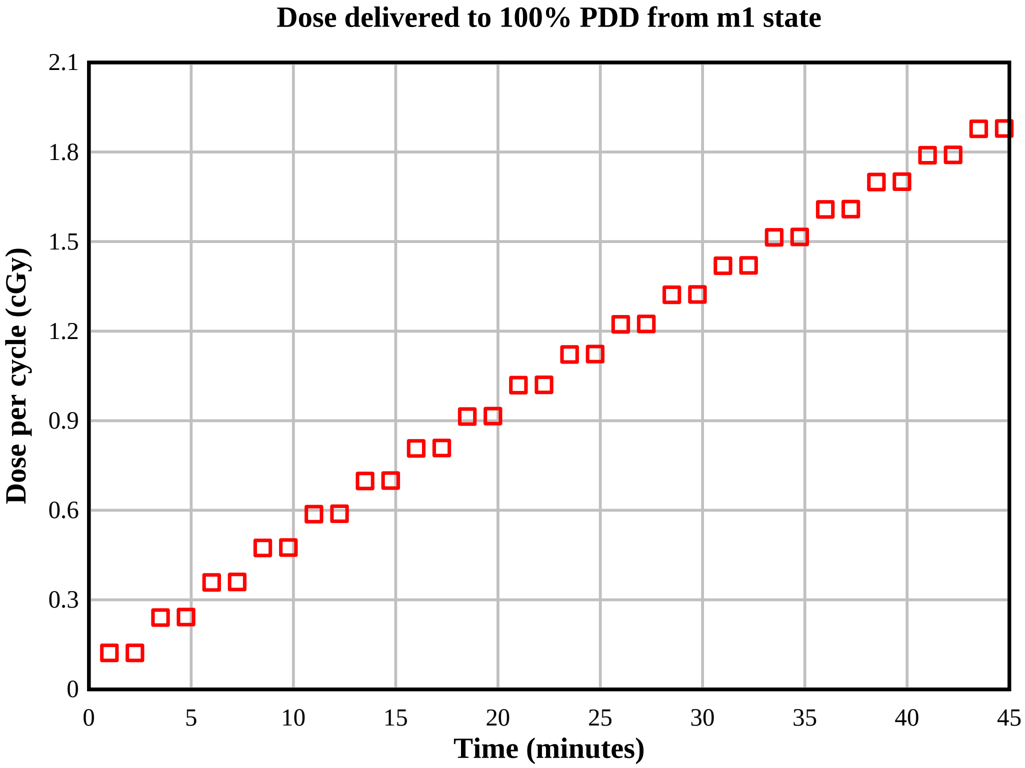

Figure 6.16. In-116 m1 state decay betas and gammas dose quantification to tissue for a 45 minute cycle of activations and decays from a pair of activation/decay boluses.

If a Clinac is used as a photoneutron source, concern about neutron dose to the patient becomes an issue. Even with the tungsten jaws fully closed, preventing X-ray dose, a patient near the Clinac will receive dose from photoneutrons “leaking” from the machine. It is reported that a 20MV Clinac produces an equivalent photoneutron dose at 1 meter equal to 1.78mSv/Gy at isocenter. This means that a Clinac delivering 1Gy of photon dose would deliver 1.78mSv of photoneutron dose with the jaws closed [37]. A Clinac operating at 600MU/min to produce maximum In-116 activation would therefore produce 10.7mSv per minute of neutron dose at 1 meter. With an annual background dose of only 6 mSv per year, it would be advisable to position the patient further than 1 meter from the source to utilize $1/R^2$ reductions or provide neutron shielding.

6.4 Production of Undesired Isotopes

A major concern when dealing with the activation of materials is unintentional creation of isotopes with decay properties that might increase dose or remain radioactive longer than expected. Ideally the GaInSn mixture would consist purely of indium, tin and gallium. However without purchase of 99.999% or 5N pure components, we can expect other isotopes. HPGe spectral analysis after neutron irradiation was used as a primary method to quantify activation of the known components (In,Sn,Ga) and identify contaminants. Where isotopes can be identified, their decay products and half-lives are presented here. Generally an isotope with a long half-life is not a concern for dose to a patient since the eutectic is only exposed to the patient for 1 minute at a time. However buildup of any long lived isotopes is a concern for continuous use of the same eutectic or for disposal.

The first components to be analyzed are those we would expect to find in a pure GaInSn eutectic consisting only of In, Sn and Ga. Table 6-7 outlines these elements and the potential activation product half-lives. Thermal capture cross sections, that assume 0.025eV neutrons, are presented for each isotopic component in the eutectic along with the dominant decay mechanism and half-life of that decay.

Table 6-7. Anticipated activation products in a pure GaInSn mixture.

Element & GaInSn %	**Isotope**	**Atomic Wt %**	**Thermal Capture $T_{1/2}$**	**σ (barns)**	**Decay Product**
Indium	In-115	95.71	14.1 sec	202	β– 3.28 MeV
22.50%	In-113	4.29	71.9 sec	12	β– 1.98 MeV
	Sn-112	0.97	115 days	0.8	γ 392 keV
Tin	Sn-120	32.6	27 hours	0.1	β- 391 keV
9.50%	Sn-122	4.63	129 days	0.15	β- 1.40 MeV
	Sn-124	5.79	9.6 days	0.13	β– 2.36 MeV
Gallium	Ga-69	60.1	21.1 min	0.3	β– 1.65 MeV
68%	Ga-71	39.9	14.1 hours	4.8	β– 961 keV

*In-116 contains 3 metastable states depending on incident neutron energy if above thermal energies

Note that for tin (Sn), the isotopes Sn-114 through Sn-119 make of 56% of natural tin by weight, however thermal neutron capture on these isotopes transitions them to heaver stable isotopes, i.e. Sn-114 transitions to Sn-115 which is stable. These isotopes of tin are therefore excluded from this table of possible activation products. In-115, the isotope of interest in this work, is the dominant activation isotope in this eutectic with the largest cross section (202 barns) for thermal capture. All other possible thermal capture isotopes in GaInSn will not contribute to dose due to: (1) Low cross section resulting in small activation quantities; (2) Low energy beta decay which results in reduced escape probability and dose. The tin isotope Sn-112 is the exception to this with a 392keV gamma. However Sn-112 activates with a capture cross section of less than 1 barn, is only 0.97% abundant in tin, and has a relatively long half-life of 115 days. Detectable levels of Sn-112 thermal capture were also not observed in the HPGe detector; and (3) Half-Lives much longer than the 1 minute dwell time over the dose site result in very little decay radiation during the dwell time.

Given that the non In-115 components of GaInSn are not a contributor to dose, gamma spectroscopy was used with the HPGe detector after Pu-Be activation to analyze any impurities or unexpected decays. A portable HPGe, the Canberra Falcon 5000, was utilized to measure a 1cc volume sample of GaInSn that underwent 1 hour of irradiation in the Pu-Be source. This hour irradiation greatly exceeded how long the eutectic would normally be exposed to neutrons but was utilized to buildup enough activation products to investigate impurities.

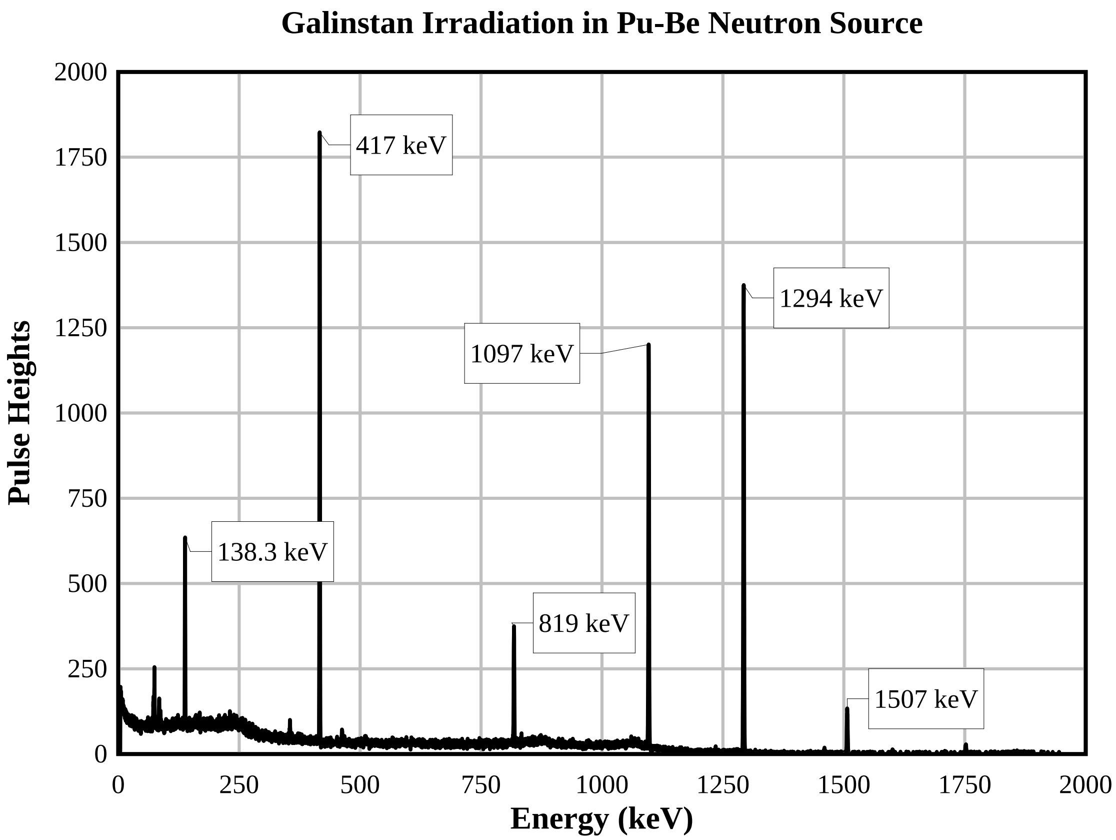

Figure 6.17. 10 minutes of decay spectrum counting on the HPGe detector from Pu-Be Activation showing strong In-116 metastable state 1 decay.

Based on Figure 6.17 it is apparent that the single major activated component detectable after 1 hour of irradiation is the first metastable state (m1) of In-116 above the ground state. This m1 isotope of indium decays with the gamma-ray energies shown below in Table 6-8 with a strong presence of all expected signature decay lines in the HPGe measured spectrum.

Table 6-8. Decay gammas and probability per decay from In-116 m1.

Decay Gamma (keV)	Probability per decay
138.3	3.70%
416.9	27.2%
818.7	12.1%
1097.3	58.5%
1293.6	84.8%
1507.6	9.92%

The strong decay presence of In-116 m1 can be expected since thermal capture on In-115 results in three possible isotopes: 1) In-116 ground state with a half-life of 14.1 seconds, 2) In-116 m1 with a half-life of 54.3 minutes and 3) In-116 m2 with a half-life of 2.2 seconds. The m2 state quickly decays to the lower m1 state during transport and can be combined with the m1 state. Relative cross sections for these isotopes are 81b, 81b and 40b respectively. Because of the long half-life of the m1 state, we can safely assume that a short 1 minute exposure to a patient will results in no measurable dose from the m1 or m2 states. However multiple irradiations of the GaInSn can result in buildup of this m1 isotope, so dose contribution was examined in previous sections. This 54.3 minute activation could be useful for neutron detection purposes, however. Other potential activation components in the eutectic from Table 6-7 are not observed on this count, due to their beta decay nature and relatively small cross sections compared to In-115. With only the In-116 m1 decay state present on the gamma-analysis, the GaInSn sample used in testing is shown to be free of any unknown contaminants.

CHAPTER 7

CONCLUSIONS

Based on modeling and experimental results, it is apparent that viable applications of this In-116 activation, transport and decay system depend heavily on the type and intensity of neutron source used to activate the material. The three neutron sources investigated here experimentally varied by several orders of magnitude in intensity from the 10^7 neutrons/sec Pu-Be, to the 10^{11} neutron per pulse DPF, and finally the photoneutron M6 source producing ~10^7 neutrons/sec into the activation target. The Pu-Be source proved to be only viable for neutron activation analysis of the GaInSn components with too few activations to provide dose in a therapy application. The DPF, likewise, did not produce enough activation for therapy but In-116 production amounts were sufficient to make yield measurements of each shot. An additional limitation of DPF neutron sources in regards to clinical usage is the variability of output with shot to shot output ranging over potentially an order of magnitude, making dose planning more difficult with varying dose delivered each time. The M6 photoneutron source did not produce sufficient activation for clinical dose but did provide experimental validation of photoneutron activation potential for the In-116. With scaling to a clinical 20MV accelerator, activations through photoneutron interactions become sufficient to perform HDR therapy with the activated GaInSn.

While activations were not sufficient to provide clinical dose from the DPF source, detector decays did track excellently with the established beryllium yield detector. This allows neutron fluence measurements to be taken at any location where insertion of a probe containing the eutectic is possible. Traditional neutron activation detectors require either placement and physical retrieval of a sample or the use of a quickly decaying material coupled to a detector. The placement and retrieval of a sample offers the benefit of immunity to harsh EMI environments and the ability to measure neutron fluence in locations where electronics will not fit or be practical. However the retrieved isotope cannot have a short half-life and must be replaced after each irradiation. Coupling of activation isotopes to detectors removes the requirements of retrieval and useable half-life, but can make measurements more limited in terms of EMI protection of the detector.   The system investigated here offers the benefits of both such measurement techniques while removing some of the limitations. Activation of a eutectic such as this that can be pumped to an EMI protected detector from a small location near a pulsed source, with short decay times and no need to retrieve or replace samples.

7.1 Clinical Applications

Clinical application of this methodology will require the neutron flux that can be delivered from a photoneutron source such as the closed jaws of a 20MV accelerator. Since these types of units are very common across the world for X-Ray external beam therapy, their use for this purpose becomes viable. As discussed in the results, a major concern is neutron dose from the machine. With a 20 minute treatment exposing a patient on the Clinac table to 214 mSv, neutron shielding or increased distance is mandatory. With movement to a distance of 5 meters from the table, the dose can be reduced to 8.6 mSv. This distance can be combined with polyethylene shielding for the patient to further reduce dose. Polyethylene 7.6 inches thick will reduce neutron dose behind the shielding by a factor of 100 according to NCRP 151. This would reduce patient dose from photoneutrons to 0.086mSv. Additional room neutron shielding for the accelerator should be considered as well if the Clinac is to be operated at high dose rates with the jaws closed.

An additional option for neutron activation of the In-115 in a clinical environment is the use of a dedicated compact continual neutron source, sometimes referred to as "sting tubes". These sealed neutron sources produce fusion neutrons, similar to the DPF source, but do so with a continual beam current and not in a pulsed fashion. While neutron yields are lower than a DPF, the activation material could potentially be placed much closer to the source. Modern tubes can operate up to $1\text{x}10^{8}$ neutrons per second with some companies producing large, fixed fusion sources that claim $3\text{x}10^{11}$ neutrons per second. While such a source would produce enough neutrons for therapeutic use of In-116, the cost burden of a large dedicated neutron source might make this impractical compared to utilizing existing clinical accelerators.

7.2 Application as a Neutron Detector

Neutron detection using the eutectic here, consisting of gallium, indium and tin, relied on the thermal capture of neutrons on indium. Thermal capture makes the detector sensitive to neutrons of all energies, however, as scattered neutrons become more likely to be captured as the cross section increases with 1/velocity as the neutrons slow. In fusion neutron research, threshold reactions would be more useful. Threshold reactions require the incident neutron to be above a certain energy, typically resulting in emission of a proton (n,p), two neutrons (n,2n), alpha (n,α), or exciting a nuclei to a metastable state. These reactions remove any sensitivity to neutrons that scatter below the threshold, making them very useful in fusion neutron research to investigate only the primary source of neutrons with energies from 2.45 to 14MeV. Dissolving significant amounts of other materials into the GaInSn would alter its melting point, so using one of the existing isotopes for threshold neutron detection is ideal.

Gallium-71, making up 40% of natural gallium and over 60% of the GaInSn by weight is a viable option for threshold reaction detection with two activation methods that could be measured using a beta decay detector. The production of a neutron through the Ga-71(n,p)Zn-71 reaction offers a threshold of 2MeV and a half-life of 2.45 minutes. Alpha emission through Ga-71(n,a)Cu-68 offers a steeply rising cross section that peaks at 14MeV, the energy of D-T fusion neutrons, and a half-life of 30.9 seconds with very energetic decay betas up to 4.4MeV. The In-115 isotope could also be used in a threshold reaction with a the In-115(n,2n)In-114 decaying with a half-life of 72 seconds and a threshold of 6.8MeV. Any isotope used here, however, would need to account for the 14.1 second decay of the thermal capture on In-115 that will always be present in a neutron environment. Therefore decay half-lives longer than about 1 minute are preferable.

APPENDIX I

NUMERICAL FLOW MODELING SOFTWARE

Computational Model of Segregated Flow in a Flowing Radioactive Metal

A computer program was developed to calculate the radioactivity of GaInSn flowing through a length of tubing from a neutron source and through a downstream radiation detector. The program also calculates the total number of beta particles that would be generated by the GaInSn at the detector and counted by the detector over some time interval. A schematic of the flow problem is shown in figure A1.

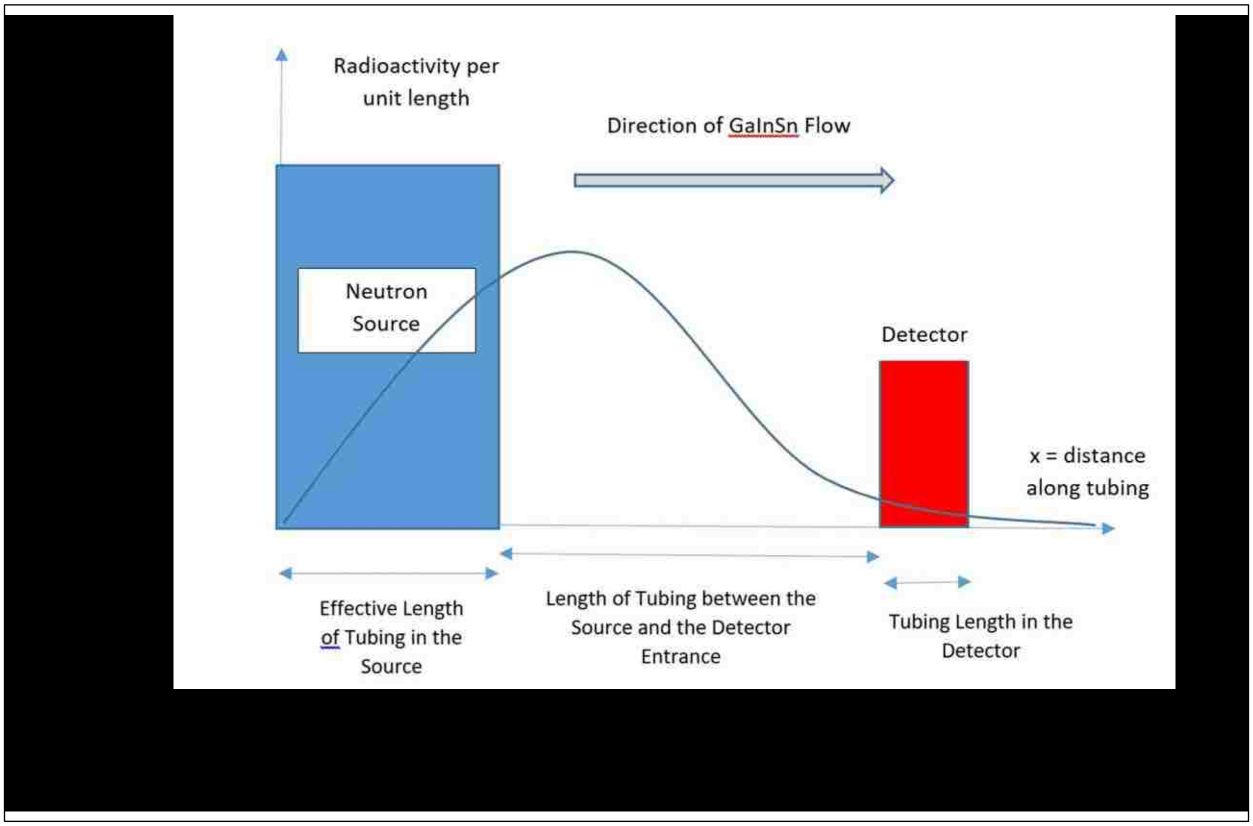

Liquid GaInSn flows through a neutron source where it is activated by a continuous source of neutrons or by a pulsed neutron source. A pump is used to move the liquid metal through the source with an effective tubing length of L_{source}. For a continuous neutron source, the GaInSn may remain in the source for a time period $t_{preflow}$ to build up the concentration of the beta emitter, In-116. At a time defined as t_{flow_start}, the pump is turned on and the “bolus” of activated GaInSn is circulated towards the detector located at a distance of L_{gap} from the exit of the neutron source. The effective length of tubing in the detector is $L_{detector}$. To capture as much of the radioactive bolus of GaInSn as possible in the detector, the flow is stopped at time t_{flow_stop}. The velocity of flow through the tubing is found by dividing the volumetric flowrate in mm^3/s by the cross-sectional area of the tubing. The detector is turned on at $t_{detector\_start}$ and left on until $t_{detector\_stop}$.

As an example, a pulsed source of neutrons with a strength of 10^{11} neutrons/pulse is used to activate GaInSn moving at 110 mm^3/s through a 1.6 mm diameter tube. The pump is turned on for 15 seconds after the neutron pulse to circulate the activated liquid metal to the detector. The resulting radioactivity of the GaInSn and the counts detected by the detector located 444 mm from the source. The fluid flows at 56 mm/s with a laminar Reynolds number of only 236. The program models this segregated flow where the fluid along the centerline of the tube moves at twice the average velocity of the flow. It takes approximately 8 seconds for the liquid metal to flow from the source to the entrance of the detector. In this simulation, the detector samples for a period of 60 seconds and the resulting of radioactivity of the liquid metal in the detector, along with the total counts (beta particles) that are released within the detector are reported as functions of time.

Figure A2 shows the bolus of radioactive GaInSn within the detector after the 15 seconds of flow. The halflife of the activated In-116 is 14 seconds resulting in a delay between the peak of the radioactivity and the growth in the number of counts (beta particles) that are released within the detector. Since this source is pulsed, the radioactivity in the activated GaInSn quickly dies off and the number of counts reaches a maximum.

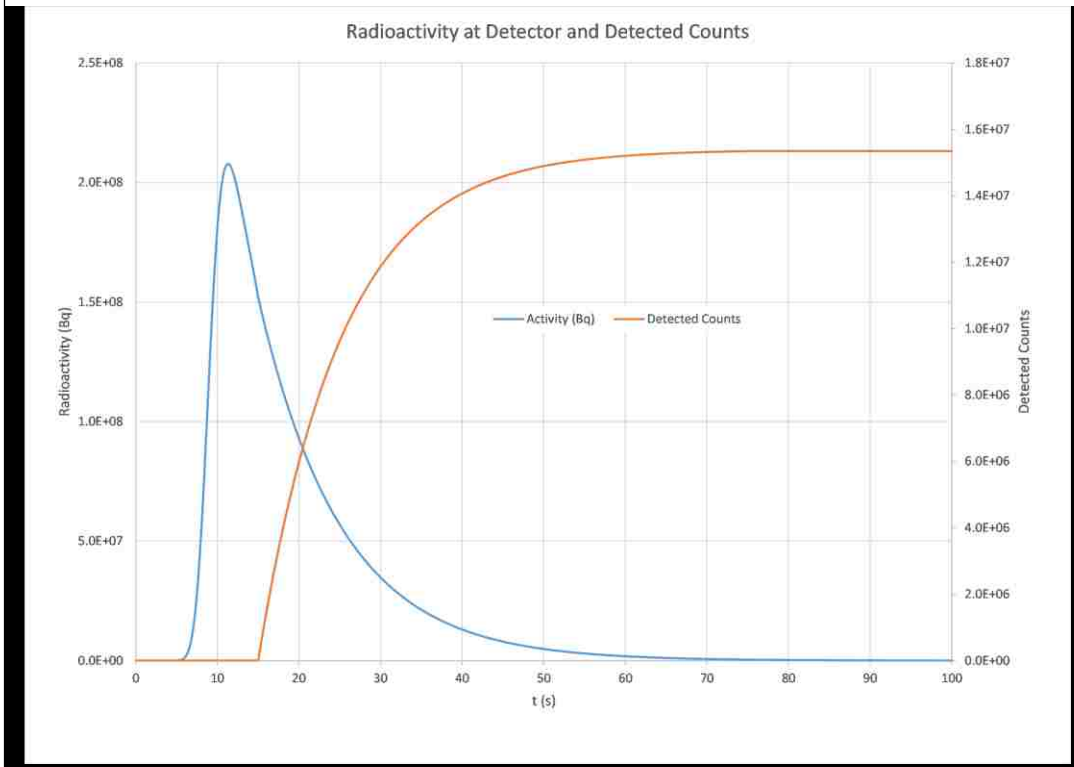

The program uses the finite difference technique to compute the radioactivity within the liquid metal as a function of time. The time increment used in the previous example is 0.1 seconds and the total length of tubing is divided into 425 intervals of 2.54 mm. The 425 resulting equations are solved at each time increment using a tridiagonal matrix solver based on the Gauss-Seidel method. The complete program, sample input file, and sample output file are included in the appendices.

```
'-------------------------------------------------------------------
'
'   Program:  GaInSn.BAS
'
'   Purpose:  Calculate the radioactivity in GaInSn introduced
'             by a neutron source.  The GaInSn is in a thin
'             tube pumped by a syringe or peristalic pump.
'             The PIP's detector is
'             located downstream of the neutron source.
'
'   Input:    1)  input.dat  - file containing input data.
'
'   Output:   1)  detector-output.dat - file containing detector
'                                output (Bq) vs time (s).
'             2)  spill              - spillout of a lot of
'                                intermediate data.
'             3)  output.dat         - organized file of output
'                                data.
'             4)  results are plotted to the screen, containing
'                 the number of In-116 atoms per m^3 as a function
'                 of time and position along the tubing.
'
'                 N_In115(i) = atoms/m^3 of In115.
'                 N_In116(i) = atoms/m^3 of In116 (radioactive).
'                 i          = increment along the length of tubing
'                              from i = 0 to i = last.
'                 Length_Increment = increment in length along the
'                                    tube.
'
'-------------------------------------------------------------------


declare sub GS(nitems as integer, max_order as integer, _
           number_of_iterations as integer, _
           x() as double, a() as double, _
           location() as integer, b() as double, _
           tolerance as double)

  '  Note that the variable location() is used to define the position of each
  '  nonzero entry in the GS coefficient matrix.

declare function Neutron_Flux_dt(x as double, t as double,  _
                        x_source_exit as double,   _
                        Time_Preflow as double,    _
                        Time_Increment as double,  _
```

```
                      Source_Strength as double, _
                      Source_Type as string) as double


dim as double Length_Total, Tube_Diameter
dim as double Flowrate
dim as double Time_Increment, Time_Maximum
dim as double Length_Increment, Length_Source, Length_Gap, Length_Detector
dim as double viscosity, density
dim as double atomic_radius_Ga, atomic_radius_Sn, atomic_radius_In
dim as double PI, Boltzmann_Constant, A_avogadro
dim as double F_In, F_Ga, F_Sn, F_In113, F_In115
dim as double halflife_In116, decay_constant_In116
dim as double atomic_weight_In, atomic_weight_Sn, atomic_weight_Ga
dim as double atomic_weight_In115, atomic_weight_In116
dim as double atomic_weight_GaInSn
dim as double cross_section
dim as double area, Re, velocity, friction_factor, pressure_drop
dim as double Diffusion_Coefficient
dim as double beta1, beta2, beta3, beta4
dim as double Source_Strength
dim as double temperature
dim as double N_In, N_In115_initial
dim as double x_source_exit, x_detector_entrance, x_detector_exit
dim as double sum

dim as integer NN = 3000, i, last
dim as double  A(3,NN), C(3,NN), B(NN), D(NN)
dim as integer location(2,NN)
dim as double  N_In115(NN), N_In116(NN)

dim as integer number_of_increments, number_of_iterations
dim as double  t, x, phi, Tolerance
dim as string  value, input_line
dim as double  null
dim as double  volume_of_GaInSn_near_detector, Detector_Diameter
dim as double  activity_at_detector
dim as integer i_detector
dim as integer page, notpage
dim as double  N_In116_Max
dim as double  x_left, x_right
dim as double  Time_Preflow, Time_Flow_Start, Time_Flow_Stop
dim as double  Time_Start_Counting, Time_Stop_Counting
dim as integer plot_increment, plot_flag
```

```
dim as double Pe_axial, Pe_radial, Pe, L, R

dim as double x_source, x_detector, x_soure_width, Detector_Efficiency

dim as string Source_Type
dim as double phi_dt, Counts, Total_Counts, Detected_Counts


  '--------------------------------------------------------------
  '
  '  A.  Read in the User Input.
  '
  '      All values are converted to SI units after being defined.
  '
  '--------------------------------------------------------------

    '
    '  A.1  Read in user data from 'input.txt.'
    '

       open "input.txt" for input as #1

     do while(eof(1) = 0)

       line input #1, input_line

       if mid(input_line,8,3) = "A.1" then Tube_Diameter    = val(mid(input_line,70,10))
       if mid(input_line,8,3) = "A.2" then Flowrate         = val(mid(input_line,70,10))
       if mid(input_line,8,3) = "A.3" then Source_Strength  = val(mid(input_line,70,10))
       if mid(input_line,8,3) = "A.4" then Source_Type      = mid(input_line,70,10)
       if mid(input_line,8,3) = "A.5" then cross_section    = val(mid(input_line,70,10))
       if mid(input_line,8,3) = "A.6" then Detector_Efficiency =
val(mid(input_line,70,10))

       if mid(input_line,8,3) = "B.1" then Time_Increment   = val(mid(input_line,70,10))
       if mid(input_line,8,3) = "B.2" then Length_Increment = val(mid(input_line,70,10))
       if mid(input_line,8,3) = "B.3" then Tolerance        = val(mid(input_line,70,10))
       if mid(input_line,8,3) = "B.4" then N_In116_Max      = val(mid(input_line,70,10))

       if mid(input_line,8,3) = "C.1" then Time_Flow_Start  = val(mid(input_line,70,10))
       if mid(input_line,8,3) = "C.2" then Time_Flow_Stop   = val(mid(input_line,70,10))
       if mid(input_line,8,3) = "C.3" then Time_Start_Counting =
val(mid(input_line,70,10))
       if mid(input_line,8,3) = "C.4" then Time_Stop_Counting  =
val(mid(input_line,70,10))
```

```
    if mid(input_line,8,3) = "C.5" then Time_Maximum     = val(mid(input_line,70,10))

    if mid(input_line,8,3) = "D.1" then Length_Source    = val(mid(input_line,70,10))
    if mid(input_line,8,3) = "D.2" then Length_Gap       = val(mid(input_line,70,10))
    if mid(input_line,8,3) = "D.3" then Length_Detector  = val(mid(input_line,70,10))

  loop

    Tube_Diameter     /= 39.3701   ' (m).
    Length_Increment  /= 39.3701   ' (m).
    Flowrate          /= 1e9       ' (m^3/s).
    Source_Strength   *= 1e4       ' (n/m^2 * s).
    Length_Source     /= 39.3701   ' (m).
    Length_Gap        /= 39.3701   ' (m).
    Length_Detector   /= 39.3701   ' (m).
    cross_section     /= 1e28           ' convert to (m^2).


    close #1


'----------------------------------------------------------------
'
'  B.  Define Constants.
'
'----------------------------------------------------------------

  '
  '  B.1  Constants.
  '

    Boltzmann_Constant = 1.380649E-23     ' (J/K).
    PI                 = 3.14159265358
    A_avogadro         = 6.02214129E23    ' (atoms or molecules/mole).

    atomic_radius_Ga   = 135e-9 / 2         ' (m).
    atomic_radius_Sn   = 140e-9 / 2         ' (m).
    atomic_radius_In   = 167e-9 / 2         ' (m).

  '
  '  B.2  GaInSn Properties.
  '

    viscosity = 0.0024               ' (kg/m*s) at 20 C.
    density   = 6.44e3               ' (kg/m^3) at 20 C.
```

```
                                  ' source:  wiki page on GaInSn.

'
'  B.3  Composition of Eutectic GaInSn and Indium.
'

   F_In113 = 0.043                ' (fraction).
   F_In115 = 0.957

   F_In    = 0.215
   F_Ga    = 0.685
   F_Sn    = 0.100

'
'  B.4  Nuclear Properties of Components
'

   halflife_In116      = 14.1              ' (s).

   atomic_weight_In    = 114.818 / 1000    ' (kg/mole).
   atomic_weight_Ga    = 69.723  / 1000    ' (kg/mole).
   atomic_weight_Sn    = 118.710 / 1000    ' (kg/mole).

   atomic_weight_In115 = 114.9038783/1000  ' (kg/mole)
   atomic_weight_In116 = 115.9052600/1000  ' (kg/mole).

'
'  B.5  Choose one of these three values for the [n,gamma]
'       cross-section for In-115.

'  cross_section       = 201.0           ' at 0.0253 eV.
'  cross_section       = 181.6           ' Maxwell averaged at 0.0253 eV.
'  cross_section       = 160.6e-3        ' Fission spectrum averaged.

                                    ' (b), for [n,gamma] in In-115.

'
'  B.6  Determine the total length of the tubing.
'

   Length_Total = Length_Source + Length_Gap + Length_Detector

   x_source_exit      = Length_Source
   x_detector_entrance = Length_Source + Length_Gap
   x_detector_exit     = x_detector_entrance + Length_Detector
```

```
'---------------------------------------------------------------
'
'  C.  Preliminary Calculations.
'
'---------------------------------------------------------------

  '
  '   C.1  Calculate Flow Parameters.
  '

    area        = (PI/4) * (Tube_Diameter)^2
    velocity    = Flowrate / area
    Re          = velocity * Tube_Diameter * density / viscosity
    Length_Total = Length_Source + Length_Gap + Length_Detector

    '   Assume smooth pipe walls.

    if Re > 2300 then
      friction_factor = 0.316 / Re^(1/4)
    else
      friction_factor = 64    / Re
    end if

    pressure_drop = friction_factor * Length_Total / Tube_Diameter * _
                density * velocity^2 / 2


  '
  '   C.2  Nuclear Properties.
  '

   '  C.2.1  Initial number density of In-115 in GaInSn.
   '        The units are (atoms/m^3).

    atomic_weight_GaInSn = F_In * atomic_weight_In + _
                     F_Sn * atomic_weight_Sn + _
                     F_Ga * atomic_weight_Ga
    N_In                = F_In * density * A_avogadro / _
                     atomic_weight_GaInSn
    N_In115_initial      = F_In115 * N_In

    decay_constant_In116 = log(2)/halflife_In116
```

```
  '
  '  C.3  Compute the Self-Diffusion Coefficient for In in GaSnIn.
  '       The units for the diffusion coefficient are (m^2/s).

   temperature          = (20 + 273)                ' (K).

   Diffusion_Coefficient = (Boltzmann_Constant * temperature) / _
                        (6 * PI * viscosity * atomic_radius_In)


  '
  ' C.4  Set up the coefficient matrix and the B matrix for solution.
  '
  '                        A p = B
  '                        C q = D
  '
  '      "p" is the number density of In-115.
  '      "q" is the number density of In-116.
  '

   number_of_increments = Length_Total / Length_Increment


  '
  ' C.5  Compute mass transfer dimensionless groups.
  '

   L         = Length_Gap
   R         = Tube_diameter / 2

   Pe        = velocity * R^2 / (Diffusion_Coefficient * L)
   Pe_axial  = velocity * L   /  Diffusion_Coefficient
   Pe_radial = velocity * R   /  Diffusion_Coefficient


'---------------------------------------------------------------
'
'  D.  Define the initial concentrations of In-115 and In_116.
'
'---------------------------------------------------------------

  '
  ' D.1  Define the initial values of N_115(i) and N_116(i).
```

```
  '


      i = 0
      t = 0
    for x = Length_Increment/2 to Length_Total step Length_Increment
      N_In115(i) = N_In115_initial
      N_In116(i) = 0
      i += 1
    next x
      last = i


'-----------------------------------------------------------------
'
'  E. Set up the screen for plotting.
'
'-----------------------------------------------------------------



  screen 20, 2  '  2 pages for screen flipping.
  notpage = 1




'-----------------------------------------------------------------
'
'  F.  Define the coefficient matrices.
'
'-----------------------------------------------------------------

    open "spill" for output as #3    '  This file contains intermediate values
                                     '  from the computations.

    open "detector-output.dat" for output as #4
    print #4, "time (s), activity (bq), Detected_Counts_Total"

open "plots.dat" for output as #5
plot_increment = 50
plot_flag = 0

    Total_Counts    = 0
    Detected_Counts = 0

  for t = 0 to Time_Maximum step Time_Increment
```

```
'
' F.1  Set the velocity of the GaInSn based on the timing.
'

  if ((t > Time_Flow_Start) and (t < Time_Flow_Stop)) then
    velocity = Flowrate / area
  else
    velocity = 0
  end if


'
' F.2  Define the beta parameters used in computing the
'      coefficient matrics, A, B, and C.  D, however, is
'      dependent upon the value of N_In115 in the new time
'      interval and is computed after solving A * N_115 = B.
'

  beta1 = velocity              * Time_Increment / Length_Increment
  beta2 = Diffusion_Coefficient * Time_Increment / Length_Increment^2
  beta3 = decay_constant_In116  * Time_Increment


'
' F.3  Define the coefficient matrices for Node at x = 0.
'
'        The boundary conditions for this node are:
'            N_In115 = initial number density.
'            N_In116 = 0

  x            =  Length_Increment/2
  phi_dt        =  Neutron_Flux_dt(x, t, x_source_exit, _
                 Time_Preflow, Time_Increment,        _
                 Source_Strength, Source_Type)
  beta4         =  phi_dt * cross_section

  A(0,0)        =  1 + beta1 + 2 * beta2 + beta4
  A(1,0)        = -beta2
  A(2,0)        =  0

  C(0,0)        =  1 + beta1 + 2 * beta2 + beta3
  C(1,0)        = -beta2
  C(2,0)        =  0

  location(0, 0) = 1
```

```
   location(1, 0) = 0

   B(0)          = N_In115(0) + (beta1 + beta2) * N_In115_initial


'  F.4  Define the coefficient matrices for Node at x = Length_Total.
'
'       The boundary conditions for this node are:
'            N_In115 = initial number density.
'            N_In116 = insulated condition.

   x             =  Length_Total - Length_Increment/2

   phi_dt        =  Neutron_Flux_dt(x, t, x_source_exit, _
                   Time_Preflow, Time_Increment,        _
                   Source_Strength, Source_Type)
   beta4         =  phi_dt * cross_section

   A(0,last)     =  1 + beta1 + 2*beta2 + beta4
   A(1,last)     = -beta1 - 2 * beta2
   A(2,last)     =  0

   C(0,last)     =  1 + beta1 + 2*beta2 + beta3
   C(1,last)     = -beta1 - 2 * beta2
   C(2,last)     =  0

   location(0, last) = last - 1
   location(1, last) = 0

   B(last)          = N_In115(last) + beta2 * N_In115_initial


'
' F.5  Define the coefficient matrices for each Interior node.
'

     print #3, "t, x(in), phi, b4"

     x = Length_Increment * 1.5

   for i = 1 to (last - 1)

     phi_dt         =   Neutron_Flux_dt(x, t, x_source_exit, _
                      Time_Preflow, Time_Increment,        _
                      Source_Strength, Source_Type)
```

```
      beta4          =   phi_dt * cross_section

      A(0,i)         =   1 + beta1 + 2*beta2 + beta4
      A(1,i)         = - beta1 - beta2
      A(2,i)         = - beta2

      C(0,i)         =   1 + beta1 + 2*beta2 + beta3
      C(1,i)         = - beta1 - beta2
      C(2,i)         = - beta2

      location(0, i) = i - 1
      location(1, i) = i + 1


      print #3, using "########.###"; "t; x(in); phi; b4 = "; t; x * 39.3701; phi;
      print #3, beta4

      x += Length_Increment

    next i


    for i = 1 to (last - 1)
      B(i) = N_In115(i)
    next i


'
'  F.6  Now, invert the matrix A*N_115 = B to find N_115(i).
'

    GS(last, 3, number_of_iterations, N_In115(), A(), location(), _
      B(), Tolerance)


'
'  F.7  Find the vector D(NN).  This changes with x, t, and N_115.
'

    x = Length_Increment/2
      phi_dt  =  Neutron_Flux_dt(x, t, x_source_exit, _
                 Time_Preflow, Time_Increment,        _
                 Source_Strength, Source_Type)
      beta4   =  phi_dt * cross_section
      D(0)    =  (1 - beta3) * N_In116(0) + beta4 * N_In115(0)
```

```
  x = Length_Total - Length_Increment/2
    phi_dt  =  Neutron_Flux_dt(x, t, x_source_exit, _
               Time_Preflow, Time_Increment,        _
               Source_Strength, Source_Type)
    beta4   =  phi_dt * cross_section
    D(last) =  (1 - beta3) * N_In116(last) + beta4 * N_In115(last)

    x = Length_Increment * 1.5
  for i = 1 to (last - 1)
    phi_dt  =  Neutron_Flux_dt(x, t, x_source_exit, _
               Time_Preflow, Time_Increment,        _
               Source_Strength, Source_Type)
    beta4   =  phi_dt * cross_section
    D(i)    =  (1 - beta3) * N_In116(i) + beta4 * N_In115(i)
    x      +=  Length_Increment
  next i


'
'  F.8  Invert the simultaneous equations C*N_116 = D to find N_116(i).
'


  GS(last, 3, number_of_iterations, N_In116(), C(), location(), _
    D(), Tolerance)

  print #3, "Iterations on N_116() = "; number_of_iterations


'
'  F.9  Print out to disk the values of t, N_115, N_116, and
'       the radioactivity of In-116.
'


    print #3, " "
    print #3, " "
    print #3, "Time = ";t
    print #3, " "
    print #3, "  i, location(0,i), location(1,i)"
  for i=0 to (last - 1)
    print #3, i, location(0,i), location(1,i)
  next i

    print #3, " "
    print #3, "  i, A(0,i), A(1,i), A(2,i), B(i)"
```

```
   for i=0 to (last   - 1)
     print #3, using "   ##.#####"; i; A(0,i); A(1,i); A(2,i); B(i)
   next i

     print #3, " "
     print #3, "  i, C(0,i), C(1,i), C(2,i), D(i)"
   for i=0 to (last - 1)
     print #3, using "   ##.#####"; i; C(0,i); C(1,i); C(2,i); D(i)
   next i

    print #3, " "
    print #3, "t(s), x(in), phi, N_In116"
   for i=0 to (last - 1)
     x = i * Length_Increment + Length_Increment/2
     phi_dt  = neutron_flux_dt(x, t, x_source_exit, Time_Preflow, _
            Time_Increment, Source_Strength, Source_Type)
     print #3, using "   ##.######"; t; x * 39.3701; phi_dt; N_In116(i)
   next i

     print #3, " "


'
'  F.10  Now, compute the radioactivity of the In-116 immediately
'       above the PIP's detector.  Add up the contribution to
'       the beta count rate from the entire length of tubing in
'       the detector.  Also, compute the total number of counts
'       that will be measured by the detector.
'


    x   = 0.0
    sum = 0.0
  for i = 0 to (last - 1)
    if ((x >= x_detector_entrance) and (x <= x_detector_exit))  then
      sum += (area * Length_Increment) * N_In116(i)
    end if
      x += Length_Increment
  next i

    activity_at_detector = sum * decay_constant_In116

  if ((t > Time_Start_Counting) and (t < Time_Stop_Counting)) then
    Counts              = activity_at_detector * Time_Increment
    Total_Counts        += Counts
    Detected_Counts     += Counts * Detector_Efficiency
```

```
        end if

        print #3, "N_In116(";i_detector;") =                ";_
          N_In116(i_detector);" at the detector, (atom/m^3)."

        print #3, "Activity (bq) at detector = "; activity_at_detector

        print #4, t; ", "; activity_at_detector; ", "; Detected_Counts


      '
      '  F.11  Plot information on the computer screen.
      '


        '
        '  F.11.1  Flip the pages to work on the nonvisible page.
        '


          if page    = 0 then page    = 1 else page    = 0
          if notpage = 1 then notpage = 0 else notpage = 1

          screenset page, notpage   ' This flips the page.

          cls

          view   (    0,    0) - (1024, 700), 9
          window (-0.05, -0.1) - (1.05, 1.1)


        '
        '  F.11.2  Draw in the Pu/Be Source as a yellow region.
        '


          x_left  = (0)             / Length_Total
          x_right = (Length_Source) / Length_Total

          line (x_left, 0) - (x_right, 1), 6, BF
          line (x_source_exit/Length_Total, -0.02) - (x_source_exit/Length_Total, 1.05),
13

          draw string (x_source_exit/(2*Length_Total) - 0.07, 0.75), "Neutron Source"


        '
        '  F.11.3  Draw in the Detector as a red region.
```

```
        '

          x_left  = (x_detector_entrance) / Length_Total
          x_right = (x_detector_exit)     / Length_Total

          line (x_left, 0) - (x_right, 0.5), 4, BF
          line (x_detector_entrance/Length_Total, -0.05) -
(x_detector_entrance/Length_Total, 0.55), 13

          draw string (x_left + 0.07, 0.35), "Detector"



        '
        '  F.11.4  Label the plot.
        '

          draw string ( 0.40, -0.05), "X Position (in)"
          draw string ( 0.01,  0.90), "N-In115 (atoms/m^3-s)"
          draw string ( 0.60,  1.00), "Time(s) = "
          draw string ( 0.85,  1.00),  str(int(t))
          draw string ( 0.60,  0.95), "Simulation ends at t(s) = "
          draw string ( 0.85,  0.95),  str(Time_Maximum)

          if (t < Time_Preflow) then
            draw string ( 0.60, 0.90), "NO FLOW UNTIL t(s) = "
            draw string ( 0.85, 0.90),  str(Time_Preflow)
          else
            draw string ( 0.60,  0.90), "Flow Velocity (mm/s) = "
            draw string ( 0.85,  0.90),  str(velocity * 1000)
          end if

          draw string ( 0.60, 0.85), "Activity at Detector (Bq) = "
          draw string ( 0.85, 0.85),  str(int(activity_at_detector))

          draw string ( 0.60, 0.80), "Actual Detected Counts = "
          draw string ( 0.85, 0.80),  str(int(Detected_Counts))

          line (-0.02, 1) - (0.02,1)
          draw string ( 0.03, 1), str(N_In116_max)



        '
        '  F.11.5  Draw the axes.  Draw in and label the x-increments, as long
        '        as there are less than 50 increments.
        '
```

```
            line (0, 0) - (0, 1.05), 14
            line (0, 0) - (1.05, 0), 14

            for x = 0 to Length_Total step Length_Increment

              line (x/Length_Total, -0.02) - (x/Length_Total, 0)
              if (Length_Total/Length_Increment < 50) then
                draw string (x/Length_Total, -0.025), str(int(x * 39.3701))
              end if

            next x


          '
          '  F.11.6  Plot the data points, N_In116(t).
          '

             pset(0, N_In116(0))
             i = 0
           for x = Length_Increment/2 to Length_Total step Length_Increment
             if (i < last) then
               line -(x/Length_Total, N_In116(i)/N_In116_max)
               i += 1
             end if
           next x


if (plot_flag = plot_increment) then
    i = 0
  for x = Length_Increment/2 to Length_Total step Length_Increment
    if (i < last) then
      print #5, t, ",",x/Length_Total, ",",N_In116(i)/N_In116_max
      i += 1
     end if
  next x

  plot_flag = 0
end if

          '
          '  F.11.7  Sleep a short time between frame displays.
          '

           sleep 10
```

```
plot_flag += 1


    next t


      input "Hit any key to continue"; value

close #5


  '----------------------------------------------------------------
  '
  '  G.  Printout.
  '
  '----------------------------------------------------------------

    open "output.dat" for output as #2

    print #2, "--------------------------------------------"
    print #2, "|                                          |"
    print #2, "|           Program GaSnIn                 |"
    print #2, "|                                          |"
    print #2, "--------------------------------------------"
    print #2, "                                           "
    print #2, "A. Input Data.                             "
    print #2, "  1.  Time increment (s):              "; Time_Increment
    print #2, "  2.  Maximum time (s):                "; Time_Maximum
    print #2, "  3.  Tube Diameter (m), (in):         "; _
      Tube_Diameter, Tube_Diameter * 39.3701
    print #2, "  4.  Tube Length (m), (in):           "; _
      Length_Total,   Length_Total   * 39.3701
    print #2, "  5.  Flowrate of GaSnIn (mm^3/s):     "; Flowrate * 1e9
    print #2, "  6.  Length of Source (m), (in):      "; _
      Length_Source,   Length_Source   * 39.3701
    print #2, "  7.  Length of the Gap (m), (in):     "; _
      Length_Gap, Length_Gap * 39.3701
    print #2, "  8.  Length of the Detector (m), (in): "; _
      Length_Detector, Length_Detector * 39.3701
    print #2, "  9.  Length increment (m), (in):      "; _
      Length_Increment, Length_Increment * 39.3701
    print #2, " 10.  Neutron source (n/cm^2*s):       "; Source_Strength / 1e4
    print #2, " 11.  Source type:                     "; Source_Type
    print #2, " 12.  Detector Efficiency (%):         "; Detector_Efficiency * 100
    print #2, " 13.  Time (start counting) (s):       "; Time_Start_Counting
```

```
    print #2, " 14.  Time (stop counting) (s):         "; Time_Stop_Counting
    print #2, "                                        "
    print #2, "B. Flow Calculations.                   "
    print #2, "  1.  Flowrate (m^3/s), (mm^3/s):       "; Flowrate, flowrate * 1e9
    print #2, "      Tube cross-sectional area (mm^2): "; area
    print #2, "  2.  Velocity (m/s), (in/s):           ", Flowrate / area, (Flowrate / area) *
39.3701
    print #2, "  3.  Reynolds Number:                  ", Re
    print #2, "  4.  Friction factor:                  ", friction_factor
    print #2, "  5.  Diffusion Coef. (cm^2/s):         "; Diffusion_Coefficient*1e4
    print #2, "  6.  Pressure Drop thru Tube (Pa/psi): "; pressure_drop, _
      pressure_drop * 14.7 / 101325
    print #2, "  7.  Effective Length (s. to d.) (m):  "; L
    print #2, "  8.  Tubing radius (m):                "; R
    print #2, "  9.  Peclet Number, Pe:                "; Pe
    print #2, " 10.  Axial Peclet Number:              "; Pe_axial
    print #2, " 11.  Radial Peclet Number:             "; Pe_radial
    print #2, " 12.  Pe_radial * (R/L):                "; Pe_radial*(R/L)
    print #2, "                                        "
    print #2, "C. Simulation Parameters.               "
    print #2, "  1.  beta 1:                           "; beta1
    print #2, "  2.  beta 2:                           "; beta2
    print #2, "  3.  beta 3:                           "; beta3
    print #2, "  4.  Number of x increments:           "; number_of_increments
    print #2, "                                        "
    print #2, "D.  Nuclear Values.                     "
    print #2, "  1.  Number density In (atoms/m^3):    "; N_In
    print #2, "  2.  Initial N of In-115 (atoms/m^3):  "; N_In115_initial
    print #2, "  3.  Time for fluid to flow from the   "
    print #2, "      source exit to detector (s):      "; _
      (x_detector_entrance - x_source_exit)/(Flowrate / area)
    print #2, "  4.  Total detector counts:            "; Total_Counts
    print #2, "  5.  Actual detected counts:           "; Detected_Counts
    print #2, "                                        "
    print #2, "E.  Summary.                            "
    print #2, "    E.1  Time:                          "; time
    print #2, "    E.2  Date:                          "; date


    close #2
    close #3
    close #4

end
```

```
function Neutron_Flux_dt(x as double, t as double,  _
                 x_source_exit as double,   _
                 Time_Preflow as double,    _
                 Time_Increment as double,  _
                 Source_Strength as double, _
                 Source_Type as string) as double

  dim as double PI = 3.14159265853, phi_dt_value


    if (Source_Type = "continuous")  then
      phi_dt_value = Source_Strength * Time_Increment
      if (x < 0)            then phi_dt_value = 0
      if (x > x_source_exit) then phi_dt_value = 0
      if (t > Time_Preflow)  then phi_dt_value = 0
    end if


    if (Source_Type = "pulsed")  then
      if (t = 0.0)  then
        phi_dt_value = Source_Strength
      else
        phi_dt_value = 0.0
      end if

      if (x < 0)            then phi_dt_value = 0
      if (x > x_source_exit) then phi_dt_value = 0

    end if


    return (phi_dt_value)

end function
```

```
Sub GS(nitems as integer, max_order as integer, _
     number_of_iterations as integer, _
     x() as double, a() as double, _
     location() as integer, b() as double, _
     tolerance as double)

'-----------------------------------------------------------------
'
'   Subroutine GS
'
'   Purpose:
'
'   Input:    a)  nitems     -- number of values in the vector x().
'               max_order  -- maximum number of non-zero diagonal
'                           terms (e.g. triagonal = 3, penta-
'                           diagonal = 5).
'               x()        -- this is used as the solution vector
'                           for output, but serves as "guesses"
'                           for the Gauss-Seidel routine as an
'                           input vector.
'               a(i,j)     -- "max_order" vectors of non-zero
'                           diagonals.  For i=0, the vector
'                           contains the central diagonal.
'               location() -- this vector contains the locations
'                           of the columns for each non-zero
'                           diagonal component.  The first index
'                           is zero for the first non-zero diagonal.
'               b()        -- right hand vector in A() x() = b().
'
'   Output:
'           a)  x(),    solution array.
'           b)  number_of_iterations -- number required to converge.
'
'-----------------------------------------------------------------


  dim as double x_old(nitems), sum, new_error, max_error
  dim as integer i, j

      number_of_iterations = 0
  do

    for i=0 to (nitems - 1)

        x_old(i) = x(i)
```

```
        sum = 0.0
      for j=0 to (max_order - 2)
        sum += a(j+1, i) * x(location(j, i))
      next j

        x(i) = (b(i) - sum) / a(0,i)

    next i

      number_of_iterations += 1

      max_error = abs(x(0) - x_old(0))

    for i=0 to (nitems - 1)
      new_error = abs(x(i) - x_old(i))
      if (max_error < new_error) then max_error = new_error
    next i

  loop until (max_error < tolerance)


end sub
```

APPENDIX II

SAMPLE MCNP INPUT DECK

```
Emission Percentage
c =============================================================
c |   Quantifying emission of beta particles from Galinstan  |
c =============================================================
c
c ========= CELLS ===========
c Galistan irradiation cell
1 29 -6.44   -1      imp:p,e=1
c
c CZT Cell
c 1 20 -5.85     -1  imp:p,e=1
c 2 20 -5.85     -2  imp:p,e=1
c
98 0           -98 1   imp:p,e=1
99 0               98  imp:p,e=0

c ========= SURFACES ========
c Galinstan Cell for emission percent
1 RCC 0 0 0  0 0 0.15875  1.27
c
c Scatter tally cell/surface
c 2 RCC 0 0 -.1  0 0 -10  5
c
c WORLD
98  RPP -10 10  -10 10  -10 10

c ========= DATA ============
c Electron source simulating In-116 decay
c
sdef par=e erg=d3 POS 0 0 0  AXS 0 0 1  RAD=d1 EXT=d2 CEL=1
SI1 0 1.27
SI2 0 0.15875
c
c In116 m1 spectrum
si3 0 2.52E-02 7.56E-02 1.26E-01 1.76E-01 2.27E-01
      2.77E-01 3.27E-01 3.78E-01 4.28E-01 4.79E-01 5.29E-01
      5.79E-01 6.30E-01 6.80E-01 7.30E-01 7.81E-01 8.31E-01
      8.82E-01 9.32E-01 9.82E-01
sp3 0 9.16E-02 9.29E-02 9.30E-02 9.13E-02 8.80E-02
      8.34E-02 7.78E-02 7.16E-02 6.44E-02 5.65E-02
      4.83E-02 4.03E-02 3.27E-02 2.52E-02 1.82E-02
      1.21E-02 7.09E-03 3.66E-03 1.55E-03 2.40E-04
c
c
c \/\/\/\/ TALLIES \/\/\/\/
c Betas exiting the Galinstan per decay
f11:e 1.2
```

```
e11 0 310i 3.11
c
c Energy depositing in the TEM for dose calcultion
c fc16 Electron Energy Deposition in Tissue (MeV/g)
c f16:e 1 2
c fc26 Photon Energy Deposition in Tissue (MeV/g)
c f26:p 1 2
c
c /\/\/\/\/\/\/\/\/\/\/\/\
c
c
mode p e
print
nps 5e8
prdmp j 5e7 1 j 5e7
c
c \/\/\/\/ MATERIALS \/\/\/\/
c
c Water as TEM
c m10 6012 1 1001 2
c
c CZT d=5.85g/cc
c Cd .96 Te 1 and Zn .04 atom fraction
c m20 48000 0.96 30000 .04 52000  1
c
c Galistan Liquid Metal
c 68.5% Ga, 21.5% In, 10% Sn
m29 31000 -0.685  50000 -0.100  49113 -0.009  49115 -0.206
c
c Components
c Indium (d=7.310g/cc)
c m49 49113 -.0429  49115 -0.9571
c Isotopes of Indium
c m113 49113 1
c m115 49115 1
c
c Moderator and System materials
c Poly (density 0.94g/cc)
c m10 1001 -0.143711  6012 -0.856289
```

APPENDIX III

CZT DETECTOR

CZT Detector with components and internal schematic used for beta measurements.

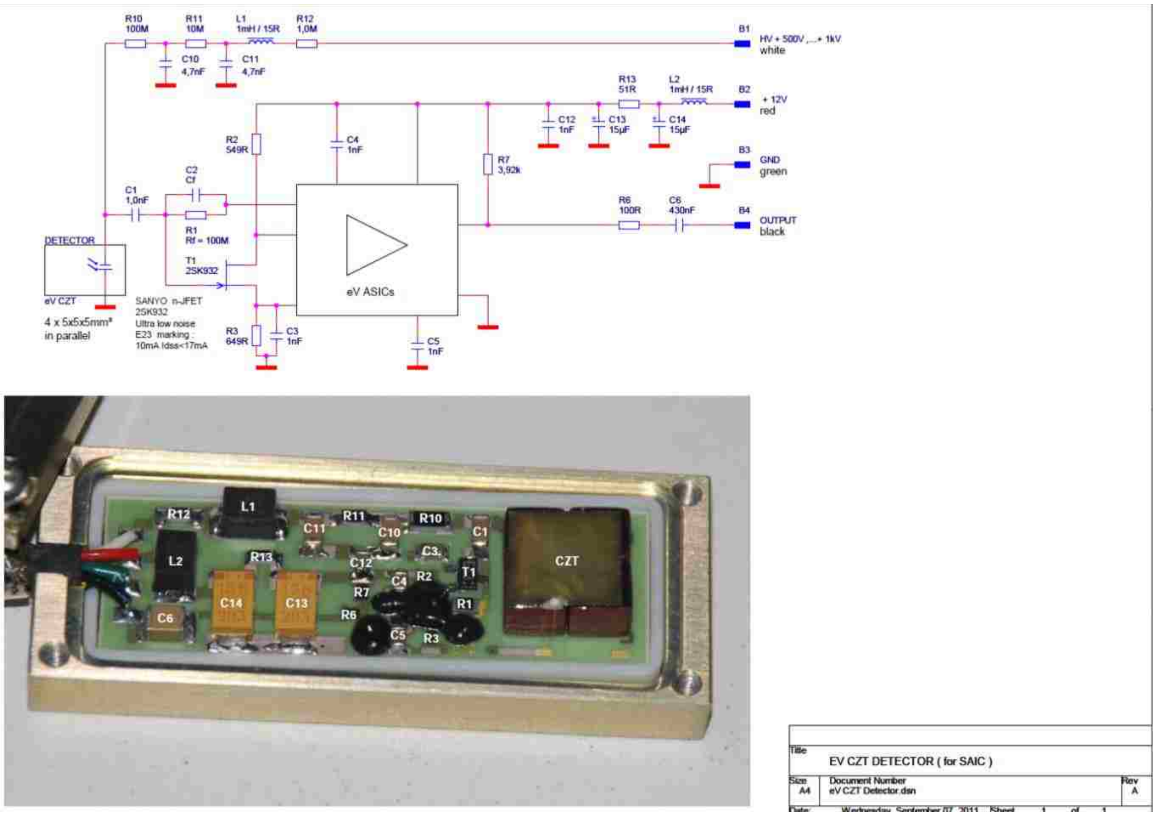

REFERENCES

[1] Pioneer in X-Ray Therapy, Science, New Series, Vol. 125, No. 3236 (Jan. 4, 1957), pp. 18-19

[2] Jäkel, Oliver. "State of the art in hadron therapy." *NUCLEAR PHYSICS METHODS AND ACCELERATORS IN BIOLOGY AND MEDICINE: Fourth International Summer School on Nuclear Physics Methods and Accelerators in Biology and Medicine*. Vol. 958. No. 1. AIP Publishing, 2007.

[3] Angha, Nader. "Muon radiation therapy." U.S. Patent No. 6,705,984. 16 Mar. 2004.

[4] Wilson, R. Radiological Use of Fast Protons. Radiology 47. (1946), pp. 487-491.

[5] Gupta, V. "Brachytherapy-past, present and future." *Journal of Medical Physics*20.2 (1995): 31.

[6] Shah, Chirag, et al. "Brachytherapy provides comparable outcomes and improved cost-effectiveness in the treatment of low/intermediate prostate cancer." *Brachytherapy* 11.6 (2012): 441-445.

[7] Lee, C., and G. Lowe. "Isotopes and delivery systems for brachytherapy."*Radiotherapy in Practice-Brachytherapy* (2011): 5.

[8] American Association of Physicists in Medicine. *Remote Afterloading Technology: A Report of AAPM Task Group No. 41, Remote Afterloading Technology*. American Association of Physicists in Medicine, 1993.

[9] Khan, Faiz M., and John P. Gibbons. *Khan's The Physics of Radiation Therapy*. Lippincott Williams & Wilkins, 2003.

[10] *Radiation Safety in Brachytherapy*. IAEA Radiation Protection of Patients. https://rpop.iaea.org/RPOP/RPoP/Content/InformationFor/HealthProfessionals/2_Radiotherapy/RadSafetyBrachytherapy.htm Accessed 17 Oct. 2014.

[11] Electron therapy basics presentation. Retrieved August 2016: http://www.slideshare.net/ajjitchandran/electron-beam-therapy

[12] L. Katz and A.S. Penfold, Rev. Mod. Phys., 24 (1952), p. 28.

[13] Kalach, Nina I., and ABS–OOTF Committee. "The American Brachytherapy Society consensus guidelines for plaque brachytherapy of uveal melanoma and retinoblastoma." *Brachytherapy* 13.1 (2014): 1-14.

[14] Einstein, Andrew J. "Breaking America's dependence on imported molybdenum." *JACC: Cardiovascular Imaging* 2.3 (2009): 369-371.

[15] Galea, R., C. Ross, and R. G. Wells. "Reduce, reuse and recycle: A green solution to Canada's medical isotope shortage." *Applied Radiation and Isotopes*87 (2014): 148-151.

[16] Liu, J.C., et al. "Calculations of Photoneutrons from Varian Clinac Accelerators and Their Transmissions in Materials." SLAC-PUB-7404 (1997).

[17] Kirwan, J. F., et al. "Beta irradiation: new uses for an old treatment: a review."*Eye* 17.2 (2003): 207-215.

[18] Andras, Alina, et al. "Intravascular brachytherapy for peripheral vascular disease." *status and date: New search for studies and content updated (no change to conclusions), published in* 1 (2014).

[19] Haynes, William M., ed. *CRC handbook of chemistry and physics*. CRC press, 2012.

[20] Nath, Ravinder, Ning Yue, and Lizhong Liu. "On the depth of penetration of photons and electrons for intravascular brachytherapy." *Cardiovascular radiation medicine* 1.1 (1999): 72-79.

[21] IAEA Final Report of a coordinated research project, "Production techniques and quality control of sealed radioactive sources of palladium-103, iodine-125, iridium-192 and ytterbium-169." 2001-2005 IAEA-TECDOC-1512

[22] Ravinder, N. "On the depth of penetration of photons and electrons for intravascular brachytherapy." Cardiovascular Radiation Medicine, V1. Issue 1. 71-79. 1999.

[23] Gueli, A.M., et al. "3D dosimetry on Ru-106 plaque for ocular melanoma treatments." Radiation Measruements 46, 2014-2019. 2011.

[24] Dickler, Adam. "Xoft Axxent® electronic brachytherapy—a new device for delivering brachytherapy to the breast." *Nature Clinical Practice Oncology* 6.3 (2009): 138-142.

[25] D. McComb, "Gallium Restorative Materials," *Journal of the Canadian Dental Association*, Vol. 64, 1998, pp. 645-647.

[26] Schreiber S, et al. "Galinstan Thermometer Is More Accurate Than Digital For The Measurement Of Body Temperature In Children. - Pubmed - NCBI ".*Ncbi.nlm.nih.gov*. N. p., 2016. Web. 7 Sept. 2016

[27] L. C. Cadwallader, Gallium Safety in the Laboratory June 21, 2003 – June 27, 2003 Energy Facility Contractors Group (EFCOG) Safety Analysis Working Group (SAWG)2003 Annual Meeting

[28] D. L. Diedhiou, D. Iero, O. de Sagazan, R. Sauleau and A. V. Boriskin, "Inset-fed liquid metal patch antenna," *The 8th European Conference on Antennas and Propagation (EuCAP 2014)*, The Hague, 2014, pp. 1739-1741.

[29] I. El Gmati, P. Calmon, A. Boukabache, P. Pons, H. Boussetta, M.A. Kallala, K. Besbes, Liquid RF MEMS variable inductor, Procedia Engineering, Volume 5, 2010, Pages 1380-1383, ISSN 1877-7058,

[30] M. Hodes, R. Zhang, L. S. Lam, R. Wilcoxon and N. Lower, "On the Potential of Galinstan-Based Minichannel and Minigap Cooling," in *IEEE Transactions on Components, Packaging and Manufacturing Technology*, vol. 4, no. 1, pp. 46-56, Jan. 2014

[31] W. Irshad and D. Peroulis, "A silicon-based galinstan magnetohydrodynamic pump," in PowerMEMS 2009, Washington, DC, December 2009.

[32] Email correspondence with authors Irshad, Peroulis. 2012.

[33] Hayes, John W., et al. "Characterization of a Thermo Scientific D711 DT neutron generator located in a low-scatter facility." *Nuclear Instruments and Methods in Physics Research Section A: Accelerators, Spectrometers, Detectors and Associated Equipment* 741 (2014): 57-66.

[34] R. Chandra, G. Davatz, H. Friederich, U. Gendotti, and D. Murer. Fast neutron detection with pressurized 4He scintillation detectors. Journal of Instrumentation, 7(03):C03035, 2012

[35] Cris W. Barnes, Alvin R. Larson, G. LeMunyan, and M. J. Loughlin. Measurements ofDT and DD neutron yields by neutron activation on the Tokamak Fusion Test Reactor. Review of Scientic Instruments, 66(1):888-890, 1995.

[36] Tim Meehan, E.C. Hagen, C.L. Ruiz, and G.W. Cooper. “Praseodymium activation detector for measuring bursts of 14 MeV neutrons.” Nuclear Instruments and Methods in Physics Research Section A: Accelerators, Spectrometers, Detectors and Associated Equipment, 620(23):397-400, 2010.

[37] Liu, J. C., et al. "Calculations of photoneutrons from Varian Clinac accelerators and their transmissions in materials." *Radiation Dosimetry and Safety, Taipei, Taiwan* (1997).

[38] Delaney, K., S. Avery, and J. Christodouleas. "Neutron Activation of Indium Foils Irradiated During Passively Scattered Proton Therapy and Implications on the Treatment of Pacemaker Patients." *International Journal of Radiation Oncology• Biology• Physics* 90.1 (2014): S748-S749.

[39] *Commercial Indium Metal.* Indium Corporation Product Data Sheet. http://www.indium.com/technical-documents/product-data-sheets/ Accessed 20 Oct. 2014.

[40] Surmann, Peter, and Hanan Zeyat. "Voltammetric analysis using a self-renewable non-mercury electrode." *Analytical and bioanalytical chemistry* 383.6 (2005): 1009-1013.

[41] Alt, Marion, et al. "Low melting gallium, indium, and tin eutectic alloys, and thermometers employing same." U.S. Patent No. 6,019,509. 1 Feb. 2000.

[42] MSDS for Galinsan. http://www.rgmd.com/msds/msds.pdf Accessed 21 Oct. 2014.

[43] Schreiber, Silvana, et al. "Galinstan Thermometer Is More Accurate Than Digital for the Measurement of Body Temperature in Children." *Pediatric emergency care* 29.2 (2013): 197-199.

[44] Harvey, Zachary R. "Neutron flux and energy characterization of a plutonium-beryllium isotopic neutron source by Monte Carlo simulation with verification by neutron activation analysis." (2010).

[45] Reniers, Brigitte, et al. "Calculation of relative biological effectiveness of a low-energy electronic brachytherapy source." *Physics in medicine and biology*53.24 (2008): 7125.

[46] M. Cardona and L. Ley, Eds., *Photoemission in Solids I: General Principles* (Springer-Verlag, Berlin) with additional corrections, 1978.

[47] Lefaivre, D., and P. Marmet. "Electroionization of D2O and H2O and study of fragments H+ and OH+." *Canadian Journal of Physics* 56.12 (1978): 1549-1558.

[48] Hoffman, R. E. "The Self-Diffusion of Liquid Mercury." *The Journal of Chemical Physics* 20.10 (1952): 1567-1570.

[49] Fogler, H. S. *Elements of Chemical Reaction Engineering.* 4th ed. pp 880-895, Pearson Education. (2006)

[50] Culbreth, W.C., O'Brien, R.J., "Computational Modeling of Segregated Laminar Flow of an Activated Liquid Metal." *Proceedings of the International Conference on Mathematics and Computational Methods Applied to Nuclear Science and Engineering (M&C 2014).*

[51] Olsen-Kettle, Louise. "Numerical solution of partial differential equations." Earth Systems Science Computational Centre School of Earth Sciences The University of Queensland (2011).

[52] White, F. M. "Viscous fluid flow. 2006." pp. 106-127 (2006)

[53] Meleshko, V. V., V. S. Malyuga, and A. M. Gomilko. "Steady Stokes flow in a finite cylinder." *Proceedings of the Royal Society of London. Series A: Mathematical, Physical and Engineering Sciences* 456.1999 (2000): 1741-1758.

[54] Garandet, J. P. "Estimation of liquid phase diffusion coefficients of gallium and antimony in germanium from segregation data in crystal growth experiments."*Journal of Crystal Growth* 310.14 (2008): 3268-3273.

[55] Hughes, "Neutron Cross Sections". Brookhaven National Lab, Permagon Press, 1957.

[56] Retrieved from Manufacturer website. September 2016: http://www.canberra.com/products/detectors/pdf/passivated_pips_C39313a.pdf

[57] Arlt, R., Ivanov, V., Parnham, K. Advantages and Use of CdZnTe Detectors in Safeguards Measurements. eV Products Documentation.

[58] Retrieved from Manufacturer website. September 2016. Fisher Scientific pumps: https://www.fishersci.com/shop/products/fisher-scientific-variable-flow-peristaltic-pumps-4/p-158215#

[59] Hodges, M. “Characterization of the radiation environment at the UNLV accelerator facility during operation of the Varian M6 linac.”, Radiation Physics and Chemistry 127. 72-77. 2016.

[60] Naseri, Alireza, and Asghar Mesbahi. “A Review on Photoneutrons Characteristics in Radiation Therapy with High-Energy Photon Beams.” *Reports of Practical Oncology and Radiotherapy* 15.5 (2010): 138–144. *PMC*. Web. 5 Nov. 2016.

[61] Ovalle, S. “Neutron Dose Equivalent in Tissue Due to Linacs of Clinical Use.” *Frontiers in Radiation Oncology*, 91-112. 2013.

[62] Liu, J.C., et al. “Calculations of Photoneutrons from Varian Clinac Accelerators and Their Transmissions in Materials.” Radiation Dosimetry and Safety Conference, 1997.

[63] Gallmeier, F.X., "General Purpose Photoneutron Production in MCNP4A." Oak Ridge National Laboratory Publications, ORNL/TM-13073. 1995.

Parts of this work were supported by National Security Technologies, LLC, under Contract No. DE-AC52-06NA25946 with the U.S. Department of Energy. DOE/NV/25946--3077

CURRICULUM VITA

Graduate College

University of Nevada, Las Vegas

Robert James O'Brien

Local Address:
UNLV Howard R Hughes College of Engneering
Department of Mechanical Engineering
4505 Maryland Parkway
Las Vegas, Nevada 89154-4027

Degrees:

Master of Science, Materials and Nuclear Engineering, 2006
University of Nevada, Las Vegas

Bachelor of Science, Applied Physics, 2005
University of Nevada, Las Vegas

Bachelor of Science, Mechanical Engineering, 2005
University of Nevada, Las Vegas

Professional Memberships and Societies:

American Association of Physicists in Medicine (AAPM)
American Nuclear Society (ANS)
American Physical Society (APS)
American Society of Mechanical Engineers (ASME)
Health Physics Society (HPS)
Society of Physics Students
Tau Beta Pi Engineering Honors Society

Special Honors and Awards:

National Science Foundation Research Experience for Undergraduates, 2003

NASA Undergraduate Space Grant, 2002-2004

Harold and Mayme Stocker Scholarship, 2001-2005

Outstanding Mechanical Engineering Student of the Year, 2004

Outstanding Graduate, Mechanical Engineering, 2005

Dean’s List 8 Semesters as Undergraduate

Honor’s College, UNLV 2000-2005

Publications:

R.J. O'Brien, W.G. Culbreth, "Neutron Detection Using a Mobile Liquid Activation Material," *IEEE Nuclear Science Syposium & Medical Imaging Conference,* Seattle, WA, 2014.

W.C. Culbreth, **R.J. O'Brien**, "Computational Modeling of Segregated Laminar Flow of an Activated Liquid Metal." *Proceedings of the International Conference on Mathematics and Computational Methods Applied to Nuclear Science and Engineering (M&C 2014).*

R.J. O'Brien, D. Lowe, Meehan, B., Hagen, E., "Fast framing camera images of neutron production cessation at high currents in a Dense Plasma Focus machine," *IEEE International Conference on Plasma Sciences,* DOI 10.1109/PLASMA.2013.6634885 (2013).

R.J. O'Brien, W.G. Culbreth, "Radiation Therapy Methods Using a Short Lived Beta-Decay Source," *2013 ANS Annual Meeting and ANS Transactions*, Atlanta, GA, 2013.

P. Guss, R. Guise, D. Yuan, S. Mukhopadhyay, **R.J. O'Brien**, et al., "Lanthanum Halide Nanoparticle Scintillators for Nuclear Radiation Detection," *Journal of Applied Physics*, 113 (2013).

R.J. O'Brien., Tsang. F., “New Methods for Electron Beam Radiotherapy*,” Invited Paper, ANS Winter Annual Meeting and ANS Transactions*, Washington, D.C., October 31, 2011.

W.G. Culbreth, D.R. Lowe, **R.J. O'Brien**., “Real-Time Alpha Detection for the Monitoring of Actinides in Air Flow,” *ANS Winter Annual Meeting and ANS Transactions,* Washington, D.C., October 31, 2011.

R.J. O’Brien, D.R. Lowe, B.T. Meehan, P.W. Patton, T.A. Wilcox, “Image Analysis of a Dual-Energy Mega-Voltage Cargo Imager Utilizing MCNPX,” *Invited presentation to ANS 2010 Winter Meeting "Best of RPSD 2010,"* Las Vegas, NV (2010).

R.J. O’Brien, D.R. Lowe, B.T. Meehan, P.W. Patton, T.A. Wilcox, “Image Analysis of a Dual-Energy Mega-Voltage Cargo Imager Utilizing MCNPX,” *ANS RPSD 2010 Proceedings,* Las Vegas, NV (2010).

R.J. O’Brien, D.R. Lowe, E.C. Hagen, B.T. Meehan, “Dense Plasma Focus Devices for Neutron Spectroscopy using MCNPX,” *IEEE Nuclear Science Symposium,* Dresden, Germany (2008).

R.J. O’Brien, D.R. Lowe, and P.W. Patton, “Dose Calculations for New Imaging Technologies Used in the Detection of Radiological Weapons of Mass Destruction,” Proceedings of Health Physics Society 52nd Annual Meeting, Portland, OR (2007).

R.J. O'Brien, “Shielding and Radiation Dose Analysis of a Dense Plasma Focus Device,” ANS Winter Meeting Proceedings, American Nuclear Society, Albuquerque, NM (2006).

R.J. O'Brien, “Shielding and Radiation Dose Analysis of a Dense Plasma Focus Device,” Proceedings of RPS 2006, American Nuclear Society, Carlsbad, NM (2006).

R.J. O'Brien, “Criticality and Heat Transfer Analysis of an Np/Pu Mixture,” Proceedings of American Nuclear Society Student Conference (2004).

Dissertation Title: Radiation Therapy Dosing and Material Transport Methodology

Thesis Examination Committee:

Chairperson, Dr. William Culbreth, Ph.D.

Committee Member, Dr. Yitung Chen, Ph.D.

Committee Member, Dr. Brendan O'Toole, Ph.D

Committee Member, Dr. Woosoon Yim, Ph.D.

Graduate Faculty Representative, Dr. Steen Madsen, Ph.D.